A New Self-Contained Electro-Hydraulic Brake System

by

Laaleh Durali

A thesis
presented to the University of Waterloo
in fulfillment of the
thesis requirement for the degree of
Doctor of Philosophy
in
Mechanical Engineering

Waterloo, Ontario, Canada, 2015

AUTHOR'S DECLARATION

I hereby declare that I am the sole author of this thesis. This is a true copy of the thesis, including any required final revisions, as accepted by my examiners.

I understand that my thesis may be made electronically available to the public.

Laaleh Durali

Abstract

The automotive brake system plays a significant role not only in the deceleration and stopping process, but also in many stability control strategies. To overcome the limitations of conventional brake systems and to improve vehicle control strategies such as traction control, and differential braking, a new generation of brake systems called the brake-by-wire system has been introduced to the vehicle industry. This generation of brake systems combines electrical, mechanical and, in some cases, hydraulic components. Although different types of brake-by-wire mechanisms have been developed in the past two decades, there still exist demands for further improvement and developing new brake mechanisms in the automotive industry due to the ever increasing demand for better safety and performance.

This research proposes a novel brake-by-wire system based on cam actuation. This system is a combination of electrical, mechanical and hydraulic components. The unique feature of the cam actuation brake system proposed in this research is that the characteristics of the motor torque amplification can be optimized by careful design of the cam shape. The compactness and self-contained characteristic of the design allow the brake system to be installed on each wheel enabling fully independent control of each wheel for better stability control. Moreover, the cam actuated brake has a fail-safe advantage by keeping the direct connection between the driver and the brake calipers in case of any system failure.

In this work, different subsystems of the brake system and their components are explained, the dynamic model of the system is found and the design parameters are optimized. Specifically, the optimal design problem has been formulated by taking the geometry of the cam as the optimization variable and the open-loop response time of the brake system as the objective function to be minimized. The solution to this problem is then obtained by the multi-layer design optimization process using the genetic algorithm (GA). Various control algorithms are applied to the developed cam actuated brake system to investigate their performance in terms of tracking a desired braking pressure.

Acknowledgements

I wish to express my sincere gratitude to my supervisors, Professor Amir Khajepour and Professor Soo Jeon, for their valuable guidance, constant support, patience and encouragement during my research.

I would like to thank my committee members, Professor. Ehsan Toyserkani, Professor. Nasser Lashgarian Azad, Professor. Hyock J. Kwon and Professor, Sedaghati for their valuable comments to improve my thesis.

I am particularly in debt to Dr. Alireza Kasaiezadeh for his friendship, guidance, advices and support in the most difficult time of my research. His presence was like a miracle for me. In addition, I would like to express my gratitude to my friend, Milad Jalali for sharing his profound knowledge with me during the past years.

I am grateful to my best friend Ms. Nazanin Najafian, for the encouragement, kindness and inspiration she gave to me my whole life. She was missed a lot in the past four years.

Words cannot express my sincere gratitude to my family, my father, Dr. Mohammad Durali, for his unconditional support, help and love during all the years of my education, my mother, Ms. Nassrin Hashemi, for what she has done for me over the years. She has never stopped loving and supporting me, and my sister, Mariam Durali, for the love and joy she gave to me in the difficult moments of my life.

Dedication

This thesis is dedicated to the people who gave me the Love, who stood by me through all the successes and setbacks during the last four years.

To my Parents, Nassrin and Mohammad

Table of Contents

List of Figures

List of Tables

Chapter 1
Introduction

The vehicle industry has become more advanced in terms of integrating electrical and mechanical components in recent decades. Researchers in vehicle industry and academia have attempted to improve vehicular performance by adding more intelligent and controllable systems. The drive-by-wire or x-by-wire is a promising technology for future commercial vehicles. Steer-by-wire and throttle-by-wire are a combination of electrical and mechanical systems that have already been installed on vehicles. Furthermore, the x-by-wire mechanism has been categorized within the Driver Assistance Systems (DAS), where the driver's role in controlling the vehicle has been replaced or reduced by some advanced control algorithms. The control signals are generated based on the vehicle's various driving conditions.

Designing and developing a robust and reliable brake system is very important both for the vehicle industry and researchers in academia. Many automobile manufacturers, like Mercedes-Benz and Toyota, have attempted to develop a brake-by-wire mechanism, but due to some safety and regulatory issues, this system has not yet been widely used in commercial vehicles. Therefore, improvement or developing a new mechanism for the brake-by-wire system is still in demand.

In this chapter, different types of brake-by-wire system are explained briefly. It is followed by the motivation behind this research and the thesis layout.

1.1 Existing Brake-by-wire Systems

1.1.1 Electro Hydraulic Brake (EHB) System

The most popular and widely used type of brake-by-wire is the Electro Hydraulic Brake (EHB) system. Compared to the conventional hydraulic brake system, EHB's braking power is provided by a hydraulic pump instead of the driver's brake pedal inputs. This system is a combination of electrical and hydraulic parts. The electrical component has the duty of providing a brake activation signal, while the hydraulic fluid builds up the necessary pressure against the braking disk during the braking process. Although the hydraulic components create the braking torque, the Electronic Control Unit (ECU) plays a more important role since it calculates the correct and necessary signal that goes to each wheel hydraulic unit. To use the EHB for the Driver Assistance System (DAS), there are sensors such as wheel speed sensor, steering angle sensor, yaw rate sensor and acceleration sensor other than

brake pedal input sensor that provide information about the vehicle's condition in calculating each wheel braking torque.

The most important advantage of EHB system over other types of brake-by-wire system is that there is a direct connection between the driver and the wheels' caliper, but it is disconnected when there is no failure in the EHB system through the isolating valve.

1.1.2 Electro Mechanical Brake (EMB) System

This type of brake-by-wire system is a combination of electrical and mechanical components. There is no braking fluid in the EMB system, therefore, it is claimed that this type of brake system is more environmental friendly than the EHB system. It is also called dry brake-by-wire in the absence of braking fluid. The electric motor provides the braking power through a mechanical mechanism, which is usually a ball screw or a power screw. Here, the electric motor input signal is calculated based on the information coming from sensors installed in the brake system to monitor the vehicle driving condition in a similar manner as the EHB.

In the EMB brake system there is no direct connection between the driver and the braking calipers. The fail safe mechanism is provided by adding an additional motor installed on the wheels.

1.1.3 Electronic Wedge Brake (EWB) System

The electronic wedge brake mechanism is a self-energized brake system. The overall mechanism of the EWB is quite similar to the EMB system. The brake power source is an electric motor which is activated by control unit's signal. The EWB has two types: upper-wedge mechanism and lower-wedge mechanism. In the upper-wedge mechanism, the electric motor is connected to the upper-wedge and the friction force between the braking disk, and the braking pad is in the same direction as the motor force. The friction force between the braking disk and the pad pulls the wedge mechanism inside and creates the self-energized ability. In the lower-wedge system, the directions of these two forces are opposite; therefore, a strong motor torque is required to pull back the wedge mechanism in case of jamming.

1.1.4 Distributed Electro Hydraulic Brake System (DEHB)

Developed by Wang et al [4], the DEHB is the most recent design in brake-by-wire category. This brake system is a combination of the EMB and the EHB. In the DEHB, an electric motor provides braking power while a screw mechanism and a hydraulic piston transform the motor torque to hydraulic pressure inside the brake cylinder.

Like the EHB system, the most important advantage of the DEHB system is its ability to directly connect the driver and brake master cylinder to the wheels' calipers should any failure happen in electrical system. On the other hand, since the hydraulic pump, which is the braking power provider in the EHB, is replaced by an electric motor, it has some similarities to the EMB system.

1.2 Motivation

In this chapter, different types of brake-by-wire mechanisms were studied. It is clear that each of the presented systems have their own advantages and drawbacks. It should be mentioned that not only is designing a novel brake system important, but developing a proper control system to create necessary activation signals for the brake system has the same importance. Therefore, this thesis is an attempt in designing, modeling, optimizing and controlling a new brake-by-wire system. The brake-by-wire system is self-contained and fail-safe in case of any unwanted failure in the brake mechanism.

1.3 Thesis Layout

The remainder of this thesis is organized as follows:

Chapter 2: In this chapter, different types of brake-by-wire systems are reviewed in a greater detail. The chapter covers the Electro Hydraulic, Electro Mechanical, Electronic Wedge and Distributed Electro Hydraulic brake mechanisms.

Chapter 3: In this chapter, the proposed brake system and its components are explained; followed by the mathematical model of the new self-contained electro-hydraulic brake system is introduced.

Chapter 4: In this chapter, the optimization of brake parameters to improve system response is formulated.

Chapter 5: In this chapter, the performance of different control algorithms for the designed brake system is examined. The controllers which include in this chapter are PI, Sliding Mode, Adaptive Sliding Mode and Model Predictive.

Chapter 6: This chapter summarizes the work done in the thesis. It also gives suggestions for the future works.

Chapter 2
Literature Review and Background

The idea of using drive-by-wire mechanisms in vehicles in place of conventional hydraulic and pneumatic systems has become popular among automotive parts manufacturers. Steer-by-wire and throttle-by-wire, examples of drive-by-wire mechanisms, are in mass production. However, commercialization of brake-by-wire design has remained as a challenge due to the passenger's safety as the top priority in the braking operation. Since the brake-by-wire systems assist the driver in different braking, control and stability conditions, improving their existing mechanism or presenting a new design is an interesting topic for the industry and academia.

This chapter discusses the past research on the brake-by-wire system with different mechanisms. In Section 2.1 the Electro Hydraulic Brake (EHB) are explained. The mechanism of the Electro Mechanical Brake (EMB) is discussed in Section 2.2. Section 2.3 covers the Electronic Wedge Brake (EWB) system, and Section 2.4 includes the Distributed Electro Hydraulic Brake (DEHB) system.

2.1 Electro Hydraulic Brake System (EHB)

As described by Buener and Bill [5], the EHB system is a braking system in which the necessary power for braking comes from a hydraulic pump that has the duty of building up the pressure in the braking system, rather than from the driver's inputs. EHB systems work in accordance to the cooperation of electrical and hydraulic components. Although their activation signals are electrical, the hydraulic fluid creates the braking force exerted to the braking disk. Other complementary parts in an EHB system, as shown in Figure 2-1, include a hydraulic control unit used to adjust the amount of transmitted hydraulic pressure to the wheel cylinders; an accumulator for storing pressurized hydraulic liquid that comes from the pump; inlet valves that conduct the output oil from the accumulator to the particular wheel cylinder; outlet valves installed in the return flow path that conduct the oil from the wheel cylinder to the reservoir (in Figure 2-1 the inlet and outlet valves are inserted in wheel-pressure modulator unit); cut-off valves that provide the direct connection between the exit of the master cylinder and the wheel cylinders; an ECU to provide a control signal for the braking process; a set of sensors to measure necessary inputs for the ECU; and a brake pedal simulator that provides an appropriate brake pedal feeling for the driver and would not let him/her feel brake pressure changes. For safety purposes, if any electrical failure occurs, the valves will be cut

from the oil's path and the necessary braking pressure will be provided directly by the driver, similar to the workings of a conventional braking system.

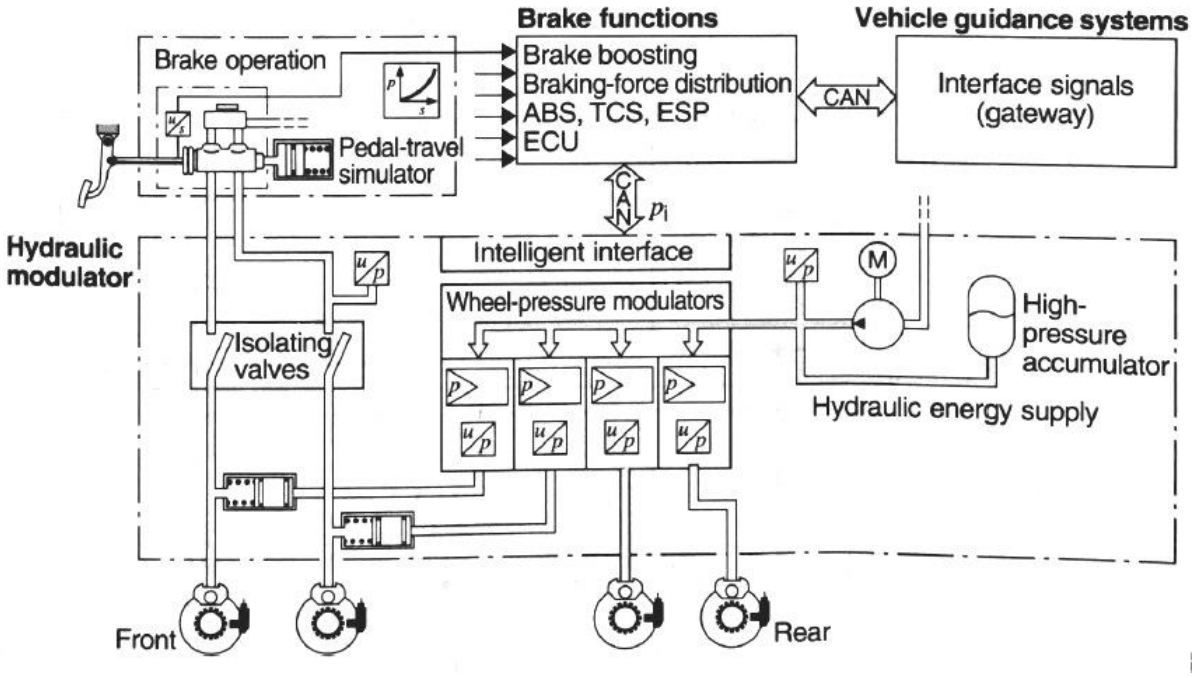

Figure 2-1 General schematic of an EHB system [1]

The inlet and outlet valves are solenoid servo valves that are activated by the electrical signal coming from ECU. The necessary electrical signal for opening the valves is calculated based on the drivers' requirements, as well as driving conditions such as the slip ratio, yaw moment, wheel speed, and steering angle. The amount of braking fluid that goes to or returns from each wheel will be calculated by the valve's spool position. How the spool position affects the flow is determined by the orifice dynamics. In some models, two solenoid valves (not a servo one) are used to control the timing of the flow into and out of the wheel cylinder. In these models, one valve works as the inlet valve, while the other is used as the outlet valve. The inlet valve works between the high pressure source (pump or accumulator) and the wheel cylinder. The outlet valve works between the cylinder and the reservoir.

In the other design, these two valves are replaced by a three-way valve, and it is assumed that the three-way valve in the braking system is a critically centered valve. This means that at the beginning, when there is no spool movement, the output port is closed. If the spool moves to the positive direction, there will be a connection between the high pressure source and the wheel cylinder. As a result, wheel pressure increases.

On the contrary, by moving the spool to the negative direction, the wheel is connected to the reservoir and wheel pressure decreases. As mentioned earlier, the passing flow from the servo valves can be calculated by the equation of flow through an orifice with a variable area,

$$Q_L = C_d h x_s \sqrt{\frac{2\Delta P}{\rho}} \tag{2-1}$$

where C_d is the discharge coefficient, h and x_s are orifice width and orifice opening, respectively. ΔP is the pressure difference between the pump and the wheel cylinder when the brake is applied. When the brake is released, ΔP becomes the pressure difference between the wheel cylinder and the tank.

The linearized form of orifice flow force for a three-way spool valve shown in Figure 2-2 is [6]

$$Q_L = 2K_q x_s - 2K_c(P_L - \frac{P_s}{2}) \tag{2-2}$$

where K_q and K_c are the flow gain and the pressure flow coefficient, respectively. x_s is the spool displacement, P_L and P_s are the load pressure and the supply pressure, respectively.

The linearized form of the orifice flow for a critically centered three-way valve depends on the spool position as: [6]

$$Q_L = K_q x_s \tag{2-3}$$

while the flow gain (K_q) can be calculated by:

$$K_q = C_d h \sqrt{\frac{2P_0}{\rho}} \tag{2-4}$$

where P_0 is the nominal pressure drop across the valve. The output flow of the valve compresses the oil inside the wheel cylinder and moves the wheel cylinder forward. The flow relation is:

$$Q_L = \dot{V}_{com} + \dot{V}_{wc} = \frac{\beta \dot{P}_{wc}}{V_{0wc}} + \frac{t_{pad} A_{wc}^2}{E_{pad} A_{pad}} \dot{P}_{wc} \tag{2-5}$$

where $\dot{V}_{com}$ is the volume changes due to the compressibility of oil inside the wheel cylinder and $\dot{V}_{wc}$ is the volume changes due to movement of wheel cylinder forward and V_{0wc} is the initial volume of the wheel cylinder.

On the other hand, if a current is applied to the solenoid servo valves, it will move the spool and open the orifice. The force components on the spool are shown in Figure 2-2. The force equilibrium equation is presented in [6]

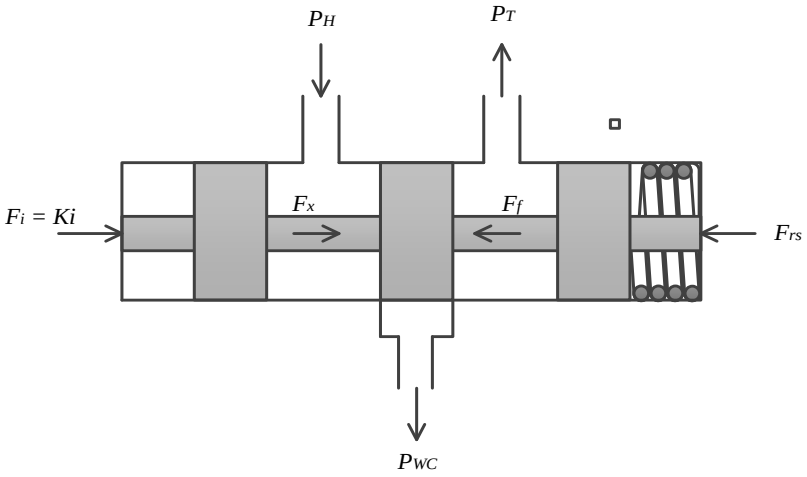

Figure 2-2 Forces applied on valve's spool

$$F_i + F_x + F_f + F_{rs} = m_s \ddot{x}_s \tag{2-6}$$

where F_i, F_x, F_f, F_{rs} are solenoid force, flow force, viscous damping force and return spring force, respectively. m_s is the spool mass and $\ddot{x}_s$ is the spool acceleration.

The linearized form of fluid force can be written as:

$$F_x = \begin{cases} -\rho L K_q \dot{x}_s - K_{fq} x_s & x_s > 0 \\ 0 & x_s = 0 \\ \rho L K_q \dot{x}_s - K_{fq} x_s & x_s < 0 \end{cases} \tag{2-7}$$

where L is the distance between two ports of the valve. K_{fq} is pressure flow force coefficient which can be calculated by:

$$K_{fq} = 2P_0 C_d^2 \cos(\theta)\, h \tag{2-8}$$

where θ is the jet angle for the valve opening as it is shown in Figure 2-3. It must be between 21 and 69 degrees. For most valve openings, 69 degrees is a good estimation for this parameter.

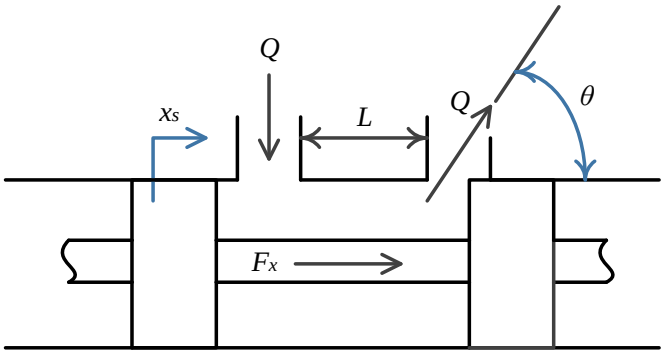

Figure 2-3 valve jet angle

Therefore, Equation (2-6) can be written as:

$$K_i i - \rho L K_q \dot{x}_s - K_{fq} x_s - K_{rs} x_s - B_f \dot{x}_s = m_s \ddot{x}_s \qquad (2\text{-}9)$$

where K_i is the current coefficient for solenoid with i as the applied current to it. K_{rs} denotes the valve's return spring stiffness. B_f is the viscous damping coefficient and m_s is the spool mass.

By solving Equation (2-9), the spool position can be found along with the solenoid current as the input of the system. This position is substituted in Equation (2-3) to calculate the flow that goes into or comes out from the wheel cylinder.

As mentioned previously, the command signal for each wheel's valve is defined by the ECU based on the driver's requirements, the master cylinder pressure, the wheel cylinder pressure, and vehicle driving conditions such as the steering angle, wheel speed, yaw rate, and vehicle acceleration. In the following pages, the researches done on the EHB system are briefly explained.

Reuter et al [7] drew some comparisons between having the EHB system on one axle or both axles of vehicles by considering braking performance and deceleration capacity in each of them. They also conducted research on braking pedal simulators to correct excessive pedal simulator displacement.

Since 2004, there have been many patents on how conventional hydraulic brake systems can be transformed into EHB systems to provide ABS, stability control, traction control, differential braking control and regenerative brake system [8]–[12]. Figure 2-4 shows an example of these systems discussed in patents. There is a sensor, shown in the Figure 2-4 by U/s, to measure pedal displacement and six pressure sensors (p/U) to detect the brake fluid pressure in each wheel and accumulator. These sensors provide information about braking condition for control unit. In the

presented system, for instance, if correction in yaw moment is needed, the control unit (ECU) will provide necessary command signal for servo valves to create asymmetric braking.

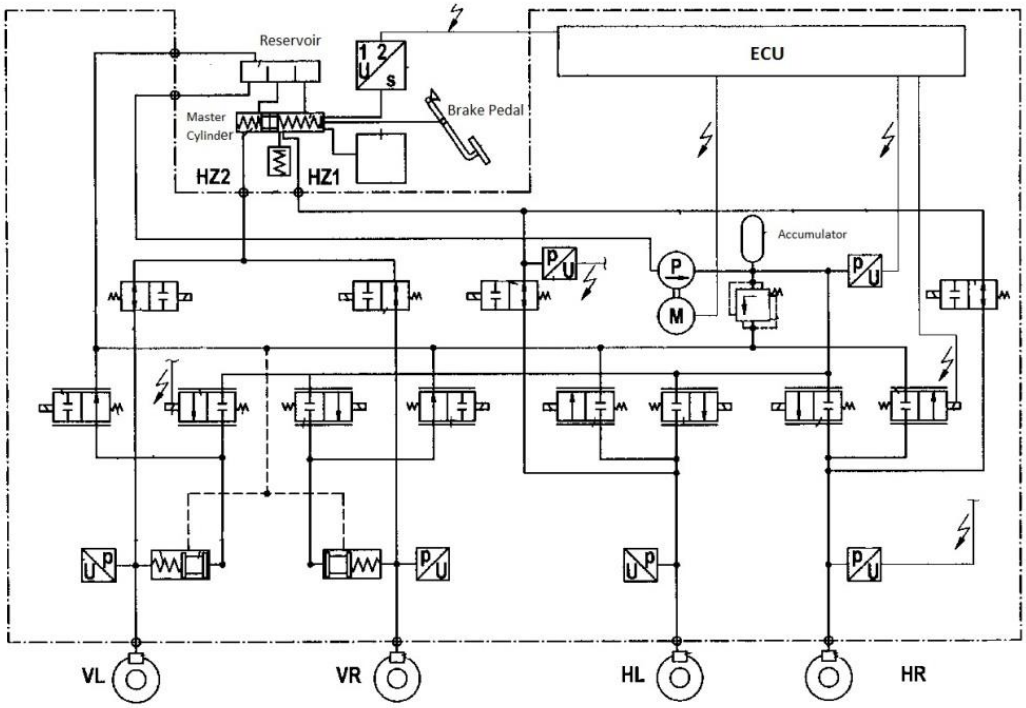

Figure 2-4 EHB system presented in [13]

The EHB system presented by Nakamura et al. [14] has the functionality to apply regenerative and frictional braking together, and can also provide other control systems such as ABS, VSC, and TCS functions. In order to generate differential braking for the vehicle, there are electrically controllable adjustment valves responsible for providing the necessary pressure for each wheel independently from the driver's input pedal force. There is a brake simulator that is connected to the master cylinder output line to provide the pedal reaction force. The control algorithm for cooperation between regenerative and frictional brake presented by Nakamura et al. is claiming to eliminate the skid and the deterioration of steering performance, and driving wheel slip; therefore, improving vehicle stability.

Soga et al. [15] designed a system similar to Nakamura's, but for the purpose of maximizing the regenerative brake torque and developing a proper ABS and VSC, a vehicle dynamic management

system is added to the EHB system. The control strategy for this system uses the wheel cylinder hydraulic pressure as feedback, which then provides a smooth driving pattern for the driver.

Park et al. [16] presented a control algorithm in which the EHB system works with a vacuum management system to provide cooperation between regenerative and frictional braking, ABS, and differential braking conditions. This vacuum management system consists of valves that are controlled by feed-forward and feedback controllers. They argued that the presented system is a cost-effective design that provides good brake performance.

A suitable EHB system for hybrid and electrical brakes that has been designed by Continental for mass production in the USA since 2008 is described by Albrichsfeld and Karner [17]. The main goal of this system is to maximize the regenerative brake system and provide a good brake pedal simulator. In this system, by activation of ABS and VSC, the regenerative brake stops working. It is said that the presented system is reliable, durable, and robust, and can follow the driver's braking demands.

Zhilin et al [18] presented an EHB system using two Matlab and AMESim software. The hydraulic section of EHB is developed in AMESim, while the controller of the system is designed in Matlab; these two are linked to examine the dynamic characteristics of EHB and how this method can affect active vehicle safety. For this purpose, the mathematical formulation of hydraulic pressure within the system and the solenoid valves are derived, and a single-neuron PID controller is designed for the controller.

Milanes et al. [19] presented an electrohydraulic brake system that was different from others. While providing ABS, the system has two electrical components that have the duty of providing braking pressure for the wheels. The first one is an electro proportional pilot valve that is used to transmit necessary flow from the pump to the wheels. The second one is a spool directional valve that is used to adjust the pressure of wheels. There is also a backup system that can be activated by the driver's force in case of any failure in the electrical components. The presented system also consists of shuttle valves that have the duty of switching between EHB and backup braking systems. It is claimed that installing the system in a car displayed good speed control behavior.

Kim et al. [20] discussed a genetic algorithm to find the satisfactory brake torque distribution between the EHB system and regenerative braking systems, which is a complimentary brake system to assist the EHB mechanism in braking. This algorithm can determine the optimal value of the torque

for the regenerative braking system and EHB. They have also developed a control method that can make the desired direct yaw moment to maintain desirable stability for the vehicle.

One of the most important uses of the EHB system is providing anti-lock brake control for vehicles. In their researche, D'alfio et al. [21] and Anwar [22] consider how the control of EHBs must be modified to work with ABS. In [23], the way the wheel slip must be controlled in the presence of the EHB brake-by-wire system is discussed.

Kim D. and Kim H [24] proposed a fuzzy rule-based algorithm that calculates direct yaw moment to provide the stability necessary for the vehicle while there is cooperation between the electrohydraulic brake system and the regenerative brake system.

2.2 Electro Mechanical Brake System (EMB)

The EMB system is a fully electrical/mechanical brake where there is no braking fluid; therefore, called a dry brake-by-wire system. As shown in Figure 2-5, the main components of an EMB brake system are the stator, rotor, planetary gear, ball screw, piston, and clamping force sensor (not shown the Figure 2-5). The motor torque drives the planetary gear and creates piston movement through the ball screw providing necessary clamping force. The brake actuator command comes from the vehicle controller in accordance with driver requirements and driving conditions.

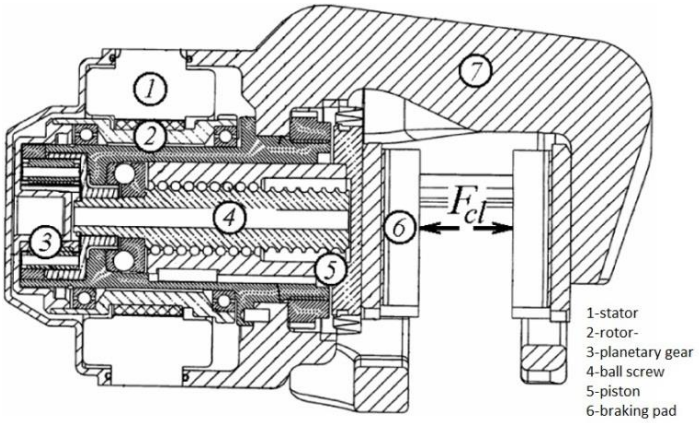

Figure 2-5 EMB components [2]

A lumped parameter model for the electromechanical brake system was developed in [25] and [26] by writing the torque equation for the electric model as:

$$T_m - T_L - T_F = J\ddot{\theta}_m \tag{2-10}$$

where T_m, T_L, T_F, J and $\ddot{\theta}m$ are motor torque, load torque, friction torque, lumped inertia and motor angular acceleration in order. By replacing motor torque and load torque relation in Equation (2-10), one may write:

$$i_q K_t - NF_{cl} - T_F = J\ddot{\theta}_m \tag{2-11}$$

where the i_q, K_t, N and F_{cl} present motor quadrature current, motor torque constant, gear ratio and clamping force in order. The clamping force has some nonlinear stiffness characteristics, which are measured by Line [26] experimentally in terms of piston position. Instead of experimental data, Jo et al. [27] used clamping force estimation between the clamping force (F_{cl}) and rotational displacement of the motor. Also, the clamping force can be presented by a characteristic curve for calipers which will be changed by temperature, environmental condition and aging during time. Therefore, it is important to calibrate the clamping force in real time. Hoseinizade et al. [28] presented a simple method to measure clamping force and calibrate the clamping force in real time. A brake torque compensator is developed in [29] to estimate and compensate for brake torque variation in EMB systems.

According to Lee et al. [30] the nonlinear friction torque can be varied based on electric motor's angular velocity as:

$$T_F = \begin{cases} D\dot{\theta}_m + (C + GF_{cl})\, sgn(\dot{\theta}) & |\dot{\theta}_m| > \varepsilon_0 \\ T_E & |\dot{\theta}_m| < \varepsilon_0 \;\&\; |T_E| < (T_s + G\,F_{cl}) \\ (\,T_s + GF_{cl})\, sgn(T_E) & otherwise \end{cases} \tag{2-12}$$

where D, C, G,T_s and T_E are the viscous friction coefficient, load independent Coulomb friction torque, load dependent friction torque coefficient, load independent static friction torque and the net external non-friction torque respectively. The ε_0 is a small zero velocity bound discussed in [31]. In the following pages, the work done on EMB mechanism is explained.

Line et al. [2] used gain scheduling, friction compensation, and feedback linearization to improve actuator nonlinearity, which is one of the main detriments of EMB systems. They also use a model predictive control to apply motor torque in a more effective manner.

Because there is no braking fluid in the system, EMB system advantages mentioned by the developers include its environmental friendliness and its improved safety by reduction of the risk of fire in case of accident. However, when it comes to applying EMB systems to real vehicles, there are some considerable safety issues since there is no direct connection between the driver and the braking

pads. Lee.Y and Lee,W [32] designed a hardware-in-loop system to test the safety and reliability of EMB systems. The presented design is flexible and the braking parameters can be changed easily.

Ahn et al. [33] investigated the control performance of EMB systems for Hybrid Electrical Vehicles (HEVs) in the presence of a regenerative braking system for different driving conditions. Kees et al. [34] conducted a comparison between EMB and Hydraulic Actuated Brakes (HAB) in regards to their performances in different ABS control conditions such as dry asphalt, wet asphalt, unpacked snow, and ice. In their study, they argued that, although the stopping distance will be shorter if EMB systems are combined with a proper control system, the reliability and safety of the system in case of failure needs further investigation.

2.3 Electronic Wedge Brake (EWB) System

The electronic wedge brake system is the most recent brake design developed in the category of brake-by-wire mechanism. The most beneficial advantage of EWB systems is their self-reinforcement ability which reduces the actuation force needed as the brake clamping force. Saving energy, providing high efficiency, faster response in comparison with hydraulic brake system which result in brake distance reduction are among the benefits of EWB systems [35]. On the other hand, EWB systems can cooperate with complimentary brake mechanism such as a regenerative brake system.

The wedge brakes are categorized into the upper-wedge brake and the lower-wedge brake as presented in Figure 2-6. In the upper-wedge category, the motor is connected to the upper wedge and moves it into the wedge. The applied force from the motor is in the same direction as the friction force created between braking pad and the disk. Therefore, the wedge is pulled in by the disk, which is the mechanism of the self-reinforcement, and less amount of force is needed for braking. On the contrary, in the lower-wedge-type, the motor applies force to the lower wedge of the EWB, so the motor's force is in the opposite direction of frictional force and the self-reinforcement ability is stopped. Also, a strong motor torque should be used to pull back the wedge in case of wedge jamming [36].

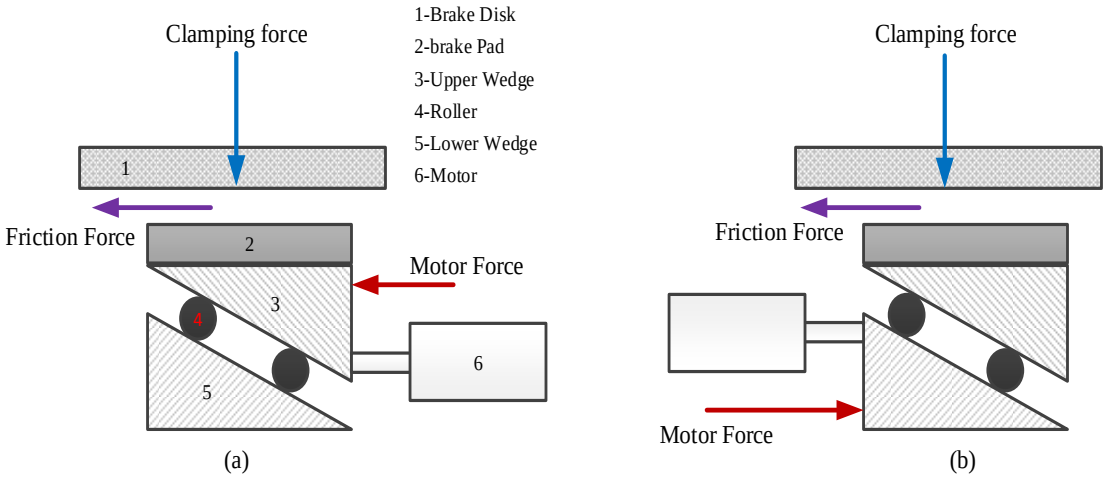

Figure 2-6 EWB mechanism; a) Upper-wedge- type. b) Lower-wedge type

The relationship between the clamping force and the actuator force can be found by writing the force equation for the wedge mechanism. As an example, forces applied on an upper-wedge-brake is shown in Figure 2-7. The frictional braking force is: [35]

$$F_b = \frac{\mu_p}{tan\,\beta - \mu_p} F_s \tag{2-13}$$

where F_b, μ_p, β and F_s are frictional brake force, friction coefficient of the pad, the wedge angle and screw force respectively. The screw is used to change the actuator's rotational motion into the wedge translational motion by

$$F_s = \frac{2\,\pi\,\eta_s\,\eta_{actuator}}{p_s} T_{actuator} \tag{2-14}$$

where the η_s, $\eta_{actuator}$ and p_s are screw efficiency, actuator efficiency and the screw pitch in order. According to Figure 2-7, the friction braking force can be calculated by the normal force (F_N) applied to the pad from the disk. Since the caliper is a flouting one, the clamping force is twice of the normal force:

$$\mu_p\,F_{cl} = \mu_p\,2\,F_N = 2\,F_b \tag{2-15}$$

Combining all the explained equations, the relation between the clamping force and the actuator torque will be found by:

$$F_{cl} = \frac{2}{tan\beta - \mu_p} \frac{2\,\pi\,\mu_s\,\mu_{actuator}}{p_s}\,T_{actuator} \tag{2-16}$$

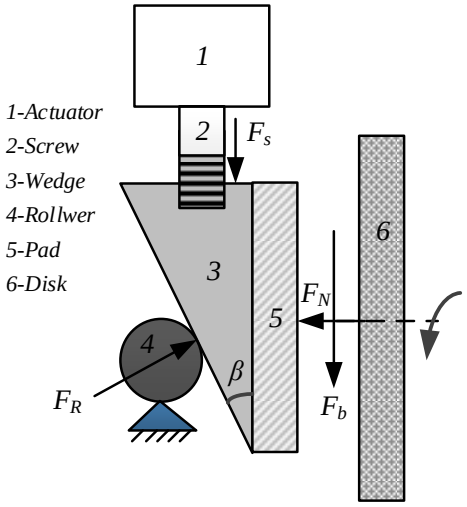

Figure 2-7 Forces applied on wedge of an EWB brake

The modeling of screw and wedge mechanism is explained in [36] in detail. The research done on EWB systems are explained briefly in the following.

Hartmann et al. [35] discussed the benefits of EWB over the conventional brake system. They presented a mathematical model between the motor force and the braking force in terms of wedge angle and friction coefficient, called the characteristic brake factor. The effect of changing the friction coefficient on the characteristic brake factor and braking force, which is needed after using the reinforcement ability, was explained in the paper. Some benefits of EWB systems such as improved reaction time compared with hydraulic brake systems, shortening the ABS cycle and reduced braking distance as well as easy maintenance, simple diagnosis and being ecological friendly due to not having hydraulic fluid are mentioned in this research.

The mathematical model of all the parts of EWB mechanism is found in [37]. The designed wedge brake has two electric motors that distribute loads and provide self-reinforcement in both directions. To validate the model, a prototype was created to show that the model accuracy for stability and control was fairly good. In continuation, Roberts et al. [38] performed a dynamometer test on the prototyped EWB to examine the wedge brake system behavior in realistic braking conditions such as continuous braking, and friction coefficient changes due to large temperature variation. The results

showed that the prototype can work well under these conditions along with having fast dynamics and low power consumption.

The EWB system has some nonlinearities due to friction coefficient changes, which was considered in the mechanical model presented by Balogh et al. [39]. The authors did some stability analysis by linearizing the system equation to get a LTI system.

Siemens VDO Automotive [40] designed a quarter car model to test the new generation of EWB system that they developed. This new model was the modification of the works done before in [35], [37] and [38]. The prototype was tested for conditions like braking disk imperfections and damages. Also, the anti-lock brake behavior of the presented wedge brake was examined by these real tests. Fox et al. [3] changed the Siemens VDO EWB system by eliminating one of the two electric motors used in previous models. This change makes the mechanism more practical due to cost reduction, as well as reduction in actuator weight and the control algorithm complexity. In terms of validation and examining the benefit of the new design, a vehicle test in low and high friction coefficient was performed. The research showed that having a 3D visualized software application for EWB allows the user to utilize analytical designs and to gain a good understanding about vehicle dynamic changes with design variations. Therefore, Semsey and Roberts [41] developed such a 3D visualized software application for the Siemens VDO wedge brake to study different braking conditions such as ABS, ESP, traction control, brake force distribution and brake behavior at low speed prior to doing real vehicle testing. The most important benefits of the software are reducing the test development processes and the costs.

Kim et al. [42] changed the general form of wedge brake mechanism by replacing the rollers with a cross-wedge mechanism as shown in Figure 2-8. They argued that using a lead screw and a worm gear instead of a roller evenly distributes the braking force. It was reported that finding the design's parameters optimized values can be helpful in reducing the brake volume. The performance of the cross-wedge system was examined throughout the ring and dynamometer tests.

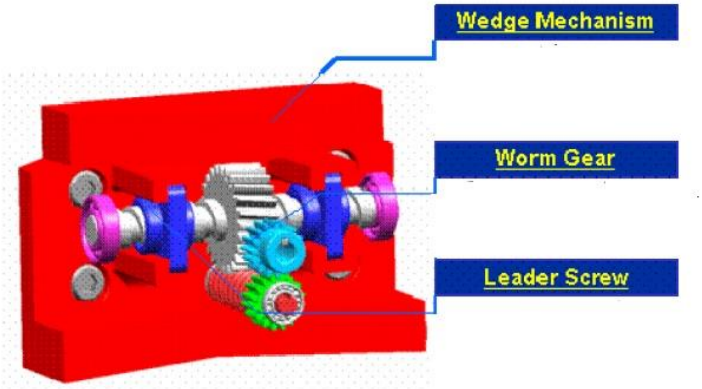

Figure 2-8 Cross wedge brake mechanism [42]

Jo et al. [36] designed an upper-wedge mechanism for EWB system where the braking process is done without the wedge jamming. Changing the friction coefficient has a direct impact in clamping force. Therefore, a push-pull control algorithm was introduced where the braking force only depends on the target clamping force despite of friction coefficient changes.

The wedge brake model in presence of the nonlinearities like backlash, friction in mechanical connections and clearance between the brake disk and pad was presented in [43]. It is known that proper clamping force control has a significant impact on brake mechanism performance. In this research, an algorithm for estimating mechanical parameters and clamping force was developed. The validity of the model was studied throughout Matlab/Simulink and examined via the prototype performance in a hardware-in-loop test.

2.4 Distributed Electro Hydraulic Brake System (DEHB)

The main idea of the DEHB was introduced by Delco Chassis in 1995 [44]. It is a brake mechanism that can be categorized between the EMB and EHB systems. DEHB is shown in Figure 2-9 [4]. The braking power is provided by an electric motor connected to a ball screw. The ball screw is responsible for converting the rotational motion to piston motion. The braking fluid inside the cylinder will be compressed and consequently generate required braking force. The most important advantage of this mechanism is that it provides differential braking that can be installed on each wheel separately. However, the brake fluid is not eliminated completely in this system as it is in the EMB; therefore, having a hydraulic back up brake is easy to arrange.

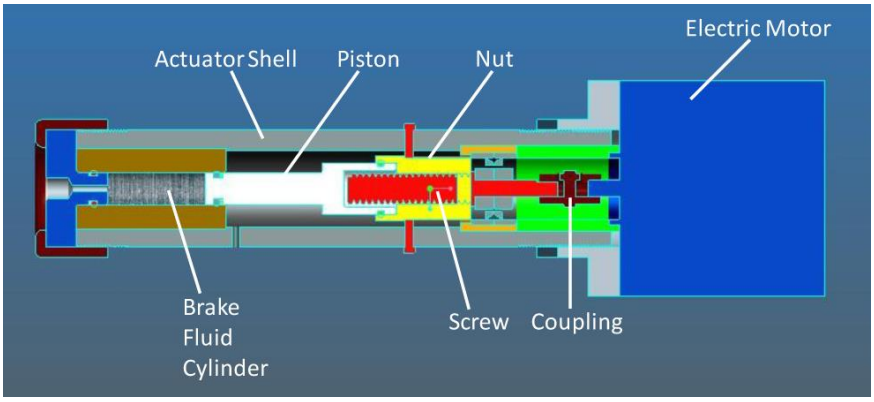

Figure 2-9 DEHB system [4]

Wang et al.[4] proposed two back up braking mechanisms for DEHB as shown in Figure 2-10. Figure 2-10 (a) shows the DEHB fail-safe strategy with the balance valve. This back up method is used when one of the installed brake mechanisms on the front or rear axle fails but the other one continues to work. In this case, the balance valve will open and let the functional brake mechanism generate the pressure of both wheels. On the other hand, as it can be seen in Figure 2-10 (b), four isolating valves connect the master cylinder to each wheel. When failure happens in both braking systems of one axle, the isolating valves connected to these wheels are opened and the driver directly generates the brake force.

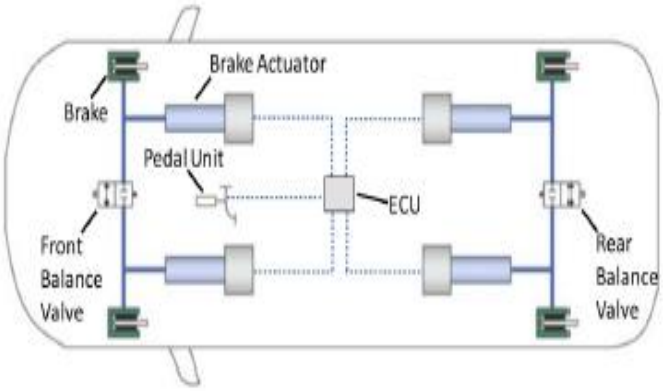

(a)

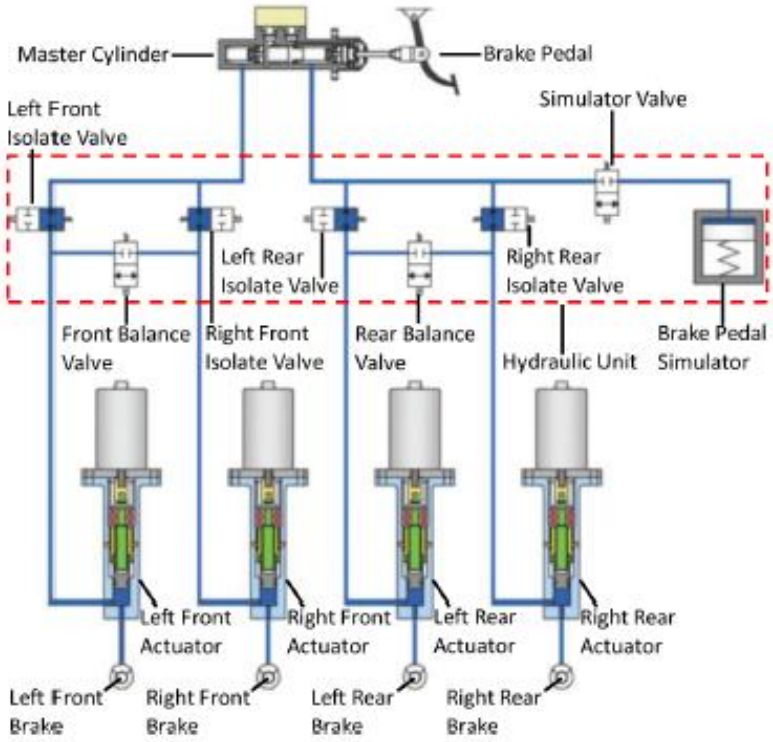

(b)

Figure 2-10 DEHB back up strategies; (a) fail safe with balance valve. (b) fail safe with balance valves and hydraulic back up [46]

A holding mechanism was added to the DEHB system by Wang et al. [45]. This is a mechanical mechanism used for long time continuous braking situations like stopping at a traffic light. The

reason for having this additional mechanism is because long term braking situations require a high level current; therefore, the motor temperature increases and harms the power supplier.

2.5 Summary

In this chapter, the researches conducted on the designs of different brake-by-wire systems were reviewed. EHB systems are a combination of hydraulic and electrical components. The braking flow to each wheel cylinder is controlled by a solenoid servo valve which provides the possibility of controlling each wheel pressure independent from the others. In EMB systems, no hydraulic fluid is used; the power provided by the electric motor will be changed to clamping force on the braking disk using a ball screw. The EWB is another brake-by-wire system with no hydraulic fluid, similar to the EMB. In wedge breaks, the motor's power transforms to the clamping force through a wedge mechanism, which provides a self-reinforcement ability showcasing an advantage of EWB systems. There is no hydraulic back up brake system for EMBs and EWBs that can be activated by the driver's force directly. To have a fail-safe mechanism, a separate electric motor and actuator must be added to the wheel. This issue creates some safety concerns when it comes to applying these systems as the primary brake system of a vehicle. One of the most recent innovative brake-by-wire systems is the DEHB, which is the combination of EHB and EMB mechanisms. In this system, the electric motor generates the needed power for braking, the power is transferred to a hydraulic piston motion by a ball screw. A benefit of this mechanism is having a hydraulic back up brake system that can be activated directly by the driver.

This thesis is an attempt to propose a novel brake-by-wire design that is self-contained, while also being compatible with active control systems and meeting the regulatory requirements for safe operation even in case of electronic systems failure.

Chapter 3
Brake System Design, Modelling

The proposed brake system can be categorized as an electrohydraulic brake system that consists of two activation sources. Activation sources include electromechanical activation and hydraulic activation. The electric source includes an electric motor that creates the necessary power for the brake system. The hydraulic section provides the necessary brake force that creates an appropriate braking torque for the vehicle when applied to the braking disk. This brake system is self-contained and can be installed on each wheel enabling differential braking for vehicle stability control.

3.1 Proposed Brake System Overview

Overall, the proposed brake system has three main subsystems; the electrical, mechanical and hydraulic as seen in Figure 3-1. The electrical system provides the required power for the brake mechanism. The mechanical subsystem converts the rotational movement created by the electrical block to the motion needed in the hydraulic module. The hydraulic subsystem uses the provided movement from the previous block to create a proper force behind the braking pads. Figure 3-6 presented in the following pages shows the general view of the proposed brake system with its components. In the following pages, the subsystems of the model are explained.

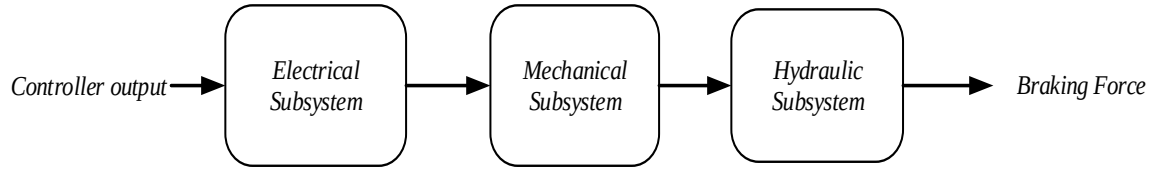

Figure 3-1 Proposed brake system overview

3.1.1 Electrical Subsystem

The electrical subsystem consists of an electric motor. This motor receives the incoming signal from the controller and creates a torque based on the braking conditions. The model used for the motor is a Permanent Magnet DC motor (PMDC). The schematic form of PMDC motor is shown in Figure 3-2.

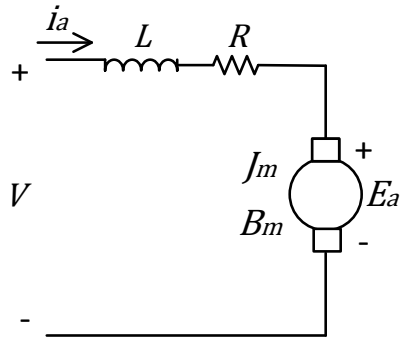

Figure 3-2 The schematic form of PMDC motor

$$T_m - T_L = J_m \dot{\omega}_m + B_m \omega_m \tag{3-1}$$

$$T_m = K_t i_a \tag{3-2}$$

where T_m and T_L are motor and external load torque. J_m, B_m, K_t, ω_m and i_a are motor inertia, motor damping coefficient, torque constant, motor speed and motor current respectively [46].

3.1.2 Mechanical Subsystem

The mechanical subsystem is responsible for changing the rotational movement to linear displacement for the hydraulic subsystem. It includes a gear mechanism and a transformer mechanism. The gear system amplifies the output torque of the motor to the necessary torque of the brake system.

As shown in the literature review, the typical mechanical components, to change rotational motion to linear motion, include a ball screw used in the EMB system or in EWB. The installed ball screw in these mechanism can provide fixed amplification as it change the motion from rotational to tangential. Figure 3-3 shows the torque-speed characteristic of a PMDC motor. As it can be seen, the speed and torque have inverse relation. The higher the motor speed is, the lower the available amount of torque for the system.

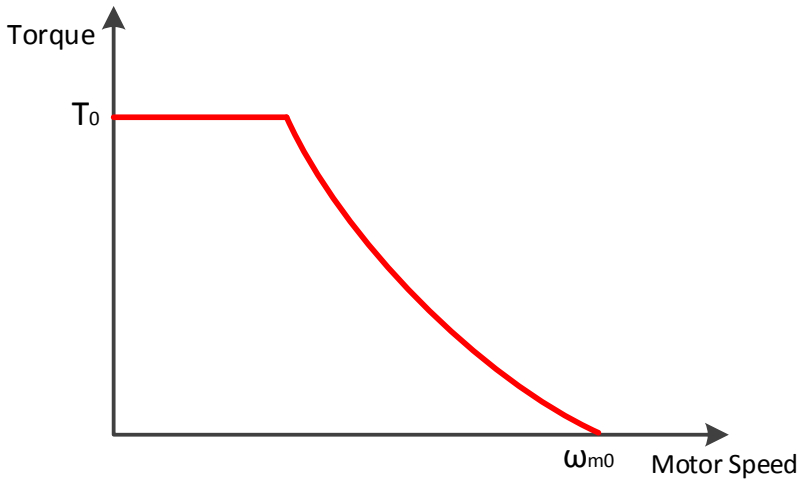

Figure 3-3 PMDC's motor torque speed characteristic

Therefore, having a mechanism that can provide a variable amplification is beneficial due to torque-speed characteristic of PMDC motor. The proposed mechanical component for variable transfer value in this research is a cam mechanism. The displacement of contacted follower to the cam profile determines the amount of amplification during motion transfer. The cam profile can be designed to create a large amplification ratio when the required braking pressure in the system changes, and to generate less amplification when the created pressure in the system is close to the target level. Also, the cam and follower mechanism is more robust compared to the ball screw mechanism in case of any malfunction in the system such as rollers breakage. Figure 3-4 shows the mechanical subsystem of Figure 3-1.

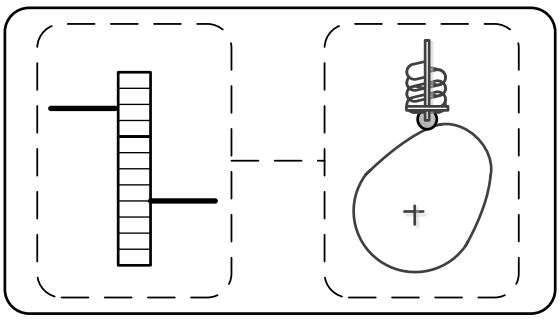

Mechanical Subsystem

Figure 3-4 Schematic form of subsection of mechanical subsystem

The detailed description of the mechanical subsystem is discussed in the system formulation and cam optimization section.

3.1.3 Hydraulic Subsystem

The hydraulic subsystem of the proposed brake system includes the actuator cylinder connected to the cam mechanism, the wheel cylinder connected to the braking pads, and the switching valve between these two cylinders for switching between the primary and secondary brake[1] systems as it is shown in Figure 3-5.

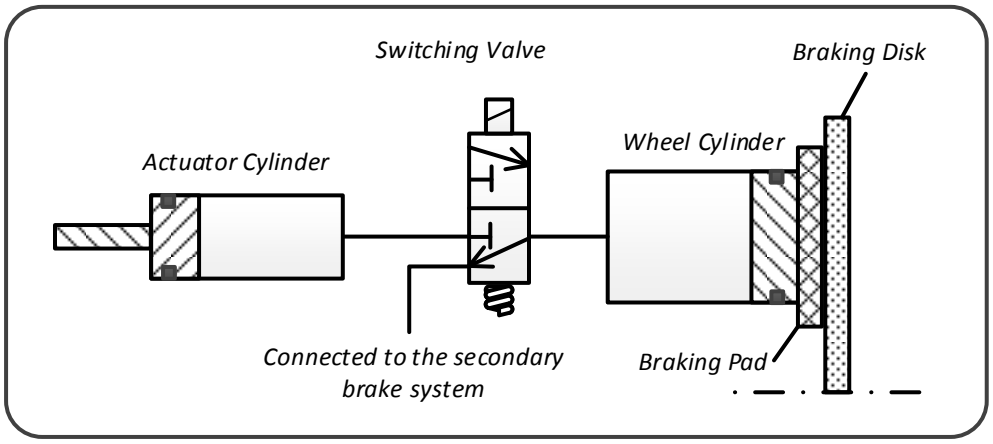

Figure 3-5 Hydraulic subsystem

In case of failure in the primary break system, the 3/2 solenoid activation valve will switch to its ideal position and let the wheel cylinder connect to the secondary brake system, which runs manually by the driver's command.

Figure 3-6 shows the components of the proposed brake system, which is the combination of the explained subsystems.

[1] The secondary brake system is explained in Appendix A

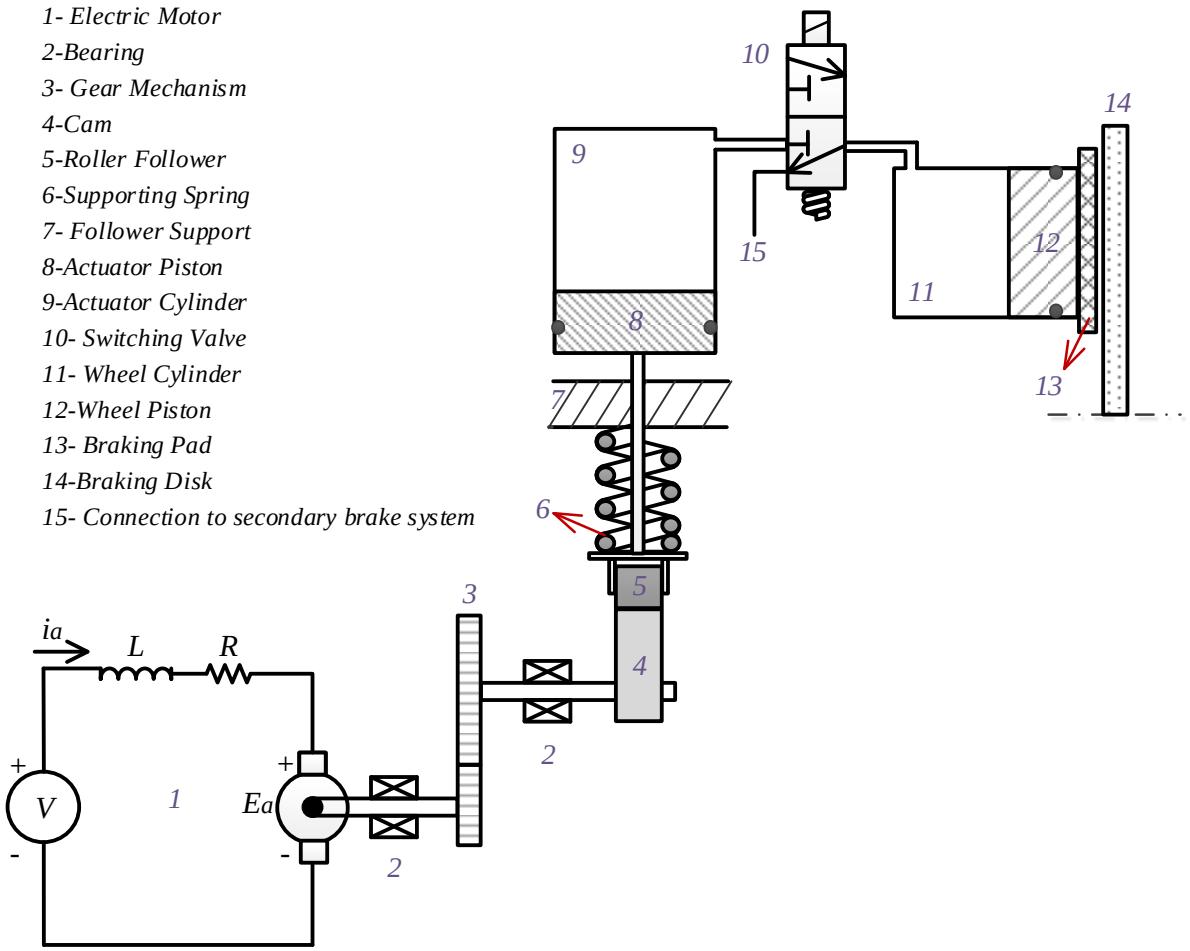

Figure 3-6 Components of design brake system

One of the advantages of the proposed brake system as mentioned before is that it can be installed on each wheel and controlled individually by the brake or vehicle controller.

Figure 3-7 shows the combination of the cam-actuated and fail-safe brake mechanisms. In case of malfunction in cam mechanism the ECU stop sending the activation signal for switching valve. The spring used in valve mechanism force it to change to its ideal position. In that position the driver will be connected to the braking pad through the fail-safe brake mechanism.

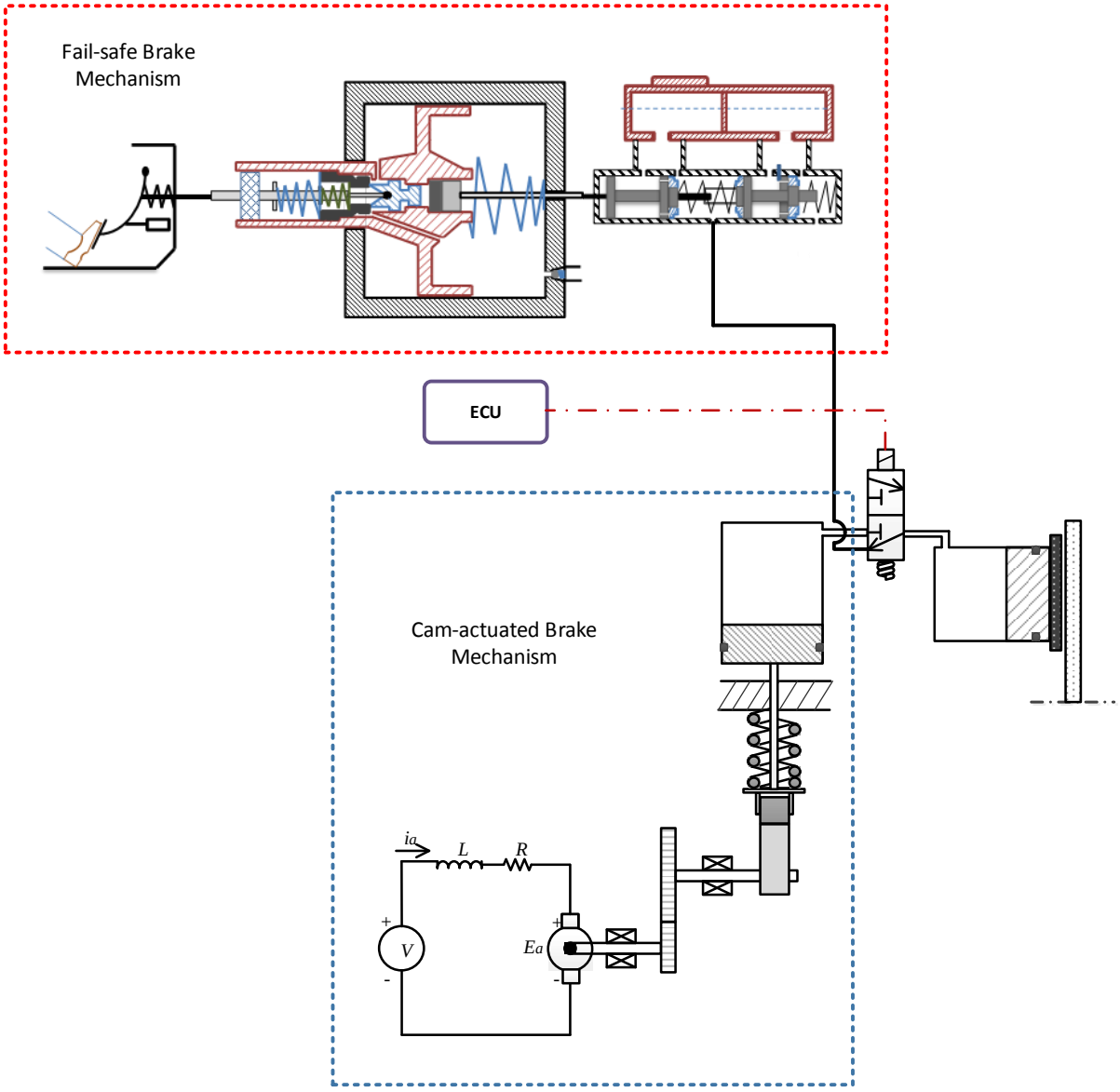

Figure 3-7 The combination of cam-actuated and the fail-safe brake mechanisms

3.2 Modelling of Proposed Brake System

In the previous section, the general form of the brake system was discussed. In this section, the mathematical formulation of the system is presented first. This is followed by an explanation of the lump model of proposed brake system, which is used later for cam optimization.

The governing equations for the electric motor were introduced in electrical subsection (Section 3.1.1). In the following sections, the other two subsystems are presented.

3.2.1 Mechanical Subsystem Formulation

As it was explained in Section 3.1.2 and shown in Figure 3-4, the mechanical subsystem includes two parts: the gear system and the cam mechanism. The gear system amplifies the output torque of the electric motor. The relation between the input and output torque of the gear system is:

$$T_{out} = G_R . T_{in} = G_R . T_m \tag{3-3}$$

where G_R is the gear ratio and T_{in} is the input torque which is equal to motor torque*(T_m)*. If it is assumed that the shaft connecting the output of the gear system and the cam mechanism is rigid, then the T_{out} of the gear system is equal to the cam's input torque.

The eccentric cam mechanism used in the proposed brake system is shown in Figure 3-8.

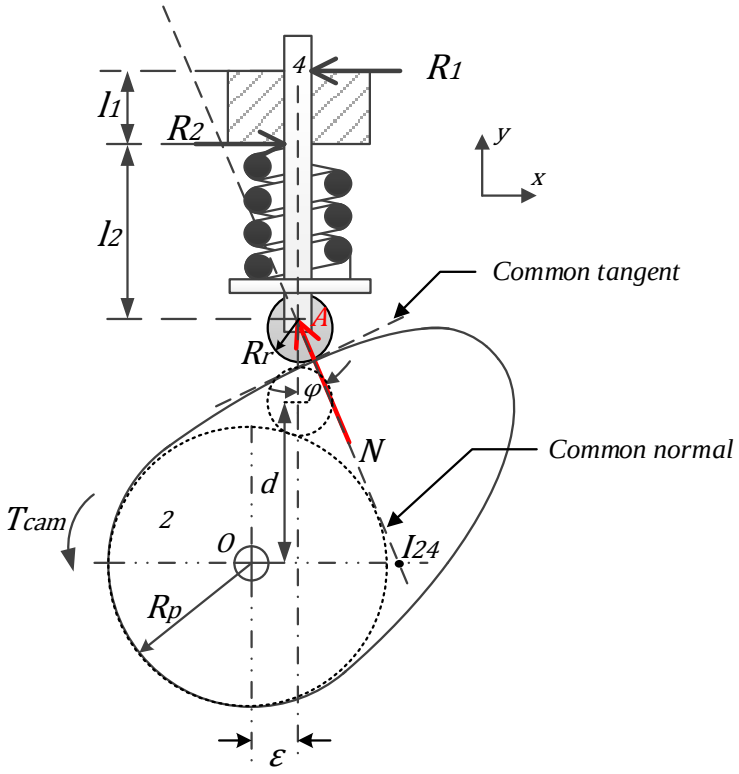

Figure 3-8 Cam mechanism

N is the contact force between the cam and the follower, which is in the direction of the common normal. The common normal direction can be indicated by pressure angle *(φ)* during the motion. The pressure angle is the angle between the common normal and the follower's direction of motion. The contact force *(N)* has two components in *x* and *y* direction. Its *y* direction's component, called F_{ycam}, pushes the follower upward or downward, compresses the oil inside the actuator cylinder, and changes the pressure inside the actuator cylinder. The *x* component of *N* is in equilibrium with the follower support reactions *(R_1* and *R_2)*. If it is assumed that the follower roller radius compared to the cam base circle radius is small, then it can be considered that applying the contact force on the follower roller center or on the contact point does not cause that much difference in calculation of contact force in the *x* direction. To find the relation between the contact force and the cam input torque, a free body diagram of the cam is shown in Figure 3-9.

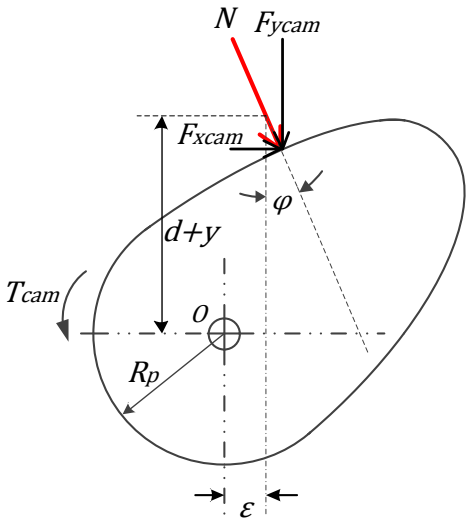

Figure 3-9 Free body diagram of cam

F_{xcam} and F_{ycam} can be defined by contact *(N)* as:

$$F_{xcam} = N \sin\varphi \tag{3-4}$$

$$F_{ycam} = N \cos\varphi \tag{3-5}$$

By writing the moment equilibrium equation for point *O* these forces will be found:

$$\sum M_o = 0$$
$$-F_{ycam}\varepsilon - F_{xcam}(d+y) + T_{cam} = 0 \tag{3-6}$$

where R_p, R_r, ε and y are cam base circle radius, follower roller radius, eccentricity of the follower and displacement of the follower respectively. T_{cam} is the input torque of the cam which is the output torque of the gear system.

By inserting Equations (3-4) and (3-5) in Equation (3-6) the contact force is calculated.

$$N\varepsilon\cos\varphi + N\left(R_p + R_r + y\right)\sin\varphi = T_{cam} \tag{3-7}$$

$$N = \frac{G_R\, T_m}{\varepsilon\cos\varphi + (d+y)\sin\varphi} \tag{3-8}$$

$$F_{ycam} = N\cos\varphi = \frac{\cos\varphi\, T_{cam}}{\varepsilon\cos\varphi + (d+y)\sin\varphi} = \frac{T_{cam}}{\varepsilon + (d+y)\tan\varphi} \tag{3-9}$$

The follower support reactions *(R_1* and *R_2)* shown in Figure 3-8 is calculated by studying the free body diagram of the follower (Figure 3-10) and writing the force equilibrium in *x* direction and momentum equilibrium for point *A*.

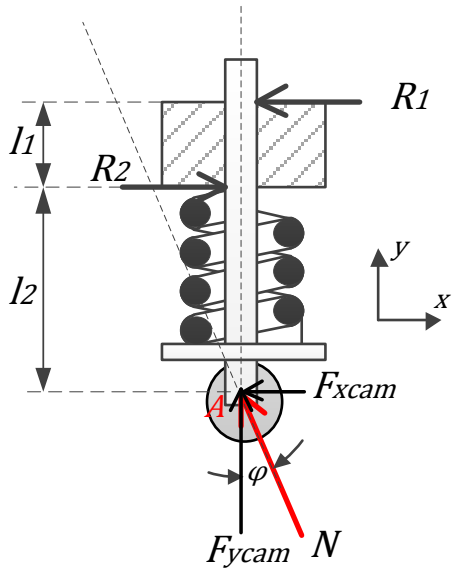

Figure 3-10 Follower free body diagram

$$\sum M_A = 0$$
$$R_1(l_1 + l_2) - R_2 l_2 = 0 \quad (3\text{-}10)$$

$$\sum F_x = 0$$
$$R_1 + F_{xcam} - R_2 = 0 \quad (3\text{-}11)$$

By solving Equation (3-10) and (3-11) at the same time, the reaction forces are calculated by:

$$R_1 = \left(\frac{l_1}{l_2}\sin\varphi\right)N \quad (3\text{-}12)$$

$$R_2 = \left(\frac{l_1 + l_2}{l_2}\sin\varphi\right)N \quad (3\text{-}13)$$

However, it should be mentioned that the vertical component of the reaction force, which is in the direction of the follower, has the main role in changing pressure inside the actuator cylinder. Its horizontal components cause sliding friction between the follower and its support; therefore, it is better to reduce the horizontal component of the friction force as much as possible. The pressure

angle can regulate this friction force and it varies when the cam rotates. Its maximum value is defined by considering cam performance and considering the concept of not having mechanical problems during cam rotation. As it will be explained in optimization section, maximum pressure angle is the most important constrain for finding and optimizing cam profile.

By considering the geometry of the cam shown in Figure 3-8, the pressure angle can be found. The I_{24} is the instant center of rotation between the cam and the follower. The cam and the follower velocity are the same at this point and it can be written as:

$$v_{I24} = \dot{y} = \omega_{cam}\overline{OI_{24}} \tag{3-14}$$

where $\dot{y}$ is the follower translational velocity and ω_{cam} is the angular velocity of the cam.

Using the chain rule for follower velocity leads to: [47]

$$\dot{y} = \frac{dy}{dt} = \frac{dy}{d\theta} \cdot \frac{d\theta}{dt} = y'\omega_{cam} \tag{3-15}$$

Comparing Equation (3-14) and (3-15), the distance between cam center *(O)* and instant center of rotation *(I_{24})* is equal to y', which is the first derivative of the cam profile with respect to the cam rotational angle as shown in Equation (3-15). The distance $\overline{OI_{24}}$ has a relation with geometrical parameters of the cam *(R_p,R_r,ε)* and the pressure angle *(φ)*.

$$\overline{OI_{24}} = \varepsilon + (d + y)\tan\varphi \tag{3-16}$$

Replacing $\overline{OI_{24}}$ by $y'$and solving Equation (3-16) provides the expression for calculating pressure angle as:

$$\varphi = \tan^{-1}\left(\frac{y' - \varepsilon}{d + y}\right) \tag{3-17}$$

where *d* is shown on Figure 3-8 and is calculated by: [48]

$$d = \sqrt{\left(R_p + R_r\right)^2 - \varepsilon^2} \tag{3-18}$$

3.2.2 Hydraulic Subsystem Formulation

The hydraulic subsystem can be modeled by a mass, spring and damper system shown in Figure 3-11. M_{act} and M_{wc} indicate the masses of actuator and wheel cylinder's piston. The existing oil in these two cylinders has a stiffness of K_{oil} and the sealing between the cylinders piston and wall has

damping coefficient shown by B_s. Also, the braking pad stiffness is indicated by K_{pad}. F is the activation force that comes from the mechanical subsystem.

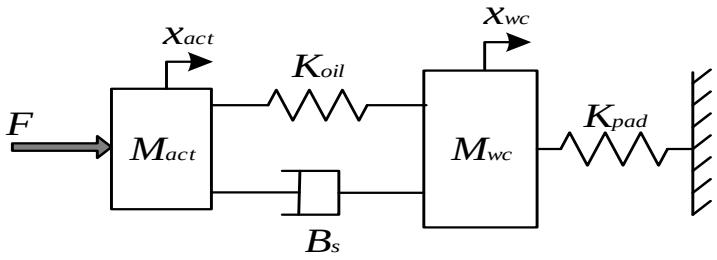

Figure 3-11 Mass, spring and damper model of hydraulic subsystem

3.2.2.1 Hydraulic Subsystem Formulation

Figure 3-12 shows the free body diagram of actuator's and wheel's cylinder mass. The dynamic equation of each mass is presented as follows:

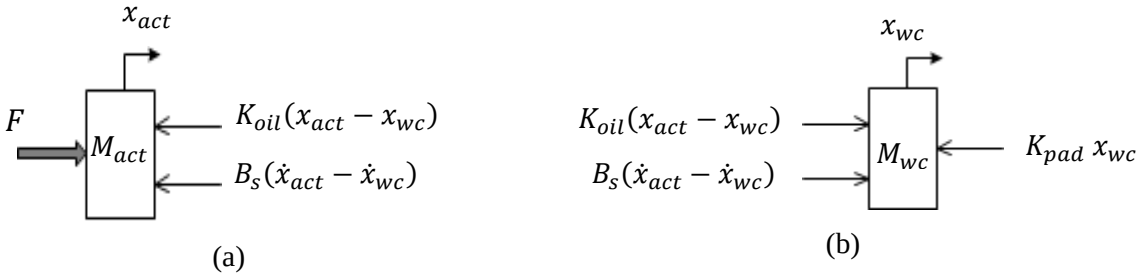

Figure 3-12 Free body diagram of (a) actuator cylinder's mass; (b) wheel cylinder's mass

$$F - K_{oil}x_{act} - B_s\dot{x}_{act} + K_{oil}x_{wc} + B_s\dot{x}_{wc} = M_{act}\ddot{x}_{act} \tag{3-19}$$

$$-(K_{oil} + K_{pad})\, x_{wc} + B_s\dot{x}_{wc} + K_{oil}x_{act} + B_s\dot{x}_{act} = M_{wc}\ddot{x}_{wc} \tag{3-20}$$

where K_{pad} is:

$$K_{pad} = \frac{E_{pad}\, A_{pad}}{t_{pad}} \tag{3-21}$$

The state space form of the system is:

$$\dot{x} = Ax + Bu \tag{3-22}$$

where matrices *x, A, B* and *u* are:

$$x = \begin{bmatrix} x_{act} \\ \dot{x}_{act} \\ x_{wc} \\ \dot{x}_{wc} \end{bmatrix}, \quad A = \begin{bmatrix} 0 & 1 & 0 & 0 \\ -\frac{K_{oil}}{M_{act}} & -\frac{B_s}{M_{act}} & \frac{K_{oil}}{M_{act}} & \frac{B_s}{M_{act}} \\ 0 & 0 & 0 & 1 \\ \frac{K_{oil}}{M_{wc}} & \frac{B_s}{M_{wc}} & -\frac{K_{oil}+K_{pad}}{M_{wc}} & \frac{B_s}{M_{wc}} \end{bmatrix}, \quad B = \begin{bmatrix} 0 \\ \frac{1}{M_{act}} \\ 0 \\ 0 \end{bmatrix}, \quad u = F \tag{3-23}$$

3.2.2.2 Frequency Analysis

The numerical values of parameters in Equation (3-23) are shown in Table 3-1. These parameters were gathered from the literatures and some engineering assumptions.

Table 3-1 Numericalvalues of hydraulic system parameters

Property	Value	Unit
K_{oil}	54.8	KN/m
B_s	0.3×10^{-3}	Nm/s
M_{act}	0.1	Kg
M_{wc}	0.3	Kg
K_{pad}	9.75×10^{6}	KN/m

The frequencies of the system are calculated by solving an eigenvalue problem with MATLAB for the system in (3-23). The eigenvalues of matrix *A* is presented in Table 3-2.

Table 3-2 Matrix *A* eigenvalues

Property	Value
$\boldsymbol{\lambda_1}$	$-1.33 \times 10^{-2} \pm 1.803 \times 10^{5} j$
$\boldsymbol{\lambda_2}$	$-4 \times 10^{-2} \pm 7.402 \times 10^{2} j$

System eigenvalues are complex number in the form: $\lambda_i = \alpha_i + j\,\beta_i$, where $\alpha_i = Re\,\lambda_i$ and $\beta_i = \mathrm{Im}\,\lambda_i$. The frequencies of the undamped system are calculated by finding the square root of the imaginary part of eigenvalues as $\omega_i = \sqrt{\lambda_i}$. Therefore, these frequencies are: $\omega_1 \cong 27.2\,Hz$ and $\omega_2 \cong 424\,Hz$. The second natural frequency which belongs to the wheel cylinder's mass is quite

large compared to the first natural frequency. This higher value for second natural frequency is due to high stiffness of the braking pad. This means that the wheel cylinder's mass has small displacement compared to actuator's mass. Therefore, it is possible to simplify the system and reduce its order. As such, the mass, spring, and damper model of Figure 3-11 can be modified to the following model.

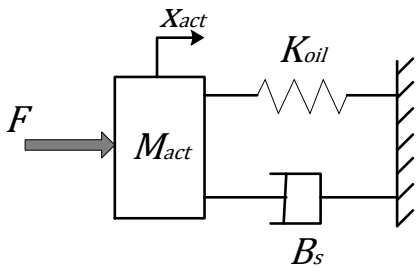

Figure 3-13 Reduced order mass, spring and damper model of hydraulic subsystem

The state space form of the reduced system can be discussed as:

$$x = \begin{bmatrix} x_{act} \\ \dot{x}_{act} \end{bmatrix}, \qquad A = \begin{bmatrix} 0 & 1 \\ -\frac{K_{oil}}{M_{act}} & -\frac{B_s}{M_{act}} \end{bmatrix}, \quad B = \begin{bmatrix} 0 \\ \frac{1}{M_{act}} \end{bmatrix}, \qquad u = F \tag{3-24}$$

The mechanical force, *(F)*, shown in Figure 3-13 is the total external forced applied to the actuator cylinder. By using the reduced order model and considering Figure 3-14, the dynamic equation of motion for the cylinder mass can be found based on the follower force (F_{ycam}).

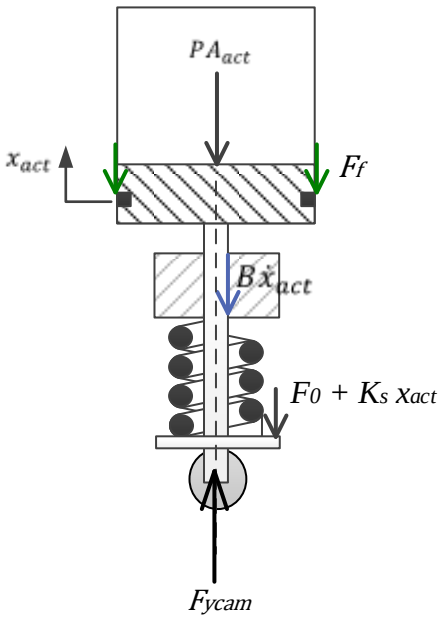

Figure 3-14 Force equilibrium for actuator cylinder

The duty of the preloaded spring used between follower support and follower head is providing contact between cam and follower all the time during cam rotation. By writing the force equilibrium, the dynamic equation of motion of the actuator piston will be found.

$$M_{act}\ddot{x}_{act} + B\dot{x}_{act} + F_0 + K_s x_{act} + PA_{act} + F_f = F_{ycam} \tag{3-25}$$

M_{act}, B, K_s and A_{act} indicate piston mass, sealing damping coefficient, follower support's spring stiffness and piston area respectively. Also, F_0, F_f and P are the follower support's preload force, friction force and pressure inside the actuator cylinder in this order.

The produced pressure inside the actuator cylinder is related to the actuator piston displacement through the compressibility of the oil [49].

$$P = \frac{\beta \Delta V}{V_0} = \frac{\beta\, A_{act}\, x_{act}}{V_0} \tag{3-26}$$

β and V_0 are effective Bulk modulus[2] of the oil and initial volume of the actuator cylinder. By inserting Equation (3-26) in (3-25) the dynamic equation will be:

[2] The calculation related to find the effective bulk modulus is presented in Appendix B

$$M_{act}\ddot{x}_{act} + B\dot{x}_{act} + F_0 + \left(\frac{\beta A_{act}^2}{V_0} + K_s\right)x_{act} + F_f = F_{ycam} \tag{3-27}$$

The friction force between the O-ring used for sealing and the cylinder wall is calculated based on the coulomb friction law as follows:

$$F_f = \begin{cases} F_k\, sgn(\dot{x}_{act}), & \dot{x}_{act} > 0 \\ sgn(F_{ext})\min(|F_{ext}|, F_s), & \dot{x}_{act} = 0 \end{cases} \tag{3-28}$$

where F_k ,F_s and F_{ext} are the sliding friction force, the static friction force and the applied external force. The sliding and static friction forces are defined by:

$$F_k = \mu_k F_N \tag{3-29}$$

$$F_s = \mu_s F_N \tag{3-30}$$

where F_N is the normal force per area, which is applied to the wall of cylinder by the sealing of O-ring. To find this normal force, the deformation of the O-ring inside the actuator piston head's groove and the produced contact stresses between O-ring and the cylinder wall should be consider as it is shown in Figure 3-15.

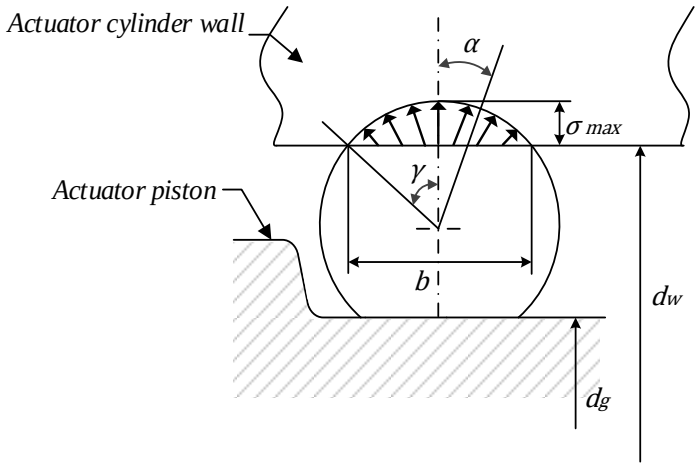

Figure 3-15 O-ring deformation inside the groove

As it is shown in Figure 3-15, the contact stress at each point depends on the cosine of the angle of contact point with the vertical axis by: $\sigma = \sigma_{max}\cos\alpha$. Since the O-ring works in the elastic section of stress and strain diagram, Hooke's law is applicable for calculating the stress according to [50], so:

$$\sigma_{max} = E\frac{\delta}{r} = E\left(1 - \frac{d_w - d_g}{4r}\right) \tag{3-31}$$

where E, δ, d_w, d_g and r are the O-ring material elasticity modulus, the O-ring radial deformation, the actuator cylinder wall diameter, the piston groove diameter and O-ring radius respectively.

The normal force per area applied to the cylinder wall will be the integral of contact force on the area of application, which is:

$$F_N = \int_{-\gamma}^{\gamma} \sigma \cos\alpha \, db = \int_{-\gamma}^{\gamma} (\sigma_{max} \cos\alpha)\cos\alpha \left(\frac{r d\alpha}{\cos\alpha}\right) = 2\,\sigma_{max} r \sin\gamma \tag{3-32}$$

where *db* is the width of contact force.

Based on the geometry of the O-ring deformation shown in Figure 3-15, it can be found that:

$$\sin\gamma = \frac{b}{2r} = \sqrt{1 - \frac{(d_w - d_g)^2}{16r^2}} \tag{3-33}$$

By replacing equation (3-33) in (3-32) and considering the whole area of contact between the O-ring and the cylinder wall, the final equation of normal force can be calculated

$$F_N = 2\pi d_w r E\left(1 - \frac{d_w - d_g}{4r}\right)\sqrt{1 - \frac{(d_w - d_g)^2}{16r^2}} \tag{3-34}$$

3.3 Lump Model of the Brake System

As it was mentioned before, the gear mechanism acts as an amplifier and no stiffness is considered for the gear's teeth. The connecting shaft between the motor/gear and gear/cam was assumed to be rigid without any stiffness. These two assumptions lead to a mathematical relation between the existing masses (J_m, J_{g1}, J_{g2}, J_{cam} and M_{act}) in the brake system. Therefore, it is possible to lump the masses and the damping of the system to one equivalent mass and an equivalent damping to get the dynamic equation of the whole brake system. By using the kinetic energy method the equivalent values will be found.

$$T = \frac{1}{2}J_m\omega_m^2 + \frac{1}{2}J_{g_1}\omega_{g1}^2 + \frac{1}{2}J_{g2}\omega_{g2}^2 + \frac{1}{2}J_{cam}\omega_{cam}^2 + \frac{1}{2}M_{act}\dot{x}_{act}^2 = \frac{1}{2}M_{eq}\dot{x}_{act}^2 \tag{3-35}$$

where J_{g1}, J_{g2} and J_{cam} are first and second gear inertia and cam inertia in order.

According to Equation (3-15), cam angular velocity is $\omega_{cam} = \frac{\dot{x}_{act}}{y'}$. It is also known that the angular velocity of the first gear is the same as ω_m and the second gear rotates with the same velocity as the cam. On the other hand, the rotation of the electric motor and the cam are related to each other by a gear mechanism amplification as:

$$\omega_m = G_R\, \omega_{cam} = \frac{G_R}{y'}\, \dot{x}_{act} \tag{3-36}$$

By substituting Equation (3-36) into (3-35) the equivalent mass is:

$$M_{eq} = \frac{(J_m + J_{g1})G_R^2 + J_{g2} + J_{cam}}{y'^2} + M_{act} \tag{3-37}$$

Using potential energy method and considering $\dot{\omega}_m = \frac{G_R}{y'}\, \dot{x}_{act}$ leads to the calculation of the equivalent damping by the following equation.

$$B_{eq} = B_m \left(\frac{G_R}{y'}\right)^2 + B \tag{3-38}$$

The dynamic equation of the lump brake system will be found by combining equations of (3-2), (3-3), (3-9) and (3-27).

$$M_{eq}\ddot{x}_{act} + B_{eq}\dot{x}_{act} + \left(\frac{\beta A_{act}^2}{V_0} + K_s\right) x_{act} + F_0 + F_f = \left(\frac{G_R\, K_t}{\varepsilon + (R_p + R_r + y)\tan\varphi}\right) i \tag{3-39}$$

This above equation shows the relation between the motor current as the input of the system and the actuator displacement. According to Equation (3-26), the actuator displacement can be converted to the pressure applied to the braking disk.

3.4 Summary

In this chapter, the proposed cam actuated brake system was discussed and its model considering all of the system's parameters was derived. The design advantages over the existing lead screw brake actuators were also discussed. In the next Chapter, the main design parameters including gear ratio, cam base circle radius, follower roller radius, and cam eccentricity will be introduced and optimized to maximize the performance of the proposed brake-by-wire mechanism.

Chapter 4
Design Optimization

In the previous chapter, the proposed brake system was modelled and formulated. The parameters of the system which can be optimized to improve system response are the gear ratio, cam design parameters *(R_p, R_r, ε)*, and the cam profile *($\frac{dy}{d\theta}$)*. These parameters can significantly affect the system response, therefore they should be properly optimized to improve system performance. The optimization algorithm is based on a multi-layer optimization method. As it was explained in Section 3.2.1, the first derivative of the follower displacement with respect to the cam angle, y', can be used to find the cam profile when it is integrated with respect to the cam angle. Determining the cam profile depends on cam design parameters which are presented in Equations (3-16) to (3-18) and the gear ratio according to Equation (3-39). Therefore, the upper layer of the optimization is related to finding R_p, R_r, ε and G_R, and the lower level calculates y', which is embedded inside the upper layer. The optimization method used for the first layer is a Genetic Algorithm (GA), and a direct search method is applied to the insider layer in the optimization process. Figure 4-1 shows the flow chart of the proposed optimization process.

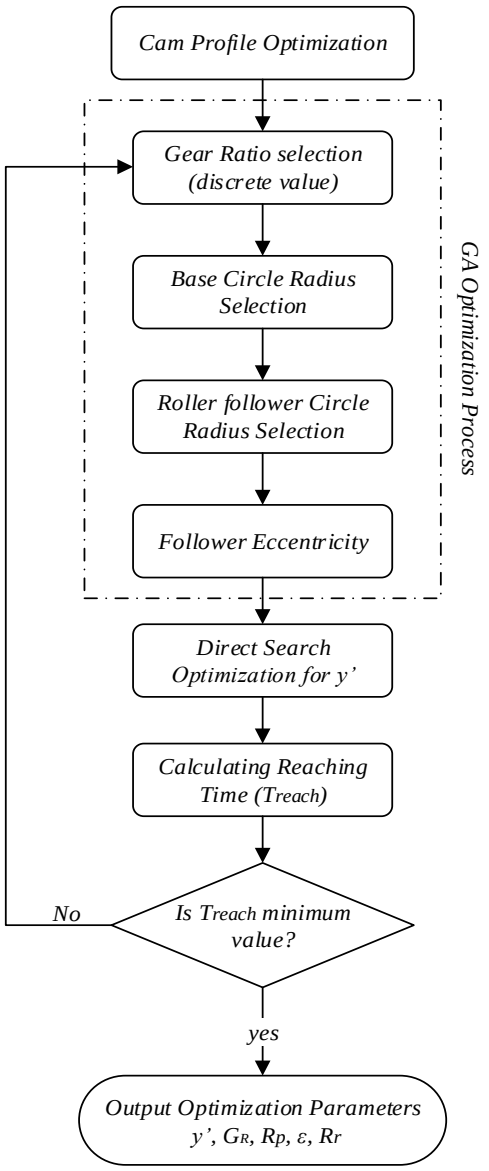

Figure 4-1 Optimization flowchart

4.1 Optimization Constraints Definition

In the following sections, the constraints of the optimization problem are discussed.

4.1.1 Pressure Angle Constraint

As it was mentioned in Chapter 3, the pressure angle is the most important constraint of the optimization. According to the hand book of cam design and manufacturing [47], the maximum value of the pressure angle for a cam mechanism with a translating follower is $\pm 30°$. If the pressure angle

increases above this limit, the cam support loads in *x* direction, R_1 and R_2 shown in Figure 3-8 increases too much and it may cause jamming between the follower and its support's wall. Furthermore, it can be seen in Figure 3-8 that the pressure angle will be zero when the cam reaches its top position, and it will have negative value as the follower starts to return. Returning of the follower means that the pressure inside the actuator cylinder decreases. Therefore, zero pressure angle can be defined as a critical value for the brake system. To be in a safe zone, a minimum angle of 5° is added to the pressure angle constraint. So, the first constraint is defined by

$$C_1: 5^{\circ} \leq \varphi \leq 30^{\circ} \tag{4-1}$$

4.1.2 Cam Design Parameters Relation Constraint

In addition to the pressure angle, there are some other geometrical and mathematical constraints for the cam design that need to be considered in the optimization process. One of these conditions can be extracted from Equation (3-18), which calculates the distant between the cam base circle center and the follower roller center, *d*, as indicated in Figure 3-8. The value under the square root of Equation (3-18) should be positive. Therefore the second constraint will be:

$$C_2: R_p + R_r \geq \varepsilon \tag{4-2}$$

Moreover, according to reference [48], two other conditions should be added to the system to ensure that the cam and the follower are easy to assemble. These constraints are:

$$C_3: R_r \leq \varepsilon \tag{4-3}$$

$$C_4: \varepsilon \leq R_p \tag{4-4}$$

4.1.3 Parameter Selection Boundary Conditions Constraints

To obtain reasonable values for the optimized parameters, some lower and upper bounds need to be imposed on the design parameters as:

$$C_5: R_p^{lb} \leq R_p \leq R_p^{ub} \tag{4-5}$$

$$C_6: R_r^{lb} \leq R_r \leq R_r^{ub} \tag{4-6}$$

$$C_7: \varepsilon^{lb} \leq \varepsilon \leq \varepsilon^{ub} \tag{4-7}$$

$$C_8: y'^{lb} \leq y' \leq y'^{ub} \tag{4-8}$$

The last boundary constraint is defined on the gear ratio. The difference between this boundary condition and others is that it is assumed that the gear ratio cannot be chosen in a continuous form. A set of predefined integers is used in the selection of the gear ratio as

$$C_9\colon\ G_R \in \left\{G_{R_1}, G_{R_2}, \dots, G_{R_i} \middle| G_{R_i} > 0\right\} \tag{4-9}$$

The boundary values used for the described constraints are summarized in Table 4-1.

Table 4-1 Boundary conditions values

Property	Value	Unit
R_p^{lb}	8	mm
R_p^{ub}	30	mm
R_r^{lb}	4	mm
R_r^{ub}	10	mm
ε^{lb}	0	mm
ε^{ub}	10	mm
y'^{lb}	4e-3	-
y'^{ub}	0.1	-
G_R	{7,10,15,20,25}	-

It is important for a brake mechanism to provide the braking pressure/force for a vehicle in the shortest possible time in the presence of a system's mechanical limitations. Therefore, the goal of optimization in this study is to minimize the response time for the actuator's cylinder pressure changing from zero to a desired pressure value. This time duration will be called the *reaching time* and will be denoted by T_{reach} hereafter. To solve the optimization problem the dynamic system governed by Equation (3-39) is considered, where the x_{act} and its first and second derivatives are replaced by the expression presented for the pressure in Equation (3-26). Therefore, the dynamic system is:

$$M_{eq}\ddot{P} + B_{eq}\dot{P} + \left(\frac{\beta A_{act}^2}{V_0} + K_s\right)P + \left(\frac{\beta A_{act}}{V_0}\right)(F_0 + F_f) = \left(\frac{\beta A_{act}}{V_0}\right)\left(\frac{G_R\, K_t}{\varepsilon + (d+y)\tan\varphi}\right) i \quad (4\text{-}10)$$

Then the optimization problem is defined as:

$$Optimization\ Problem: \min T_{reach}|_{y', G_R, R_p, \varepsilon, R_r} \quad (4\text{-}11)$$

where T_{reach} denotes the first time the solution of ordinary differential equation in (4-10) hits the desired value pressure and $y', G_R, R_p, \varepsilon$ and R_r are the designed paramaters and the constrains are C_1 to C_9 as discussed in Equations (4-1) to (4-9).

It should be mentioned that setting a fixed predefined pressure as the desired value of solving optimization problem function will give out a set of design parameters that provide the best and most optimized answer for that specific pressure. However, in braking, the necessary braking pressure will change between a minimum and a maximum pressure in response to the driver's demand and the driving conditions. To have an optimized answer in almost all the working brake ranges, the optimization problem definition needs to be modified. Four different pressure levels between zero and maximum pressure are considered in solving Equation (4-10). Each of these pressure levels create a corresponding reaching time. Now, the optimization problem is to minimize the summation of these reaching times as:

$$M_{eq}\ddot{P}_i + B_{eq}\dot{P}_i + \left(\frac{\beta A_{act}^2}{V_0} + K_s\right)P + \left(\frac{\beta A_{act}}{V_0}\right)(F_0 + F_f) = \left(\frac{\beta A_{act}}{V_0}\right)\left(\frac{GR\, K_t}{\varepsilon + (d+y)\tan\varphi}\right) i\Big|_{\substack{P_i \\ i=1,2,3,4}} \quad (4\text{-}12)$$

$$Optimization\ Problem: \min \sum_{i=1}^{4} T_{reach_i} \quad (4\text{-}13)$$

Table 4-2 shows the pressure levels used for calculating the reaching time in solving Equation (4-12).

Table 4-2 Desired pressure values used in objective function calculation

Property	Value	Unit
P_1	3.44 (500)	MPa (Psi)
P_2	6.89 (1000)	MPa (Psi)
P_3	10.34 (1500)	MPa (Psi)
P_4	13.78 (2000)	MPa (Psi)

The MATLAB GA optimization Toolbox has been used to find the optimum parameters. The MATLAB GA optimization command can be described as:

$$[x_{best}\ f_{val}] = ga\ (@CostFunction,\ n_{var},\ A_{ineq},\ B_{ineq},\ A_{eq},\ B_{eq}, lb, ub, nonlcon, n_{IntVar}) \quad (4\text{-}14)$$

where *CostFunction*, n_{var} and n_{IntVar} are optimization's objective function, number of optimization variables and the integer variables number in order and the equation returns the optimum parameters. The other arguments relate to the defined constraint for the optimization process. A_{ineq}, B_{ineq} indicate the linear equality constraints presented through the Equation (4-2) to (4-4) in the form of $A_{ineq} * x \leq B_{ineq}$. A_{eq}, B_{eq} and *nonlcon* represent the equality constraint and the nonlinear constraint respectively. lb and ub are upper and lower bounds on design variables given in Equations (4-5) to (4-9). These arguments' values are presented in Table 4-3 .

Table 4-3 GA input arguments' values

Property	Value
n_{var}	4
A_{ineq}	$\begin{bmatrix} -1 & 1 & 0 & -1 \\ 0 & -1 & 0 & 1 \\ -1 & 1 & 0 & 0 \end{bmatrix}$
B_{ineq}	$\begin{bmatrix} 0 \\ 0 \\ 0 \end{bmatrix}$
A_{eq}	[]
B_{eq}	[]
$nonlcon$	[]
n_{IntVar}	3

In addition to the discussed input argument's value, there are some other options for the genetic algorithm which have to be set when using MATLAB software to get a proper answer from the optimization [51]. These options are presented in Table 4-4.

Table 4-4 GA's option setting

Property	Value
PopulationType	DoubleVector
PopulationSize	50
Generations	400
TolFun	1e-6
TolCon	1e-3
CreationFcn	gacreationlinearfeasible
FitnessScalingFcn	fitscalingrank
SelectionFcn	selectionstochunif
CrossoverFcn	crossoverintermediate
MutaruinFcn	mutationadaptfeasible

4.2 Optimization Results

Presented formulation for the proposed brake system and optimization process in the previous section was simulated in MATLAB software to find the optimized parameters. These parameters are shown in Table 4-5 as the following.

Table 4-5 Optimization parameters

Property	Value	Unit
R_p	28.9	mm
ε	7.2	mm
R_r	5.9	mm
G_R	15	-

The parameters presented in Table 4-5 are the GA optimization results. It is a good idea to examine how the design parameters are changed using the optimization results. Figure 4-2 shows the pressure angle based on Equation (3-17) when Equation (3-39) is solved by the optimized parameters.

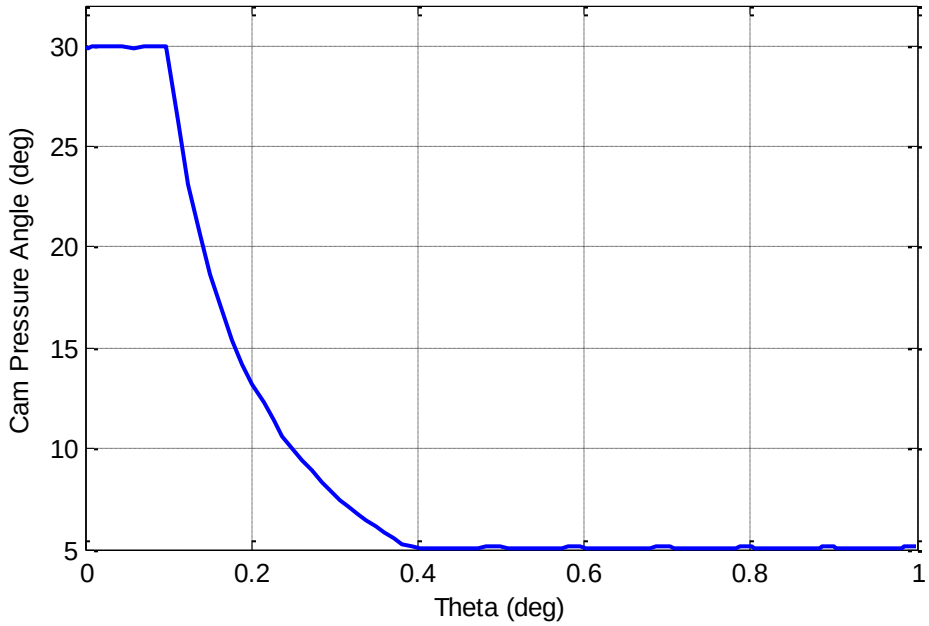

Figure 4-2 Pressure angle vs. cam rotational angle

In the defining constraints in section 4.1, fixed lower and upper bound were set for y'. Therefore, it is expected that at each time step of solving Equation (4-12), the GA calculates the best answer with respect to these fixed bounds. Rearranging Equation (3-17), which is presented in Equation (4-15), shows that y' limits depend on the follower raise at each time step with a fixed pressure angle value.

$$\frac{dy}{d\theta} = y' = (\tan\phi)(d + y) + \varepsilon \tag{4-15}$$

For example, if the follower raise *(y)* is 6.6 mm at the time of 28 millisecond, with 30º and 5º as the maximum and minimum allowable pressure angle, y' bounds are $0.01 \leq y' \leq 0.035$. Figure 4-3 shows y' upper and lower limit changes over the time with the follower raise variation at each time step.

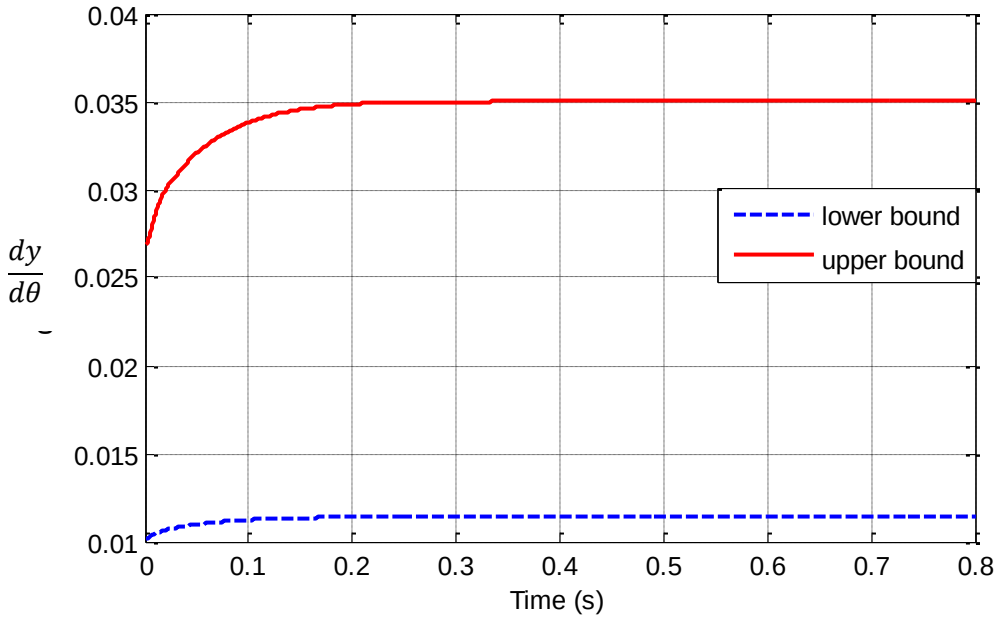

Figure 4-3 y' boundary changes vs. time

The direct search optimization that leads to y' is shown in Figure 4-4 as a graph drawn based on the cam rotational position.

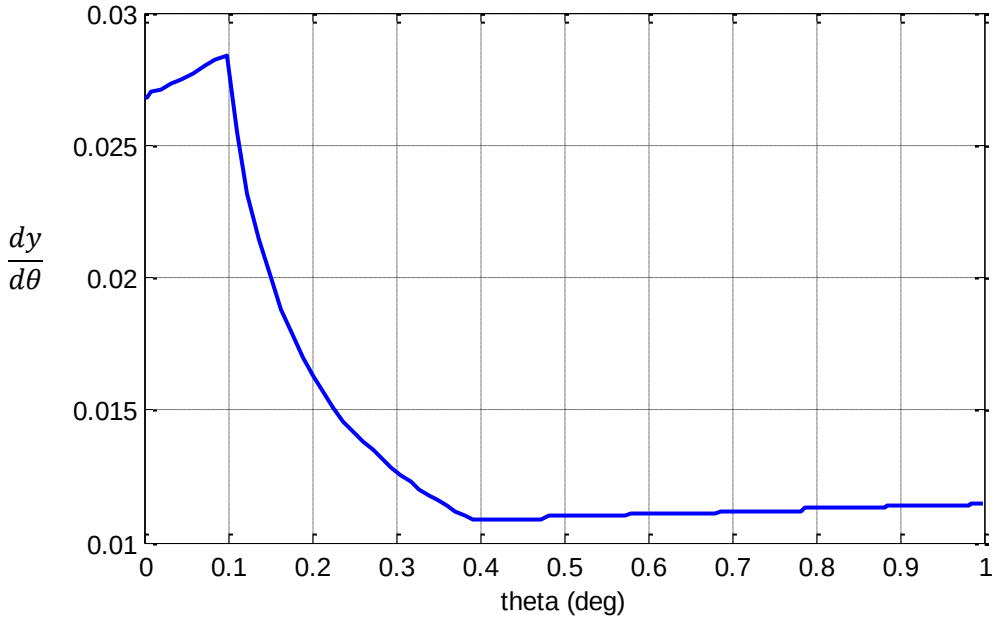

Figure 4-4 y' vs. Cam rotational angle

The follower raise *(y)* can be found by taking the integral of y' with respect to θ as shown in Figure 4-5.

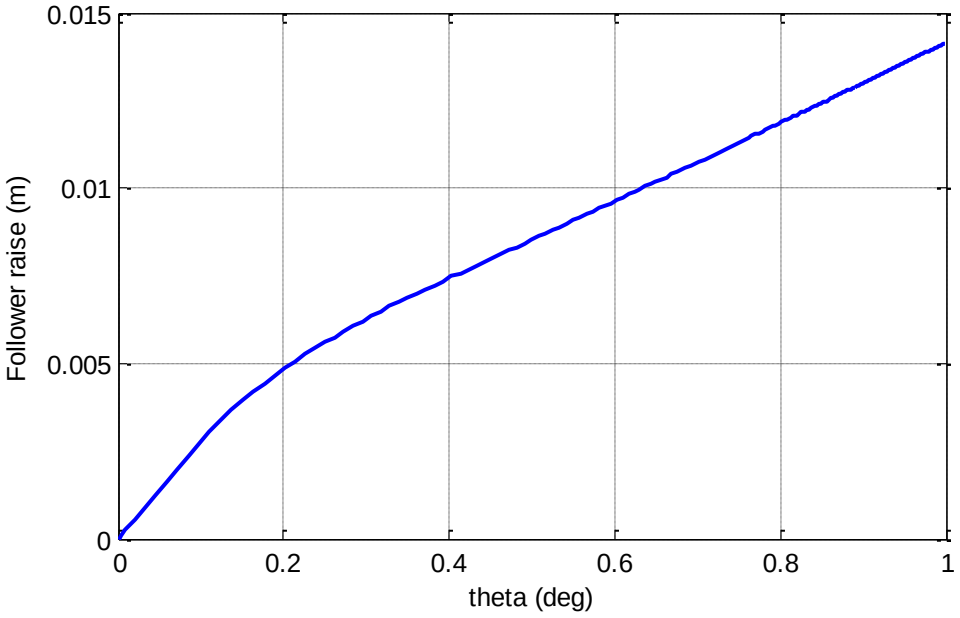

Figure 4-5 Follower raise vs. cam rotational angle as the result of optimization

It should be mentioned that since the cam mechanism is used for the brake design, there is no need to have 2π (rad) rotation. Nevertheless, a cam profile is defined up to 360 degrees in Figure 4-6.

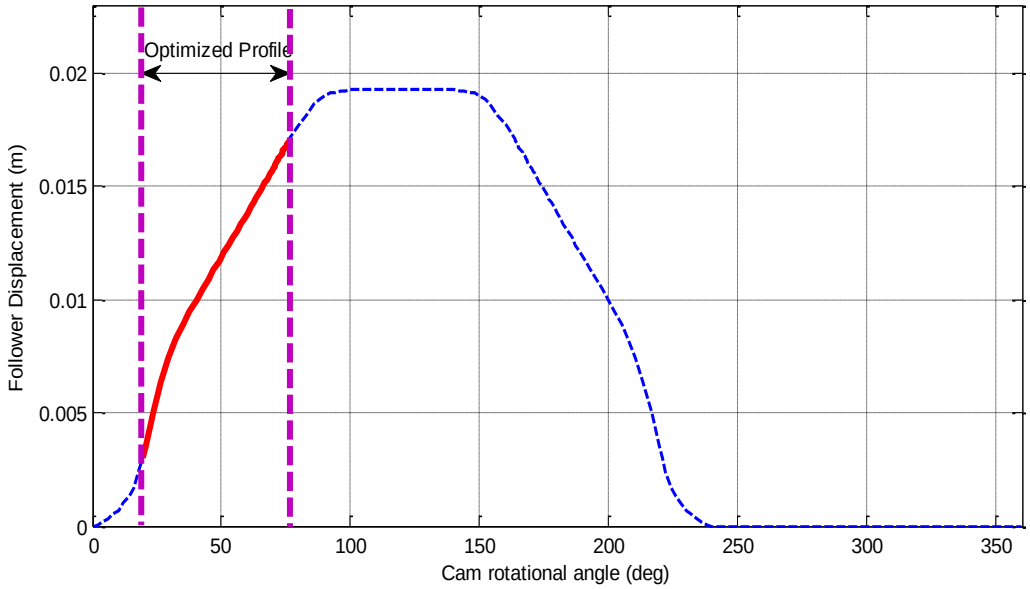

Figure 4-6 Follower Displacement vs. Cam Rotational Angle

The cross sectional area of the cam is shown in Figure 4-7.

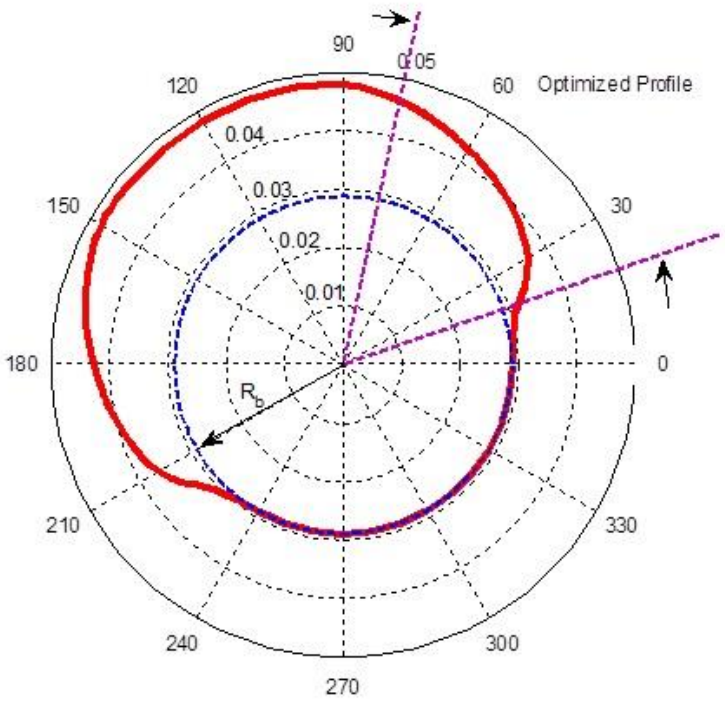

Figure 4-7 Cross section of the cam profile

By using Equation (3-26), the created pressure for the braking can be calculated. This is shown in Figure 4-8. Although the maximum target pressure was *13.87 (MPa)*, the calculated pressure by using the optimized cam profile can reach near *20 (MPa)*. This amount of pressure above the maximum target pressure can provide a safety factor around 1.4, which keeps the design in a safe zone in case some unmolded factor, such as braking pad wear, affects the necessary pressure.

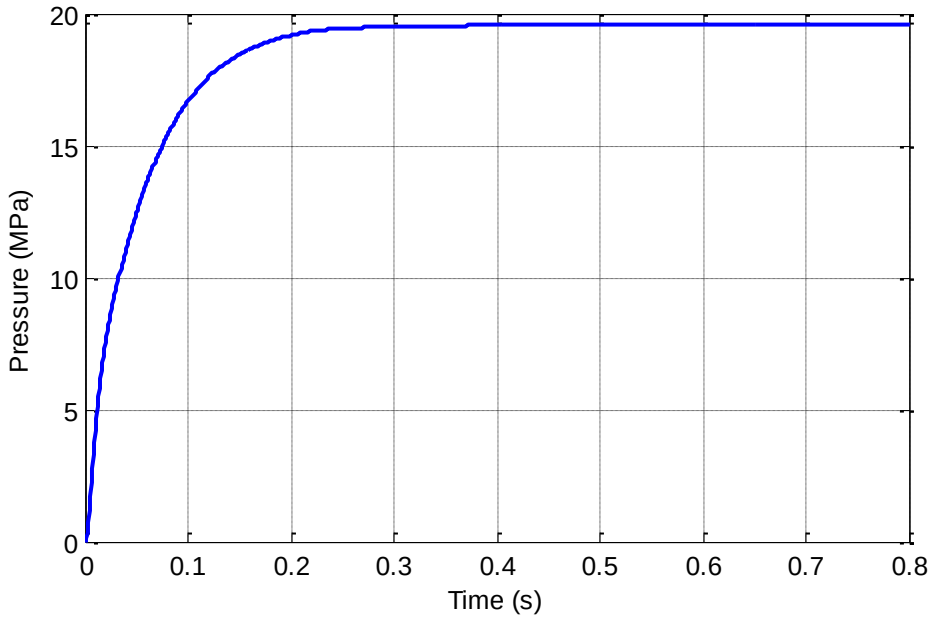

Figure 4-8 Created brake pressure vs. time for a cam actuated brake mechanism

To check the feasibility of the optimized cam-actuated brake system, the response time of increasing braking pressure from zero to its maximum is compared with a not optimized cam-actuated mechanism (in which the eccentricity and gear ratio is half of the optimized values)and an EMB system with ball screw mechanism in Figure 4-9 . As shown in this figure the cam mechanism is faster compared to the ball screw design. Using the variable amplification provided by the cam is the main reason of having improvement in this system as it was mentioned in Section 3.1.2.

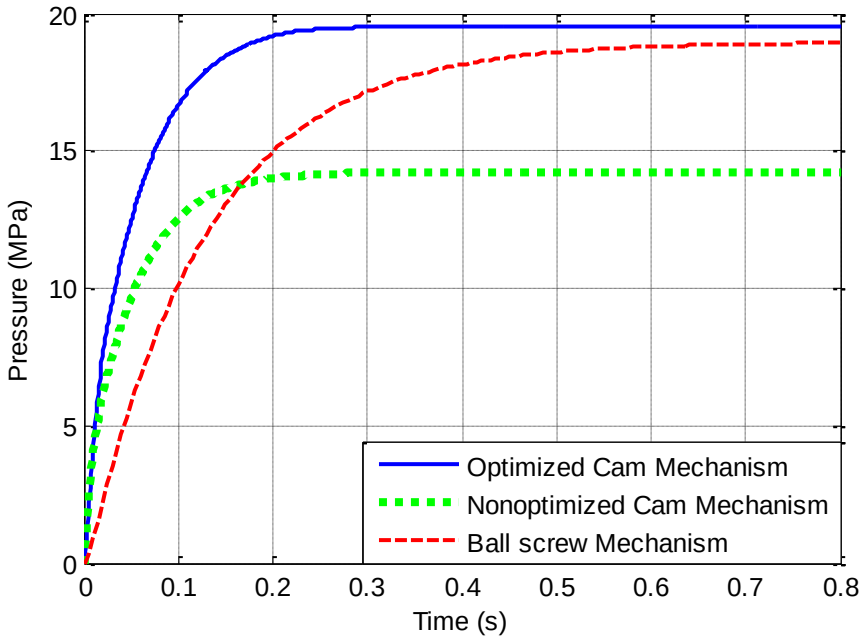

Figure 4-9 Brake pressure comparision

The design of cam actuated brake system was discussed in previous chapter. Table 4-6 shows a comparison between characteristics of cam actuated brake system and other types of brake-by-wire mechanisms that were explained in literatures in Chapter 2.

Table 4-6 Comparison between different type of brake-by-wire characteristics and cam-actuated brake mechanism

Brake Type	EHB	EMB	EWB	BEHB	Cam-actuated Brake
Activation signal	Electrical	Electrical	Electrical	Electrical	Electrical
Braking power source	Hydraulic	Electrical	Electrical	Hydraulic	Hydraulic
Characteristics	Fail-safe Modular	Fully electrical No braking fluid	Fully electrical No braking fluid Self-energized ability	Providing distributed braking force Modular	Self-contained Having redundancy Fail-safe Fast response

4.3 Summary

In this chapter, the design parameters of the cam actuated brake system were optimized. The optimization algorithm was a multilayer algorithm. The first stage of the optimization was related to finding the optimized values for the cam base circle radius, follower eccentricity, follower circle radius and the gear ratio. The second stage was a direct search algorithm to find the cam profile shape. The objective of the optimization was finding design parameters to have the fastest possible response for the brake mechanism while the maximum allowable motor current is applied to the system. The solution to the optimization problem showed that the open loop response time can be reduced down to around 63 millisecond, which is an acceptable response time for a brake mechanism.

Chapter 5
Control Design

In this chapter, different control methods are examined to find the best method for providing a desirable braking pressure for the brake system with the cam actuator design. The first section of chapter 5 is related to the PI controller. In the second section, the performance of the Sliding Mode Controller (SMC) is studied with further investigation into its adaptive version called Adaptive Sliding Mode Controller (ASMC). In the following pages, the Model Predictive Controller for the designed brake system is discussed. Finally, the last two sections discus about the system's closed loop response to an arbitrary input and uncertainty compensation of different types of controllers.

The dynamic equation of the cam actuated brake system is recalled in this chapter as follows.

$$M_{eq}\ddot{P} + B_{eq}\dot{P} + K_{eq}P = \left(\frac{\beta A_{act}}{V_0}\right)\left(\frac{GR\ K_t}{\varepsilon + \left(R_p + R_r + y\right)\tan\varphi}\right) i + d(P,\dot{P},t) \tag{5-1}$$

The state space form of this equation, can be presented as:

$$\begin{bmatrix}\dot{x}_1\\ \dot{x}_2\end{bmatrix} = \begin{bmatrix}0 & 1\\ -\frac{K_{eq}}{M_{eq}} & -\frac{B_{eq}}{M_{eq}}\end{bmatrix}\begin{bmatrix}x_1\\ x_2\end{bmatrix} + \begin{bmatrix}0\\ \left(\frac{\beta A_{act}}{V_0}\right)\left(\frac{GR\ K_t}{\varepsilon + \left(R_p + R_r + y\right)\tan\varphi}\right)\end{bmatrix} u + d(P,\dot{P},t) \tag{5-2}$$

where x_1 and x_2 represent the pressure *(P)* and the rate of pressure changes $(\dot{P})$ respectively. $d(P,\dot{P},t)$ is the disturbance term which includes the coulomb friction of the system that is discussed in the previous chapter. It is assumed that the disturbance term is bounded, i.e.$\left|d(P,\dot{P},t)\right| \leq W$, with the bound *W* known. It bears reminding that Equation (5-2) is a nonlinear system because the system parameters K_{eq}, B_{eq} and M_{eq} depend on the cam angles.

Table 5-1 shows the numerical values of parameters used in simulation. The calculations of equivalent mass, stiffness and damping are explained in Section 3.3.

Table 5-1 Simulation parameters numerical value

Property	Value	Unit
J_m	5.95×10^{-8}	$Kg.m^2$
K_t	0.0465	$N.\frac{m}{A}$
B_m	0.008	$N.\frac{s}{m}$
J_{g1}	2.1×10^{-7}	$Kg.m^2$
J_{g2}	3.95×10^{-5}	$Kg.m^2$
J_{cam}	6.12×10^{-7}	$Kg.m^2$
M_{act}	0.1	Kg
A_{act}	1.58×10^{-4}	m^2
β	0.375	GPa

The input of the system (u) is the electric motor current provided by the controller based on the reference pressure value. The closed loop block diagram of the system is shown in Figure 5-1.

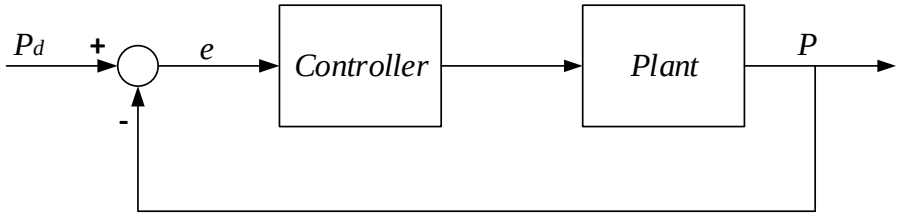

Figure 5-1 Closed loop block diagram of the system

The controller calculates the proper current for the plant based on the value of the error. It should be mentioned that there is a current limit for the given current to the electric motor used in the braking system, i.e. $-30 \leq I \leq 30$ Ampere. This limit should be considered in the control design.

5.1 PI Controller

The first controller studied for the cam actuated brake system is the well-known PI controller. The schematic form of the system with PI controller is shown in Figure 5-2.

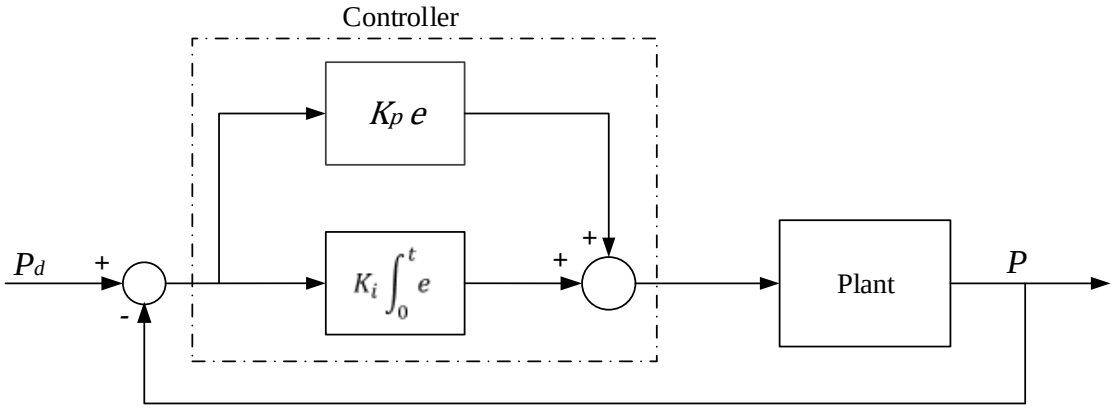

Figure 5-2 PI controller clock diagram

As it can be seen from Figure 5-2 that the error is introduced by the difference between a pre-defined pressure, called P_d, and the actual output pressure of the plant. It should be mentioned that a step function with the final value of 13.8 MPa (2000 psi) is used as the reference pressure during the controller's design. The PI controller's gains *(K_i* and *K_p)* can be chosen in a way that achieves the best performance for the closed loop system. The controller behavior after normalizing the system with respect to the reference pressure is presented in the following sections for different values of K_i and K_p. The effect of changing the integral gain on the closed loop system's error is shown in Figure 5-3 while the proportional gain was kept constant. Figure 5-4 presents a picture of the closed loop system for different K_p and constant K_i.

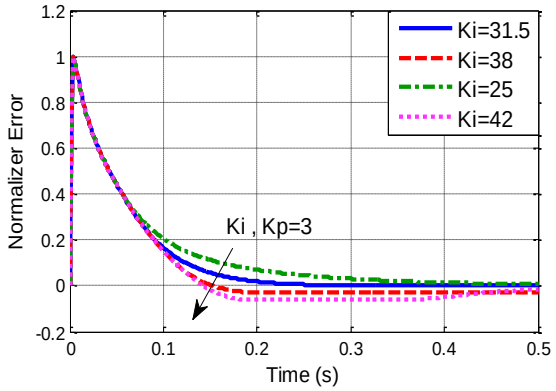

Figure 5-3 Effect of different values of K_i on the normalized error with constant K_p

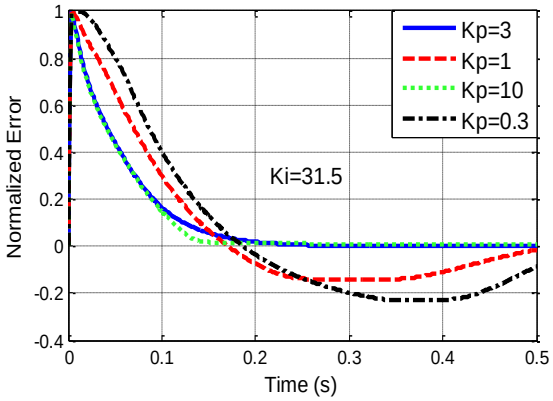

Figure 5-4 Effect of different values of K_p on the normalized error with constant K_i

These two figures lead to tuning the PI controller gains as these are shown in Table 5-2.

Table 5-2 PI controller's gains

Property	Value
Proportional Gain (K_p)	3
Integral Gain (K_i)	38.5

The PI controller performance with the tuned gains is shown in Figure 5-5, and Figure 5-6 shows the control action which goes to the main plant.

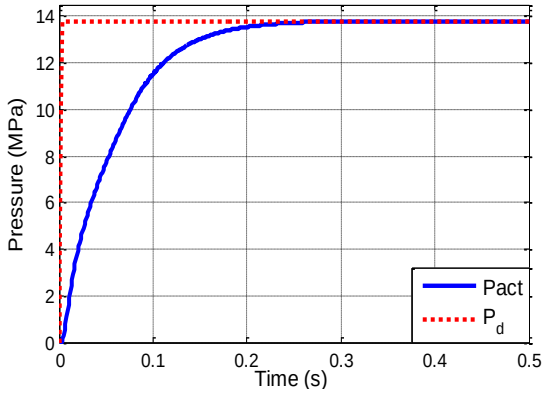

Figure 5-5 Closed loop tracking performance for PI controller

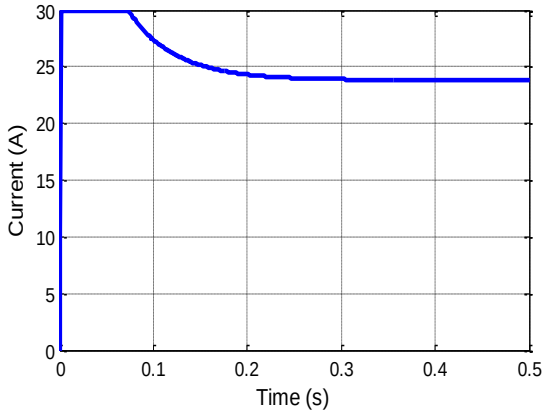

Figure 5-6 Control action of PI controller

5.2 Sliding Mode Controller and Adaptive Sliding Mode Controller Design

One of the control methods that show promise in dealing with uncertainties and tracking a desired value is the Sliding Mode Controller (SMC). However, the main drawback of the SMC is that the discontinuous form of the SMC may cause chattering in the control signal. The control action chatter may not be accepted in some applications. For example, the chattering may not be acceptable in the vehicle's braking pressure and torque. Oscillation in braking torque can affect not only the performance of the vehicle but also what the driver feels during the braking process. One of the methods used for eliminating the chattering of the control signal is the boundary layer method [52], which is a tradeoff between the tracking performance of the controller and the chattering elimination. An alternate method to the boundary layer theory is using the Adaptive Sliding Mode Control (ASMC) [53], [54]. This type of controller is known to be capable of dealing with unmolded parameters and external uncertainties while being free from chattering.

5.2.1 SMC Design

The error between the desired and the actual pressure created by the system's plant can be used in defining the sliding surface in the following equation.

$$e = P - P_d \tag{5-3}$$

Generally the dynamics on the sliding surface dynamic can be shaped in the form of: [52]

$$S(x,t) = \left(\frac{d}{dt} + \lambda\right)^{n-1} e \tag{5-4}$$

where λ is some positive number and n is the order of the system. As it is shown in Equation (5-1), the order of the system is equal to 2, so the sliding surface will be

$$S = \dot{e} + \lambda e \tag{5-5}$$

In order to guarantee the asymptotical convergence of the error and its time derivative to zero, the sliding surface presented in Equation (5-5) should be reached in a finite time by applying the appropriate control signal u to the system. One way to find such a control signal is using Lyapunov function techniques.

By taking the derivative of Equation (5-5) twice and substituting $\ddot{P}$ with (5-1), the time derivative of the sliding surface is:

$$\dot{S} = \left(\ddot{P} - \ddot{P}_d\right) + \lambda\dot{e} = -\ddot{P}_d + \left(-\frac{B_{eq}}{M_{eq}}\dot{P} - \frac{K_{eq}}{M_{eq}}P + \frac{G}{M_{eq}}\,u + \frac{1}{M_{eq}}d\left(P,\dot{P},t\right)\right) + \lambda\left(\dot{P} - \dot{P}_d\right) \tag{5-6}$$

where:

$$G = \left(\frac{\beta A_{act}}{V_0}\right)\left(\frac{G_R\,K_t}{\varepsilon + \left(R_p + R_r + y\right)\tan\varphi}\right) \tag{5-7}$$

The sliding mode control signal has two parts; one part is the equivalent control signal, and the other part is the switching control signal:

$$u_{SMC} = u_{eq} + u_{sw} \tag{5-8}$$

Equivalent control action is found for a perfect system without disturbance by equating the derivative of the sliding surface (Equation (5-6)) to zero. Therefore,

$$u_{eq} = \left(-\frac{M_{eq}}{G}\right)\left(\ddot{P}_d + \lambda\dot{P}_d + \left(\frac{B_{eq}}{M_{eq}} - \lambda\right)\dot{P} + \left(\frac{K_{eq}}{M_{eq}}\right)P\right) \tag{5-9}$$

The other part is the switching control signal found by introducing a proper Lyapanov function. For sliding surface dynamic shown in Equation (5-5), the Lyapunov function used is in the form:

$$L = \frac{1}{2}S^2 \tag{5-10}$$

According to [55], to have the asymptotical stability for surface dynamic around the equilibrium point *S=0*, two conditions must be satisfied:

I. $\dot{L} < 0$ for $S \neq 0$

II. $\lim_{|S|\to\infty} L = \infty$

Due to the definition of the Lyapanov function in Equation (5-10), the second condition is satisfied. It was mentioned that the surface should reach zero in a finite time. For this purpose, the first condition can be changed to:

$$\dot{L} = S\dot{S} \leq -\beta|S| \tag{5-11}$$

where $\beta>0$ is a design parameter. By taking the integral of Equation (5-11) over the time interval i.e., $0 \leq t \leq T$ in two cases of $S>0$ and $S<0$, the reaching time will be:

$$t_r \leq \frac{|S(t=0)|}{\beta} \tag{5-12}$$

Equation (5-12) shows the finite time in which the control action calculated by (5-11) will drive the sliding surface to zero and keep it there afterwards. The switching control signal is calculated by solving Equation (5-11) in the presence of the disturbance and assuming that the final control is in the form of: $u = -u_{eq} + \bar{u}$. If the $\dot{S}$ is replaced by Equation (5-6), the derivative of Lyapanov function is calculated as:

$$\dot{L} = S\dot{S} = S\left(-\ddot{P}_d - \lambda\dot{P}_d + -\left(\frac{B_{eq}}{M_{eq}} - \lambda\right)\dot{P} - \frac{K_{eq}}{M_{eq}}P + \frac{G}{M_{eq}}\left(-u_{eq} + \bar{u}\right) + \frac{1}{M_{eq}}d(P,\dot{P},t)\right) \tag{5-13}$$

By substituting the equivalent control signal from (5-9) in the above equation, Equation (5-13) can be written as:

$$\dot{L} = S\left(\frac{1}{M_{eq}}d(P,\dot{P},t) + \frac{G}{M_{eq}}\bar{u}\right) = S\frac{1}{M_{eq}}d(P,\dot{P},t) + S\frac{G}{M_{eq}}\bar{u} \tag{5-14}$$

By choosing $\bar{u} = -\eta sign(S)$, where $\eta > 0$ and the *sign* denotes the sign function. By inserting $\bar{u}$ in the (5-14), the $\dot{L}$ will be:

$$\dot{L} = |S|\frac{W}{M_{eq}} - |S|.\frac{G}{M_{eq}}\eta = -|S|\frac{1}{M_{eq}}(G\eta - W) \tag{5-15}$$

Considering the modified form of the first condition of Lyapunov function showed in Equation (5-11) and combining it with (5-15), it will be:

$$\dot{L} = -|S|\frac{1}{M_{eq}}\,(G\eta - W) = -\beta|S| \tag{5-16}$$

Indeed the control design parameter η can be chosen as:

$$\eta = \frac{1}{G}\left(M_{eq}\beta + W\right) \tag{5-17}$$

Consequently, the control signal *u* that forces the tracking error to zero in a finite time is:

$$u = -u_{eq} - \eta\, sign(S) \tag{5-18}$$

5.2.2 ASMC Design

The ASMCs are known to provide a chatter free behavior for the closed loop system while also having the capability to deal with external uncertainties and unknown parameter variations. In the previous chapter, the cam actuated brake system is modeled and optimized based on some assumed values for the brake system parts like the masses of the gears, the cam and the actuator cylinder and the bulk modulus of braking oil. Rewriting Equation (5-1) with respect to $\ddot{P}$ gives:

$$\ddot{P} = -Z_1(t)\dot{P} - Z_2(t)P + B\,u + d(P,\dot{P},t) \tag{5-19}$$

where $Z_1 = \frac{B_{eq}}{M_{eq}}$, $Z_2 = \frac{K_{eq}}{M_{eq}}$ and $B = \frac{G}{M_{eq}}$ in which G was introduced before. Since the exact values of mentioned parameters used in calculating M_{eq}, K_{eq} and G are unknown, Z_1, Z_2 and B can be written as a known value plus the uncertain part of each one

$$Z_1 = \hat{Z}_1 + \Delta Z_1\,, Z_2 = \hat{Z}_2 + \Delta Z_2\,, B = \hat{B} + \Delta B \tag{5-20}$$

where $\hat{Z}_1, \hat{Z}_2$ and $\hat{B}$ are the known parts of parameters and ΔZ_1, ΔZ_2 and ΔB are the unknown parts. Therefore Equation (5-19) can be transformed to:

$$\ddot{P} = -\hat{Z}_1\dot{P} - \hat{Z}_2P + \hat{B}\,u - \Delta Z_1\dot{P} - \Delta Z_2P + \Delta B\,u + d(P,\dot{P},t) \tag{5-21}$$

All the uncertainties can be lumped together as follows: [53]

$$\tilde{Z} = -\Delta Z_1\dot{P} - \Delta Z_2P + \Delta B\,u + d(P,\dot{P},t) \tag{5-22}$$

Therefore, Equation (5-21) can be written as:

$$\ddot{P} = -\hat{Z}_1\dot{P} - \hat{Z}_2 P + \hat{B}\,u + \tilde{Z} \tag{5-23}$$

The first step in designing the ASMC is to define a proper surface. A good candidate for the tracking purpose is the integral form for the surface. The integral term guarantees that the surface will reach zero and stay there while the steady state error will also be zero. The sliding surface is found by choosing *n-1=2* and $\int e$ instead of *e* in Equation (5-4), so

$$S = \left(\frac{d}{dt} + \lambda\right)^2 \int e = \dot{e} + 2\,\lambda\, e + \lambda^2 \int e \tag{5-24}$$

$$\dot{S} = \ddot{e} + 2\,\lambda\,\dot{e} + \lambda^2 e \tag{5-25}$$

The ASMC signal consist of three parts [54].

$$u = u_{eq} + u_p + u_d \tag{5-26}$$

where u_{eq}, u_p and u_d are the equivalent control signal, the proportional control signal and the disturbance rejection control signal respectively. The equivalent control signal is calculated like before, i.e., $\dot{S} = 0$ for completely known system. This condition calculates the equivalent control signal as:

$$u_{eq} = \hat{B}^{-1}\left(\ddot{P}_d + \hat{Z}_1\dot{P} + \hat{Z}_2 P - 2\,\lambda\,\dot{e} - \lambda^2 e\right) \tag{5-27}$$

The proportional control signal *(u_p)* is used to improve the transient performance of the system and it will be calculated by modifying the derivative Lyapunov function as: $\dot{L} = S\dot{S} \leq -SKS$, where *K>0* is the ASMC design parameter. Therefore,

$$S\left(\dot{S} + KS\right) = 0 \tag{5-28}$$

If $\dot{S}$ found by (5-25) is substituted in the above equation, the control action will be:

$$u = \underbrace{\hat{B}^{-1}\left(\ddot{P}_d + \hat{Z}_1\dot{P} + \hat{Z}_2 P - 2\,\lambda\,\dot{e} - \lambda^2 e\right)}_{u_{eq}} - \underbrace{\hat{B}^{-1}KS}_{u_p} \tag{5-29}$$

It can be seen from Equation (5-23) that, by adding an additional term to the control signal, the lumped disturbance term can be compensated. This additional control signal is in the form of $u_d = -\hat{B}\tilde{Z}$. $\tilde{Z}$ is unknown and its estimate needs to be used instead, so the final form of ASMC is:

$$u = -\hat{B}^{-1}\left(-\ddot{P}_d - \hat{Z}_1\dot{P} - \hat{Z}_2 P + 2\,\lambda\,\dot{e} + \lambda^2 e + KS + \tilde{Z}_{est}\right) \tag{5-30}$$

where $\tilde{Z}_{est}$ is the online estimation of lumped disturbance term and its values will be calculated in next subsection taking the stability and robustness into consideration.

5.2.2.1 Stability and robustness analysis of ASMC

If the control presented in Equation (5-30) is applied to a nonlinear and uncertain system like (5-23), the robust stability of the closed loop system needs to be considered. To estimate the unknown lumped disturbance $\tilde{Z}$ in Equation (5-23), a Lyapunov function may be used.

$$L = \frac{1}{2}\left(S^2 + \frac{E^2}{\Gamma}\right) \tag{5-31}$$

where E is the error between the estimated uncertainty ($\tilde{Z}_{est}$) and its actual value ($\tilde{Z}$) i.e. $E = \tilde{Z}_{est} - \tilde{Z}$, and $\Gamma>0$ is the design parameter. The derivative of the above Lyapunov function is:

$$\dot{L} = S\dot{S} + \Gamma^{-1}E\dot{E} \tag{5-32}$$

As shown in (5-25) $\dot{S} = \ddot{P} - \ddot{P}_d + 2\lambda e + \lambda^2 e$. If the calculated control action in (5-30) is inserted in the $\ddot{P}$ equation presented by (5-23), then $\dot{S} = -KS - E$. Thus

$$\dot{L} = -SKS - SE + E\Gamma^{-1}(\dot{\tilde{Z}}_{set} - \dot{\tilde{Z}}) \tag{5-33}$$

Now, if the following control law is chosen:

$$\dot{\tilde{Z}}_{est} = \Gamma S \tag{5-34}$$

The Equation (5-33) will be

$$\dot{L} = -SKS - E\Gamma^{-1}\dot{\tilde{Z}} \tag{5-35}$$

To have the asymptotical stability, the condition $\dot{L} \leq 0$ must be applied. The worst case scenario happens when the term $E\Gamma^{-1}\dot{\tilde{Z}}$ is negative; therefore, the Equation (5-35) can be written as follows:

$$\dot{L} = -SKS - E\Gamma^{-1}\dot{\tilde{Z}} \leq -SKS + \left|E\Gamma^{-1}\dot{\tilde{Z}}\right| \leq -K|S^2| + \frac{\left|E\dot{\tilde{Z}}\right|}{\Gamma} \leq -K|S^2| + \frac{|E||\dot{\tilde{Z}}|}{\Gamma} \tag{5-36}$$

$$\dot{L} < 0 \ \rightarrow |S| > \left(\frac{|E||\dot{\tilde{Z}}|}{K\Gamma}\right)^{0.5} = \varepsilon \tag{5-37}$$

where ε is a positive value. From Equation (5-37), it can be concluded that for all $|S| > \varepsilon$, $\dot{L}$ is negative definite; therefore, L is bounded and all trajectories will reach ε neighborhood of the

$S(t)=0$ [3]. At the same time, by increasing the design parameters K and Γ, the ε can be chosen arbitrarily small, which causes the magnitude of the surface to become small in the presence of uncertainties. In conclusion, the control signal found by ASMC will be:

$$u = -\hat{B}^{-1}\left(-\ddot{P}_d - \hat{Z}_1\dot{P} - \hat{Z}_2 P + 2\,\lambda\,\dot{e} + \lambda^2 e + KS + \int \Gamma S dt\right) \tag{5-38}$$

5.2.3 SMC and ASMC Simulation Results

Both SMC and ASMC were modeled in simulation. Like PI controller, the reference pressure was set at 13.8 MPa. The simulation sampling time was set to 1 millisecond and the design parameters of SMC and ASMC are shown in Table 5-3.

Table 5-3 SMC and ASMC's parameters

Controller	*Property*	Value
SMC	λ	100
	η	5e11
ASMC	λ	8
	K	3e3
	Γ	75

In the following pages, the SMC and ASMC simulation results are shown.

[3] See Appendix B for further stability analysis

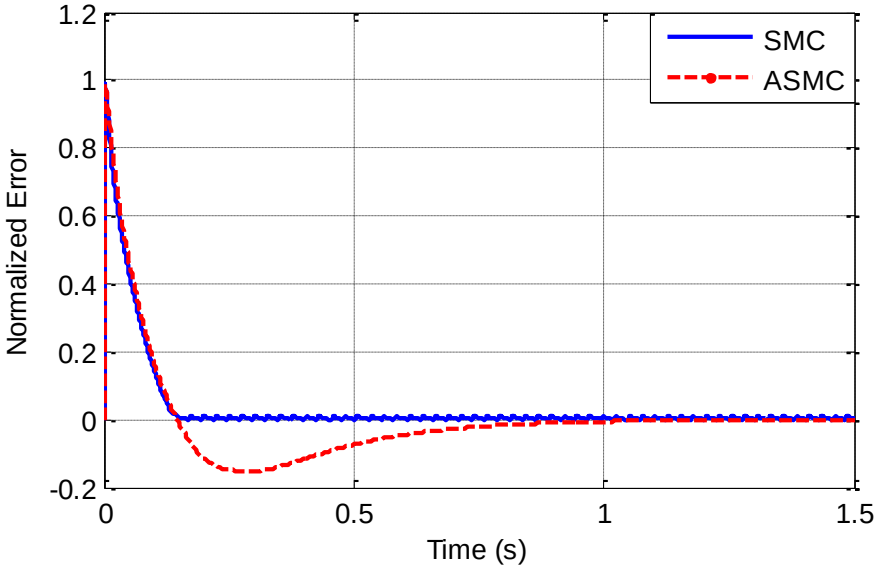

Figure 5-7 Normalized error for SMC and ASMC

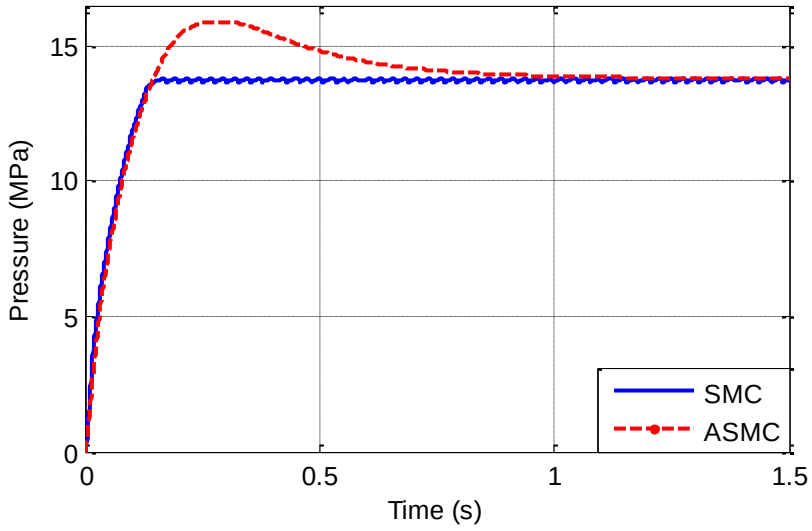

Figure 5-8 Closed loop tracking performance for SMC and ASMC

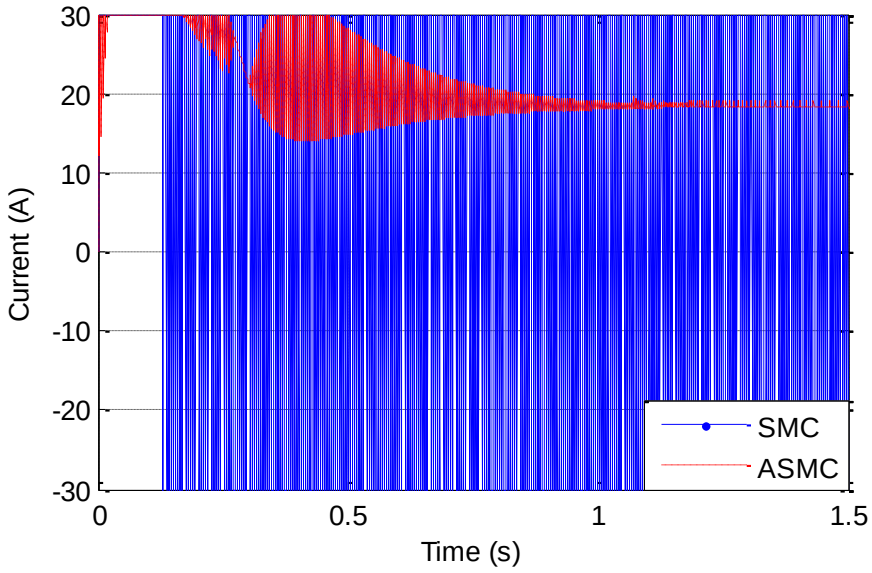

Figure 5-9 Control action of SMC and ASMC

As seen in Figure 5-8, the pressure created by the control action of the SMC has some chatter due to the sign function used in the definition of its control action in Equation (5-18). On the other hand, these chatters are smoother when the ASMC is used, but at the same time, the created pressure by the ASMC input signal has a considerable overshoot in the output. This phenomenon can be explained by considering the definition of the sliding surface for ASMC in Equation (5-24). As it can be seen in this equation, the defined surface is similar to the definition of a PID controller with the proportional, integral and derivative gains equal to 2λ, $\lambda^2$and 1 in order. The term λ affects the proportional and integral gain. Obviously, the large proportional gain causes large changes in output when the error signal is large. On the other hand, higher integral gain forces the system to reach its set point faster and eliminates the steady state error. However, because it deals with past error, it can create an overshoot in the system, which is known as the integrator wind-up in the literature. Figure 5-10 shows closed loop response for the system with ASMC for different λ.

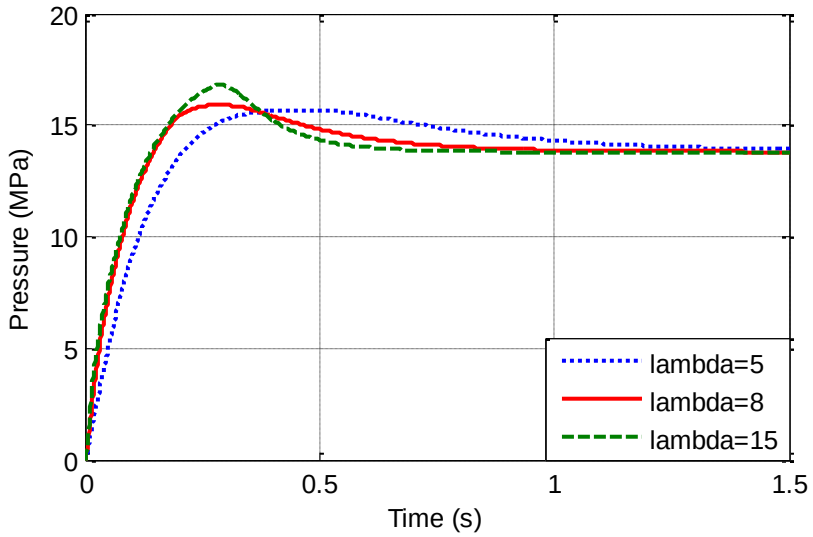

Figure 5-10 System closed loop response for different values of λ

As shown in Figure 5-8, the SMC closed loop response has chattering for created pressure for the braking system. This pressure chattering can cause oscillation in the braking torque, which is not desirable. However, ASMC is smooth and chatter free, but it has noticeable overshoot in closed loop response making it unsuitable for braking applications.

As mentioned before, the limit of ± 30 A is used as a saturation limit for the control signal. The existence of the current limit led to the design of another type of controller that can explicitly consider the constraints during calculation of the control action. A good candidate for this type of controller is the Model Predictive Controller (MPC), which is explained in the following section.

5.3 Model Predictive Controller Design

As mentioned in the previous sections, there is a constraint for control action applied to the electric motor of the brake system. This constraint has not been considered in designing PI, SMC and ASMC. One of the promising control methods that can explicitly handle input and state constraints is the Model Predictive Control (MPC) method. The MPC is an optimal control method that predicts the future response of the system at each time step by considering the measured plant's output value at the current time. At first, a finite prediction horizon of *N*-step is determined. Then, a cost function is defined to obtain the optimal control inputs for *N*-step prediction. The control action applied to the plant is the first element of the calculated optimal control sequence. If there are any inputs or state constraints, they will be applied as an inequality during the optimization process. All these

calculations are repeated at each sample time to find the new set of the optimal inputs over the shifted prediction horizon [56]. Figure 5-11 shows the basic strategy of MPC at time step *t* and *t+1*[57].

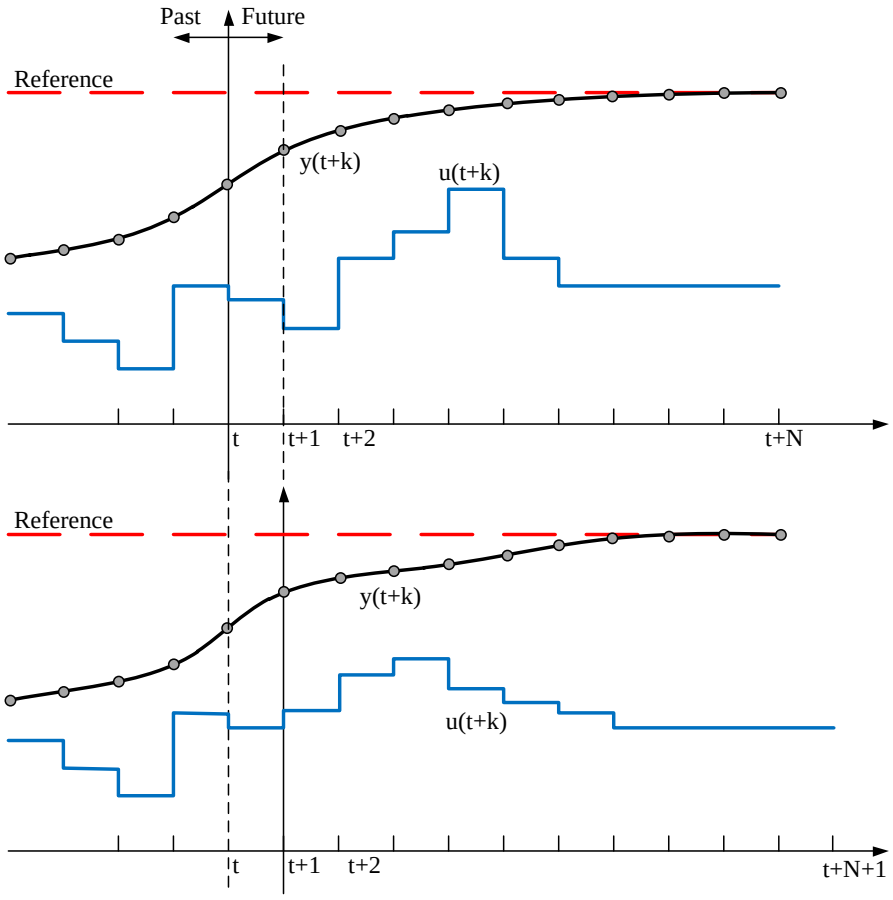

Figure 5-11 MPC strategy

The state space form of the plant is:

$$\dot{x} = Ax + Bu \tag{5-39}$$

where $x = \left[P\ \dot{P}\right]^T$ and matrices *A* and *B* are presented in Equation (5-2). To use the MPC theory, the continuous system must be discretized. Remember that the system is nonlinear since *A* and *B* elements depend on the cam angle. To use the Zero-Order Hold (ZOH) discretization method, these matrices should be constant. For this, *A* and *B* are calculated at each sampling time using the current cam angle and assumed to be constant during this period; therefore, the ZOH discretization is done at each sampling time as follows:

$$x_{k+1} = A_d x_k + B_d u_k$$

$$A_d = e^{AT} \tag{5-40}$$

$$B_d = \left(\int_0^T e^{AT} d\tau \right) B = A^{-1}(A_d - I)B$$

where T is the sampling time and matrix A is nonsingular. The main goal of using this controller for the brake system is its previously discussed reaching of the actual braking pressure with its reference pressure. Therefore, the MPC controller is formulated to solve a tracking problem for the closed loop system. The optimal control cost function is written for a new term, which is the difference between the desired states $\left[P_d \ \dot{P}_d\right]^T$ and the actual states $\left[P \ \dot{P}\right]^T$ of the plant as:

$$\tilde{x} = x_d - x_x \tag{5-41}$$

So the defined quadratic cost function for the MPC controller over a finite horizon of N steps will be:

$$J_0(x_0, U_0) \triangleq \tilde{x}_N^T \, P_x \, \tilde{x}_N + \sum_{k=0}^{N-1} \tilde{x}_k^T \, Q \, \tilde{x}_k + u_k^T \, R \, u_k \tag{5-42}$$

where the P_x and Q are the state weights and they are positive semi definite matrices, i.e., $P_x = P_x^T \succcurlyeq 0, Q = Q^T \succcurlyeq 0$ and R is the positive definite input weight $R = R^T \succ 0$. Also, $U_0 \triangleq [u_0, u_1, \dots, u_{N-1}]$ is the current and future inputs sequence. Therefore, the finite time optimal control problem considering the input limit can be written as:

$$\begin{aligned} J_0^*(x_0) &= \min_{U_0} \ J_0(\tilde{x}(0), U_0) \\ subject\ to \quad & x_{k+1} = A_d x_k + B_d u_k \\ & u_k \in u = \{u \mid -30 \le u_k \le 30\} \end{aligned} \tag{5-43}$$

One method to solve the presented quadratic cost function is eliminating the intermediate states by using the consecutive substitution of the states as it is shown below: [58]

$$
\begin{aligned}
x(0) &= x(0) \\
x(k=1) &= A_d x(0) + B_d u(0) \\
x(k=2) &= A_d x(1) + B_d u(1) = A_d\big(A_d x(0) + B_d u(0)\big) + B_d u(1) \\
&= A_d^2 x(0) + A_d B_d u(0) + B_d u(1) \\
&\vdots \\
x(k=N) &= A_d^N x(0) + A_d^{N-1} B_d\, x(0) + A_d^{N-2} B_d\, x(1) + \cdots + B_d\, u(N-1)
\end{aligned}
\tag{5-44}
$$

The above set of equation can be rewritten in a matrix format as follows:

$$
\underbrace{\begin{bmatrix} x(0) \\ x_1 \\ x_2 \\ \vdots \\ x_N \end{bmatrix}}_{\mathcal{X}} = \underbrace{\begin{bmatrix} I \\ A_d \\ A_d^2 \\ \vdots \\ A_d^N \end{bmatrix}}_{\mathcal{S}^x} x(0) + \underbrace{\begin{bmatrix} 0 & 0 & \dots & 0 \\ B_d & \dots & \dots & 0 \\ A_d B_d & \ddots & \ddots & \vdots \\ \vdots & \ddots & \ddots & \vdots \\ A_d^{N-1} B_d & \dots & \dots & B_d \end{bmatrix}}_{\mathcal{S}^u} \underbrace{\begin{bmatrix} u_0 \\ u_1 \\ u_2 \\ \vdots \\ u_N \end{bmatrix}}_{U_0}
\tag{5-45}
$$

Equation (5-45) shows that the future steps can be presented as functions of the present state *(x(0))* and the future inputs specifically. As it is suggested in [58], it can be stated in a compact form as:

$$
\mathcal{X} = \mathcal{S}^x\, x(0) + \mathcal{S}^u\, U_0 \tag{5-46}
$$

Since Equation (5-39) shows that the system has 2 states, the dimension of matrices $\mathcal{S}^x$ and $\mathcal{S}^u$ are $(2N+2) \times 2$ and $(2N+2) \times N$ in order.

The introduced objective function in (5-42) can be rearranged to:

$$
J(\tilde{x}(0), U_0) = \tilde{x}^T \bar{Q} \tilde{x} + U_0^T \bar{R} U_0 \tag{5-47}
$$

where $\bar{Q}$ is the combined initial state and future states weight in the form of $\bar{Q} = blockdiag\,\{Q, \dots, Q, P_x\}, \bar{Q} \succcurlyeq 0$ and $\bar{R} = blockdiag\,\{R, \dots, R\}, \bar{R} \succ 0$. If in Equation (5-47), $\tilde{x}$ is replaced by (5-41) the objective function changes to

$$
\begin{aligned}
J(\tilde{x}(0), U_0) &= (x_d - x_k)^T \bar{Q} (x_d - x_k) + U_0^T \bar{R} U_0 \\
&= x_d^T\, \bar{Q} x_d - 2\, x_k^T\, \bar{Q}\, x_d + x_k^T \bar{Q} x_k + U_0^T \bar{Q} U_0
\end{aligned}
\tag{5-48}
$$

x_k can be replaced by Equation (5-46) to find the objective function based on current value of the state and the future inputs. Thus, it will be:

$$J(x(0),U_0) = U_0^T \underbrace{\left(\mathcal{S}^{u^T}\,\bar{Q}\,\mathcal{S}^u + \bar{R}\right)}_{H} U_0 + 2\underbrace{\left(x^T(0)\,\mathcal{S}^{x^T}\,\bar{Q}\,\mathcal{S}^u - x_d^T\,\bar{Q}\,\mathcal{S}^u\right)}_{F} U_0 + x_d^T\,\bar{Q}x_d$$
$$- 2x^T(0)\,\mathcal{S}^{x^T}\,\bar{Q}\,x_d + x^T(0)\,\mathcal{S}^{x^T}\,\bar{Q}\,\mathcal{S}^x\,x(0) \tag{5-49}$$

Equation (5-49) is in the form of a Quadratic Programing (QP) optimization problem subjected to the input constrains presented in (5-43). According to literature, there are different solvers and programing languages such as Maple [59], CGAL [60], MATLAB, etc. to find the minimum value of QP function numerically.

The first element of optimal inputs will be applied to the plant as the MPC control signal. The MPC design parameters are presented in Table 5-4. In the following, the result of simulation, found by using the quadratic programing solver of MATLAB, for the brake system with a MPC is shown.

Table 5-4 MPC design parameters

Property	Value
$\boldsymbol{N}$	5
$\boldsymbol{Q}$	$\begin{bmatrix} 9.5\times10^{-10} & 0 \\ 0 & 0 \end{bmatrix}$
$\boldsymbol{\bar{R}}$	$9.87\times10^{-2}\,I_{5\times5}$

The simulation results are shown in the Figure 5-12 to Figure 5-14 .

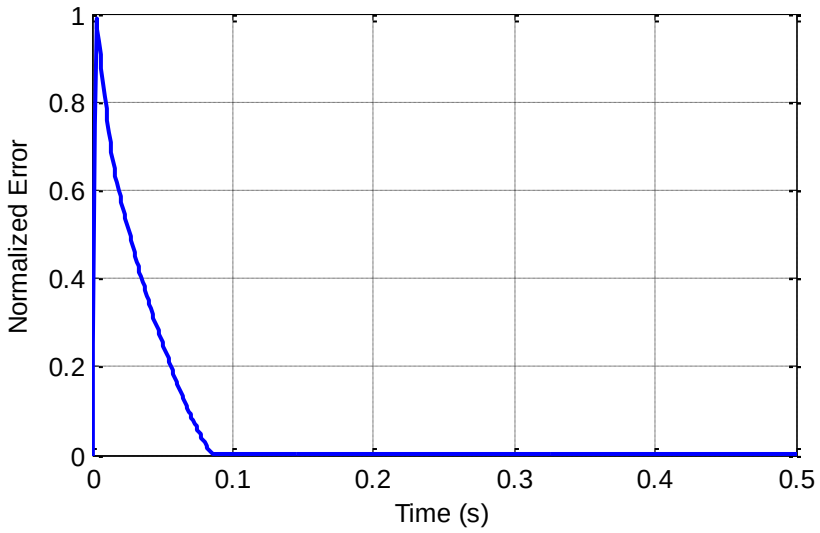

Figure 5-12 Error between the target and the actual pressure with MPC

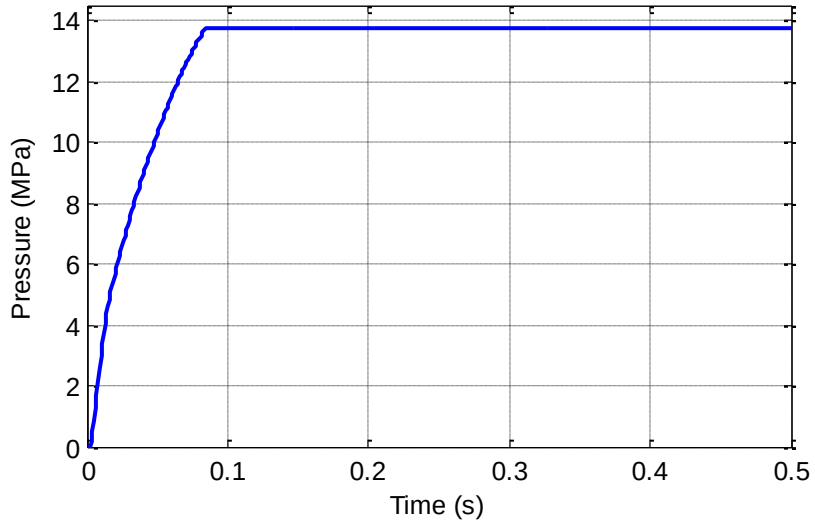

Figure 5-13 Closed loop tracking performance for MPC

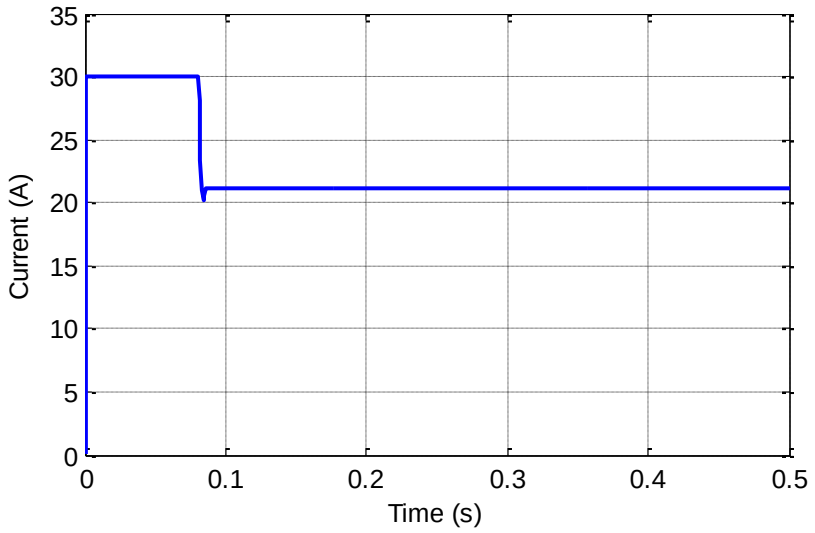

Figure 5-14 Control action of MPC

As shown in Figure 5-13, the plant pressure can reach the desired pressure smoothly without any overshoot or chattering. Figure 5-14 presents the control action signal, which is found by considering the existing physical limit for the brake system electric motor. The control action is on the upper limit before the response reaches to the desired value, then, it will reduce to the steady state current for keeping the pressure at the desired level.

5.4 Closed Loop Response to an Arbitrary Desired Value

As mentioned in previous section, to choose the best controller for the cam actuated brake system, it is not enough to consider the step response of the closed loop while the real braking process is a combination of increases and decreases in demanding braking pressure. A good controller has to be able to compensate any combination of braking pressure and to show reasonable behavior to the demanded arbitrary desired value. Figure 5-15 shows an arbitrary desired pressure and the closed loop response of the system with mentioned controllers in previous sections. The control action for the arbitrary reference with MPC and PI controller are shown in Figure 5-16. The SMC and ASMC outputs are not shown in this figure since they have too much chattering that make the figure unclear.

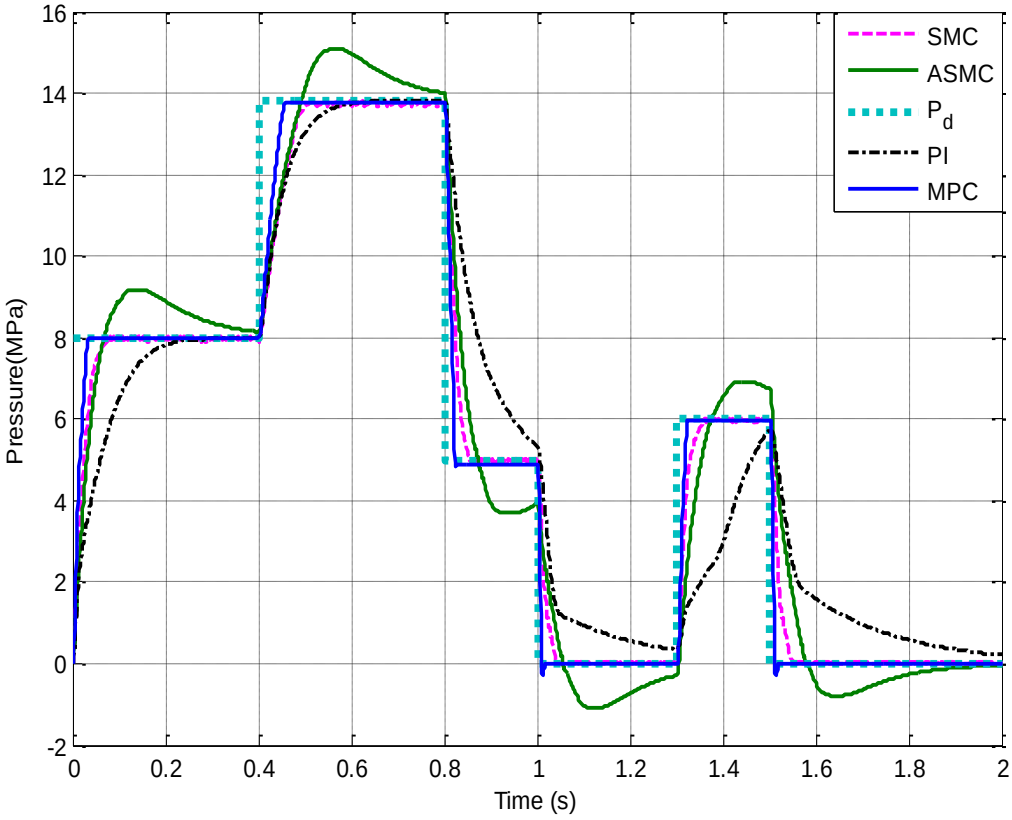

Figure 5-15 Closed loop response of cam actuated brake system to an arbitrary desired pressure

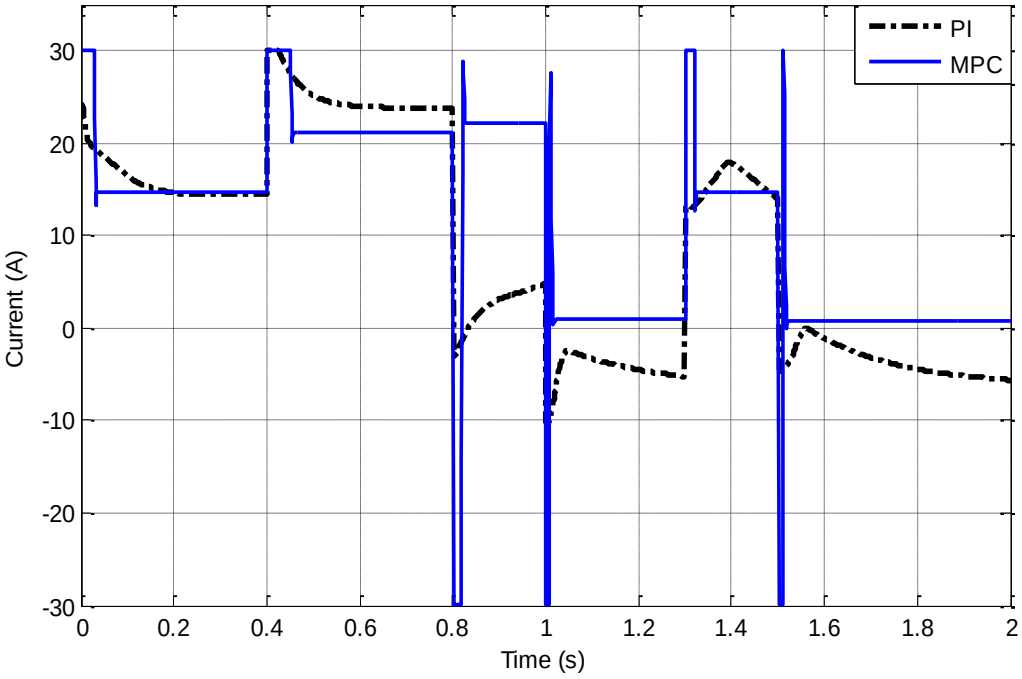

Figure 5-16 Control action of the PI, MPC and DISM-MPC controller for an arbitrary desired pressure

Figure 5-17 shows the normalized error between the desired and the actual pressure for different types of controller.

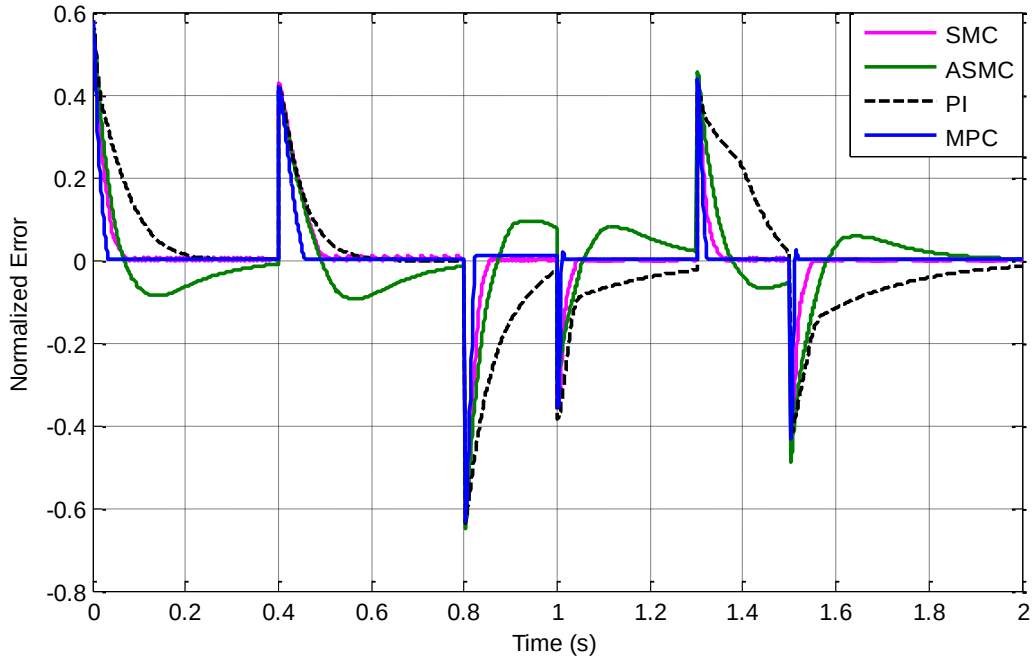

Figure 5-17 Error between arbitrary desired pressure and actual pressure for different types of controller

As shown in Figure 5-15, among all the controllers considered in this Chapter, the MPC controller has a better closed loop response in terms of tracking performance and speed of response. The response of the plant with MPC not only removes the overshoot (like the ASM controller), but it also eliminates the chatter.

5.5 MPC Robustness Performance

Based on the simulation results in the previous section, it can be concluded that the MPC controller may be the best choice for the cam actuated brake system. The only thing that should be examined before accepting MPC as the final answer is studying its behavior with the present parameter's uncertainty. It was assumed that the bulk modulus of the real system is 40% less than the value used for designing the controller. This can happen due to existence of air in the fluid of the brake system. Figure 5-18 shows the closed loop response of the system for β value used during the controller design and the reduced bulk modulus.

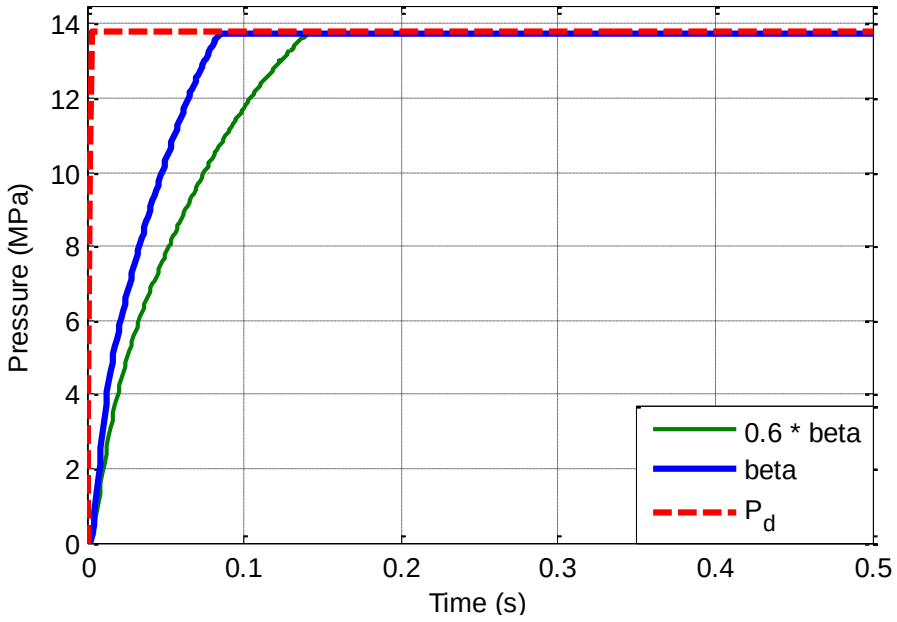

Figure 5-18 The effect of Bulk modulus changes as a parameter's uncertainty on closed loop response

Figure 5-18 indicates that although the bulk modulus had a considerable change, the response of the plant is still smooth without overshoot or any oscillation. Also, the time in which the actual pressure reaches the desired pressure did not increase dramatically.

In conclusion, according to the presented results for different types of the controller it is possible to state that the MPC controller can be used for the cam actuated brake system to provide good tracking and fast behavior in the presence of parameters' uncertainties such as variation of bulk modulus, and unknown friction forces.

5.6 Summary

In this chapter, the control design for cam actuated brake system was studied. The PI controller was first examined as the simplest form of controller in practical application. Then, a sliding mode controller was investigated for the brake system, which showed chattering in steady state response due to characteristics of the SMC. To remedy the chattering effect, the adaptive sliding mode controller (ASMC) was examined. Although the oscillations were eliminated, the closed loop response generates overshoot, which is not suitable for braking purposes. To take the input constraint into consideration, a model predictive control (MPC) was also studied. The results presented in this

chapter showed that among all the studied controllers, the MPC had the best behavior in terms of tracking and speed of response compared to the other types of controllers. Finally, the plant closed loop response with the MPC was examined while including a parameter uncertainty of bulk modulus changes in the braking fluid. The results showed that the MPC is a good controller for the cam actuated brake system if the computational load is not a major issue.

Chapter 6
Conclusions, Contributions and Future Work

6.1 Conclusions and Summary

In this thesis, a new, self-contained brake-by-wire mechanism (called the cam actuated brake system) was introduced.

To achieve the goal of this thesis, the following tasks were conducted:

- Design and modelling of the cam actuated brake system: the subsystems of the cam actuated brake system were explained and the mathematical model of each subsystem was presented. These subsystems are electric, mechanical and hydraulic. The main component of the mechanical section is an electric motor, which is the braking system power provider. The mechanical subsystem consists of a gear and a cam-follower mechanism to amplify the electric motor torque and to change rotational motion to the cylinder's displacement. The actuator cylinder, wheel cylinder, and the cut-off valve are the main parts of the hydraulic subsystem that create the necessary pressure for braking. The frequency analysis showed that considering the braking pad as a rigid and neglecting wheel cylinder displacement is a valid assumption. Therefore, the dynamic model of brake system with the motor current as the input and the actuation cylinder's displacement as the output of the system was determined.

- Design optimization: the main parameters of the cam actuated brake system were identified and then optimized. The optimized parameters are cam base circle radius, follower radius, follower eccentricity value, gear ratio, and cam profile. The objective of the optimization was finding these parameters so that the braking pressure reaches to pre-defined target pressure in the shortest possible time with respect to existing mechanical constraints. The optimization algorithm was a two-layer algorithm in which the direct search and the genetic algorithm (GA) were combined. The GA method was used to find the cam geometric parameters and gear ratio. The direct search method was applied to calculate the best possible profile for the cam.

  The results showed that the designed system can reach the target pressure in an acceptable response time when simulated in open-loop form.

- Control design: different types of controllers were designed, and simulated for the cam actuated brake system. The controllers considered in this work include the PI controller, the Sliding Mode Controller, the Adaptive Sliding Mode Controller, and the Model Predictive Controller.

  There are some limitations for brake systems that should be considered in control design. These limitations include keeping in mind the maximum allowable current in the electric motor and making sure that the braking pressure is free from any high frequency chattering. Among the examined controllers, the MPC method showed the best possible response in tracking the target pressure and creating a chatter free response. This controller could calculate the input of the system, motor's current, while it concurrently considered the input constraint during the calculations.

6.2 Contributions

Completing the above tasks led to the following contributions achieved during this research:

- Being self-contained and having redundancy: the designed cam actuated brake system is a modular brake mechanism. Each braking module can be installed on each wheel and connected to the electronic control unit separately. Therefore each wheel participates in braking process individually as a self-contained brake system. Individual control of brake modules creates redundancy for the braking system. If one of the modulus does not work properly, the other three can provide necessary braking torque for stopping the vehicle or reducing the vehicle speed.
- Adding fail-safe characteristic for the cam actuated brake mechanism: the designed brake system keeps the direct connection between the driver and the braking pad through the switching. In case of malfunction in cam actuated brake mechanism the switching valve disconnect the cam system and connect the secondary brake system, which is activated by the driver force directly, to provide necessary braking pressure for the system.
- Providing fast response time for changing the brake pressure: the created variable amplification by cam mechanism can compensate the low amount of torque provided by the motor at vehicle high speed. Therefore the response time can be improved compared to the mechanism used ball crew in transferring torque from motor to braking pad.

6.3 Future Work

To have the cam actuated brake mechanism as a practical brake system for vehicles, the following directions for future research are suggested:

- The design parameters optimization was done by considering the boundary conditions and the cam pressure angle constraint. Although these constraints were the most important conditions during the conceptual development of the system, there are other additional limitations such as manufacturing constraints and manufacturer supply limitations that have to be considered during the optimization process.
- After examining different type of controller, it was concluded that the MPC is the proper type of control strategy for the cam actuated brake mechanism. Some further studies will be done on stability and feasibility of the MPC controller to make sure that it can provide a good performance for the system in all possible conditions.
- The performance of the developed brake system and the results of simulation can be validated by having a prototype of the mechanism. Two phases can be defined for experimental studies. In the first phase, a table top set up can be built to examine the performance of the system. Upon satisfactory performance, the designed brake system should be implemented on a real vehicle to examine the performance of the cam actuated brake in real driving conditions

Appendix A

Secondary Brake System Mechanism

The secondary brake system has the role of fail-safe brake mechanism for the designed brake system. Its structure is similar to the conventional brake system installed on the vehicles and it is activated by the driver's force applied to the brake pedal.

A Secondary brake system consists of a brake pedal, a booster, a master cylinder, a caliper (cylinder, piston and braking pad) and a braking disk. In this section, mathematical models of these parts are explained. The general form of the system is shown in Figure A- 1. The driver's force causes a displacement in the pedal. This force causes a displacement in the brake pedal that then transfers to the booster through the push rod. The booster amplifies the force and pushes the master cylinder forward when the brake is applied. The movement of master cylinder's piston changes the volume of the master cylinder subsequently moving the braking oil from master cylinder to the wheel cylinder of the caliper and increasing the pressure behind the braking pad.

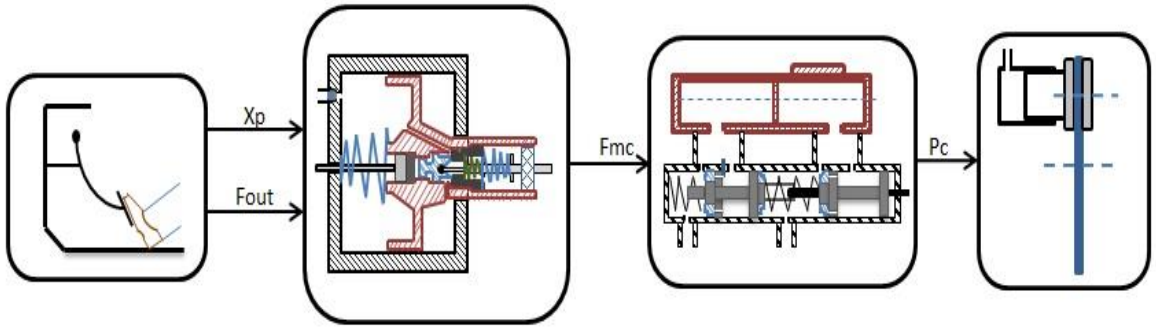

Figure A- 1 Secondary brake system configuration

In the following the mathematical model of each shown subsystems in Figure A- 1 is explained.

Brake pedal

The driver's force on the pedal is amplified by the pedal linkage and the pedal ratio set for the pedal mechanism. As shown in Figure A- 1, the transmitted force to the rest of the system (F_{out}) is the multiplication of the driver's pedal force and the pedal ratio as shown in Equation (A-1).

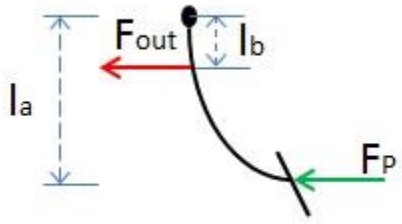

Figure A- 2 Pedal linkage

$$F_{out} = \frac{l_a}{l_b} F_p \tag{A-1}$$

Booster

To reduce the driver's effort in providing the necessary force for the master cylinder, there is a device between the pedal push rod and the master cylinder called the booster shown in Figure A- 3. The main function of the booster is to assist the driver's pedal force in pressurizing the master cylinder. As it is shown in Figure A- 3, one of the two chambers of the booster is a vacuum chamber. The vacuum is provided by the induction manifold in vehicles with an Internal Combustion Engine (ICE), and the other vacuum source is used in electrical or hybrid cars to provide assistant for the driver during braking process. This is done to assist the driver's effort in pressurizing the output fluid of the master cylinder.

The vacuum booster is comprised of two chambers separated by a diaphragm; as previously explained, the first chamber is connected to the atmospheric pressure while the second chamber is connected to the vacuum source. When the brake is not applied, the pressure of both chambers is equal to the vacuum source pressure. When the brake is activated, the pressure of the chamber connected to the vacuum source stays constant. Meanwhile, the air goes to the other chamber through the air valve. The pressure difference produces a force on the diaphragm, which is transmitted to the master cylinder through the reaction disk. While the brake pedal is on hold, the pressure of both sides remains unchanged. When the driver reduces the pedal force and releases the braking pedal, the return and outer springs move the push rod to the right and close the air valve. In the meantime, the vacuum valve opens and the pressurized air moves from the first chamber to the second one reducing the boosting effect.

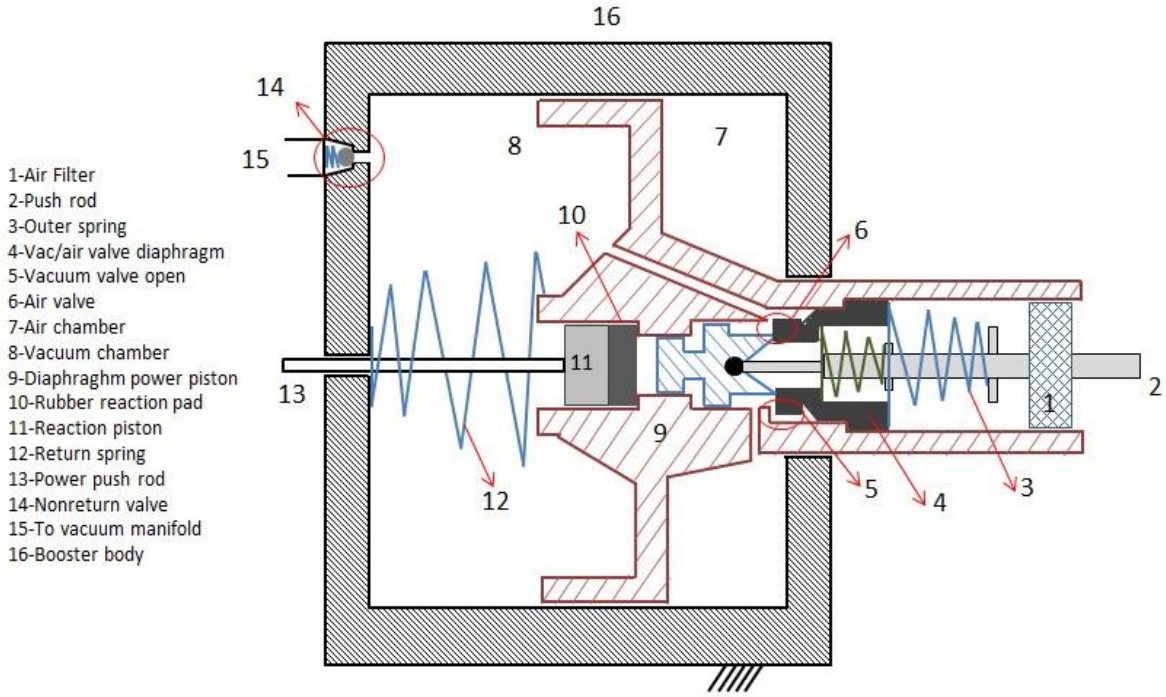

Figure A- 3 Cross sectional area of booster

The vacuum booster model is mathematically formulated in the following paragraphs. The pressure difference is applied on the effective booster area (A_B), which is the difference between the diaphragm and push rod area as:

$$A_B = \frac{\pi}{4} D_d^2 - \frac{\pi}{4} D_{pr}^2 \tag{A-2}$$

where D_d is diaphragm diameter, and D_{pr} is push rod diameter.

The vacuum that the booster can hold in time is indicated by mechanical efficiency. The vacuum capacity can change by the temperature and altitude. Now the boost force (F_B) produced by the effective pressure (pressure difference) for the booster is calculated by:

$$F_B = P_B A_B \eta = (P_a - P_v) A_B \eta \tag{A-3}$$

where P_B, P_v and P_a are the effective pressure, the pressure of the second chamber and that of the first chamber, respectively. η is the mechanical efficiency of the booster.

As shown in Figure A- 3, there is a return spring in the back of the diaphragm on the second chamber that functions to return the diaphragm to its initial position after releasing the brake pedal at the end of the braking process. Using a free body diagram of the diaphragm, the displacement of the diaphragm can be found. These applied forces include the force created by the pressure difference on both sides of the diaphragm, the return spring force, forces created by the rubber reaction disk, and the damping force produced by the sealing inside the booster. This results in:

$$F_B - F_{rs} - F_{rrd} - F_s = M_d \ddot{x}_d \tag{A-4}$$

where F_B, F_{rs} , F_{rrd} and F_s are the boosting force, the return spring force, the rubber reaction pad force and the sealing damping force. M_d is the diaphragm mass and $\ddot{x}_d$ is the diaphragm acceleration.

The difficult part in modeling the booster is finding the first chamber pressure (P_{ai}, i indicates the value of the first chamber at each instant during the brake process) of the booster because the value of these pressures depend on the mass of air that enters to or releases from each chamber.

There are two orifice valves in the vacuum booster as shown in Figure A- 3. One is called a vacuum valve, and it is between two chambers that are closed immediately when brake is applied; the other orifice valve is called an air valve, and is located between the atmospheric pressure and the first chamber. When air enters the first chamber, the diaphragm is moved to the left by the effective boost force. If it is assumed that the air in the booster chamber is an ideal gas undergoing isothermal expansion or compression, the instant pressure of the first chamber can be calculated by:

$$P_{ai} V = M_{air} R T \tag{A-5}$$

where V is the volume of first chamber, M_{air} is the mass of air inside the first chamber, R is specific gas constant which is equal to 287.04 [J/kgK], and T is the gas temperature.

The total volume of the first chamber is calculated by the summation of initial volume and change of volume at each instant stem as:

$$V = V_0 + A_d x_d \tag{A-6}$$

where V_0 is initial volume of the first chamber, A_d is the diaphragm area and x_d is the diaphragm displacement. The transmitted air mass through the inlet orifice valve is calculated by the air flow into the first chamber through the orifice of air valve as:

$$M_{air} = \int_{t_0}^{t} \rho Q dt \tag{A-7}$$

$$Q = C_d A_{or} \sqrt{\frac{2\Delta P}{\rho}} = C_d A_{or} \sqrt{\frac{2(P_{atm} - P_{ai})}{\rho}} \tag{A-8}$$

where C_d is orifice discharge coefficient and A_{or} is orifice open area. The orifice open area can be found as follows giving different signs for applying and releasing the brake pedal by the driver:

$$A_{or} = w x_{or} = \begin{cases} w\,(x_p - x_d) & Apply \\ w\,(x_d - x_p) & Release \end{cases} \tag{A-9}$$

where w is the width of the orifice opening, x_p and x_d are push rod and diaphragm displacement.

The mass inside the first chamber in the three phases of braking (apply, hold and release) can be written as:

$$M_{air} = \begin{cases} \int_{t_0}^{t} \rho\, C_d w (x_p - x_d) \sqrt{\frac{2(P_{atm} - P_{ai})}{\rho}}\, dt + M_{i-1} & Apply \\ M_{i-1} - C_{leak}(P_{ai} - P_v) & Hold \\ \int_{t_0}^{t} \rho\, C_d w (x_d - x_p) \sqrt{\frac{2(P_{ai} - P_v)}{\rho}}\, dt + M_{i-1} & Release \end{cases} \tag{A-10}$$

where M_{i-1} is the existing mass inside the first chamber at previous time step and C_{leak} is the leakage coefficient between first and second chamber.

Master cylinder

The cross sectional view of the master cylinder is shown in Figure A- 4.

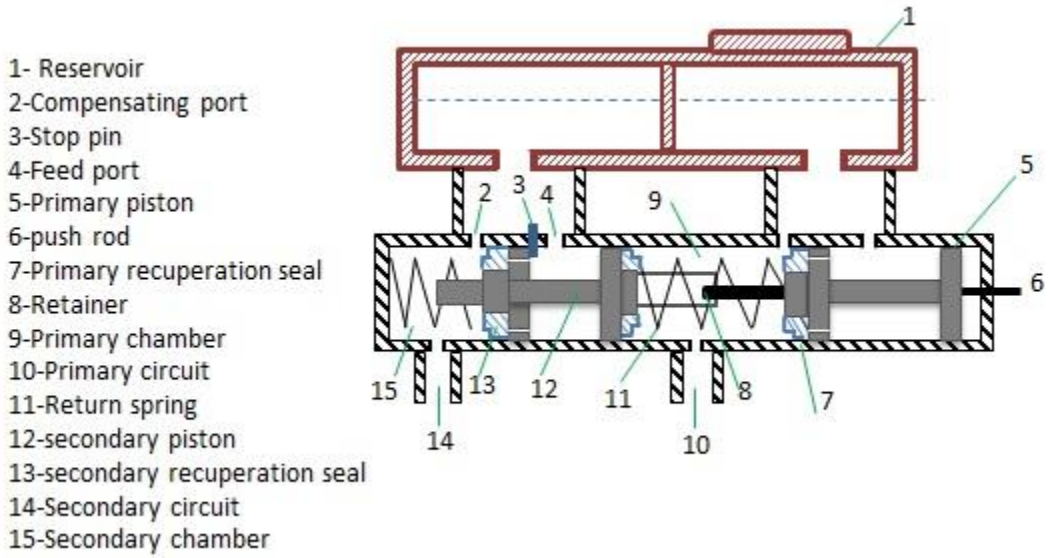

Figure A- 4 Cross sectional view of master cylinder

The master cylinder, instead of being modeled as a double circuit model, can be modeled as a single circuit model with a primary piston and a cylinder structure [61] as it is shown in Figure A- 5. The input master cylinder force moves the primary piston to the left. There are some opposing forces against the master cylinder's input force. As it is shown, the piston movement compresses the braking fluid in the master cylinder so that the master cylinder's internal pressure increases. There are springs inside the master cylinder that assist in returning the master cylinder to its initial position when the braking process ends. The spring reaction force is another opposing force in addition to the braking fluid damping force. The dynamic equation of the master cylinder is given by:

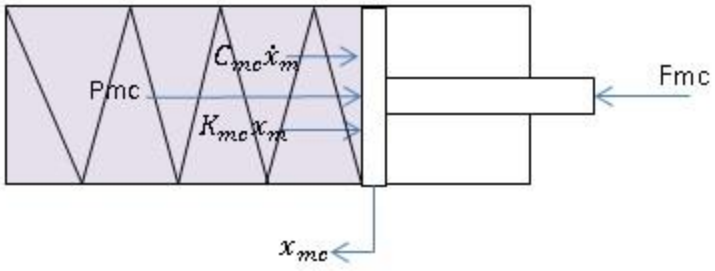

Figure A- 5 Free body diagram of primary piston of master cylinder

$$F_{mc} - P_{mc}A_{mc} - C_{mc}\dot{x}_{mc} - K_{mc}x_{mc} = M_{mc}\ddot{x}_{mc} \tag{A-11}$$

where F_{mc} is the input force of the master cylinder applied by the booster, P_{mc} is the master cylinder pressure, C_{mc}, K_{mc}, M_{mc} are damping coefficients of piston seal, spring stiffness, and master cylinder mass, respectively. $x_{mc}, \dot{x}_{mc}, \ddot{x}_{mc}$ refer to the displacement, velocity, and acceleration of the master cylinder, respectively.

To find the effect of the wheel cylinder on the master cylinder displacement, additional equations are considered. One is the equality between the output flow of the master cylinder and the transmitted flow from the pipe, which can be written as:

$$Q_{out-MC} = Q_{pipe} \tag{A-12}$$

$$Q_{out-MC} = A_{mc}\dot{x}_{mc} - \dot{V}_{cmc} = A_{mc}\dot{x}_{mc} - \frac{\dot{P}_{mc}V_{0mc}}{\beta_{oil}} \tag{A-13}$$

$$Q_{pipe} = sgn(P_{mc} - P_{wc})C_{qp}\sqrt{|P_{mc} - P_{wc}|} \tag{A-14}$$

where $\dot{V}_{cmc}$ and V_{0mc} are the rate of volume changes due to compressibility of oil inside the master cylinder and initial volume of the master cylinder, respectively. C_{qp} is flow coefficient.

The other is the equality between the volume of displaced oil out of the master cylinder and the changed volume in the wheel cylinder and pipe[61].

$$\Delta V_{mc} - \Delta V_{cmc} = \Delta V_{wc} - \Delta V_{cwc} - \Delta V_{ocp} - \Delta V_{pexp} \tag{A-15}$$

ΔV_{mc}, is the change of volume in master cylinder because of movement of push rod and ΔV_{cmc} is the change of volume inside the master cylinder due to compressibility of oil. ΔV_{wc} is the change of volume in the wheel cylinder. ΔV_{cwc} and ΔV_{ocp} are volume changes due to compressibility of oil inside the wheel cylinder and the pipe line. ΔV_{pexp} is the expansion of the pipe line.

It must be mentioned that V_{wc} can be found by considering the brake pad as a spring with its stiffness denoted by K_{pad}.

$$V_{wc} = A_{wc}x_{wc} = \frac{F_{pad}}{K_{pad}}A_{wc} = \frac{P_{wc}A_{wc}}{K_{pad}}A_{wc} = \frac{t_{pad}A_{wc}^2}{E_{pad}A_{pad}}\ P_{wc} \tag{A-16}$$

t_{pad} , E_{pad} and A_{pad} represent the thickness, the Young's modulus, and the area of the braking pad, respectively. A_{wc} is the cross sectional area of the wheel cylinder piston. To calculate volume changes due to compressibility of oil inside the pipe and expansion of pipe line in Equation (A-15), the

average pressure of wheel cylinder (P_{wc}) and master cylinder pressure (P_{mc}) are used in the bulk modulus expression.

$$A_{mc}x_{mc} - \frac{P_{mc}V_{mc}}{\beta_{oil}} = \frac{t_{pad}A_{wc}^2}{E_{pad}A_{pad}}\,P_{wc} + \frac{P_{wc}V_{0wc}}{\beta_{oil}} + \frac{(P_{mc}+P_{wc})V_{pipe}}{2\beta_{oil}} + \frac{(P_{mc}+P_{wc})V_{pipe}}{2\beta_{pipe}} \qquad \text{(A-17)}$$

V_{pipe} and β_{pipe} refer to the total volume and the bulk modulus of the pipe, respectively. β_{oil} is the bulk modulus of the oil and V_{0wc} is the initial volume of the wheel cylinder.

Braking caliper and disk

As shown in Figure A- 6, the output pressure of the master cylinder is applied to the brake caliper, and the resulting friction creates a braking force on the braking disk. By knowing the effective braking radius, we can determine the braking torque that participates in the braking process and acts as a negative torque in the longitudinal vehicle model. This torque is:

$$T_b = F_f r_{pad} = \mu_{pad} F_N r_{pad} = \mu_{pad} r_{pad} A_{pad} P_{wc} \qquad \text{(A-18)}$$

where F_f is the tangential force applied to the caliper, μ_{pad}, and r_{pad} are the effective friction coefficient and the effective radius of the braking pad, respectively.

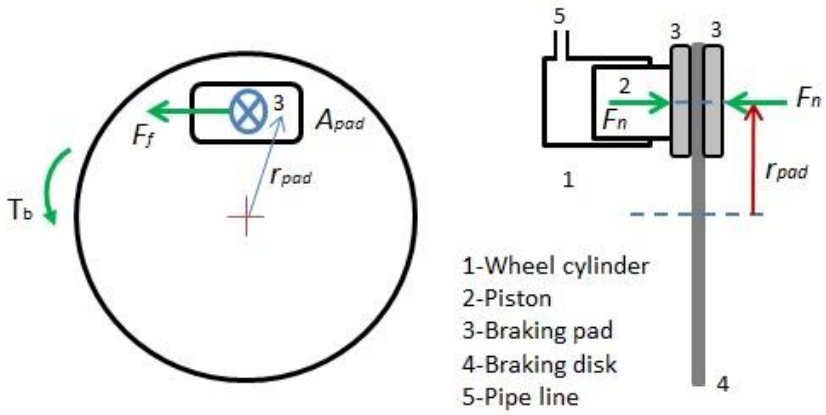

Figure A- 6 Free body diagram of the braking disk

Appendix B

Effective Bulk Modulus

The undissolved air in braking fluid can reduce the system bulk modulus considerably compared to the pure oil bulk modulus. Figure B- 1 which shows the combination of oil and undissolved air used to calculate the effective bulk modulus as:

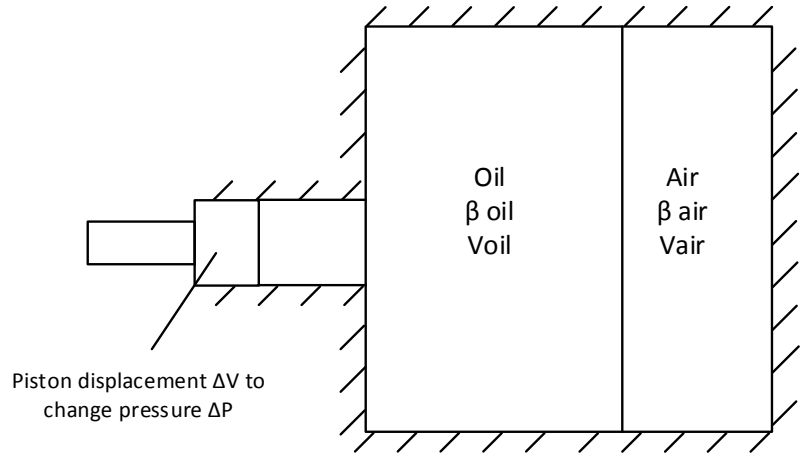

Figure B- 1 Bulk modulus of an oil and undissolved air mixture

Piston displacement creates a volume change of ΔV which increases the pressure inside the cylinder as ΔP. The volume change inside the cylinder is defined by the summation of the compression of the oil and of the air as:

$$\frac{1}{\beta_e} = -\frac{\Delta V}{\Delta P\, V} = -\frac{\Delta V_{oil} + \Delta V_{air}}{\Delta P\, V_T} \tag{B- 1}$$

where $\Delta V_{oil}, \Delta V_{air}\ and\ V_T$ are oil volume changes, air volume changes and the total volume. If the above equation rearranged, it conducts to:

$$\frac{1}{\beta_e} = \frac{1}{\beta_{oil}}\left(\frac{V_T - V_{air}}{V_T}\right) + \frac{1}{\beta_{air}}\,\frac{V_{air}}{V_T} \tag{B- 2}$$

since $\frac{V_{air}}{V_T} \ll 1$ the presented equation for effective bulk modulus can be simplified as:

$$\frac{1}{\beta_e} = \frac{1}{\beta_{oil}} + \frac{1}{\beta_{air}}\,\frac{V_{air}}{V_T} \tag{B- 3}$$

Appendix C

ASMC Stability Analysis

The global asymptotic stability of the sliding surface can be proved by two methods; a) examining asymptotically stability of Lineard equation; b) solving the sliding surface dynamic equation. These two methods are explained in the following.

a) Global asymptotic stability of Lineard equation:

If the calculated control action in (5-30) is inserted in $\ddot{P}$ equation ((5-23)), the closed-loop dynamic will be:

$$\dot{S} + KS = -E \tag{C- 1}$$

By replacing *E* with its definition ($E = \tilde{Z}_{est} - \tilde{Z}$), Equation (C- **1**) changes to:

$$\dot{S} + KS = -\tilde{Z}_{est} + \tilde{Z} \tag{C- 2}$$

$\tilde{Z}_{est}$ can be replaced by Equation (5-34), therefore (C- 2) is in the form of:

$$\dot{S} + KS + \int \Gamma S = \tilde{Z} \tag{C- 3}$$

Considering constant value for *K*, the derivative of Equation (C- 3) is:

$$\ddot{S} + K\dot{S} + \Gamma S = \dot{\tilde{Z}} \tag{C- 4}$$

The global asymptotic stability of a generalized second order equation in the form of $\ddot{x} + f(x)\dot{x} + g(x) = 0$ is studied in [62]. According to this reference, to have the global asymptotical stability, three conditions should be satisfied:

I. $xg(x) > 0$

II. $f(x) > 0$

III. $\lim_{x\to\infty} \int_0^x g(\xi)d\xi = \infty$ [63]

These aforementioned conditions have to be satisfied for closed-loop system presented in (C- 4). Considering the first condition for the system leads to:

$$S^2\left(\Gamma-\frac{\dot{\tilde{Z}}}{S}\right)>0 \implies S^2\Gamma - S\,\dot{\tilde{Z}}>0 \implies S^2\Gamma > S\dot{\tilde{Z}} \tag{C- 5}$$

$$\Rightarrow \begin{cases} S>0 \Rightarrow S\Gamma > \dot{\tilde{Z}} \Rightarrow \Gamma > \dot{\tilde{Z}}S^{-1} \\ S<0 \Rightarrow S\Gamma < \dot{\tilde{Z}} \Rightarrow \Gamma > \dot{\tilde{Z}}S^{-1} \end{cases}$$

It can be concluded that the first condition is satisfied if $\Gamma > \frac{\dot{\tilde{Z}}}{S}$. It is assumed that the lumped uncertainty rate is bounded as $\left|\dot{\tilde{Z}}\right| < \nu < \infty$. Therefore, $\Gamma > \frac{\dot{\tilde{Z}}}{S}$ can be satisfied everywhere except a small neighborhood of the sliding surface where$|S| < \delta$, if $\Gamma = \frac{\nu}{\delta}$. Thus, by considering the bounded rate for uncertainty assumptions, there is a Γ for which the first condition is satisfied everywhere except in the small neighborhood of the sliding surface.

Since the design parameter *K* is positive the second condition is satisfied, in the third condition by replacing *g(x)* with $S\left(\Gamma-\frac{\dot{\tilde{Z}}}{S}\right)$, it can be seen that:

$$\lim_{S\to\infty}\int_0^S \xi\left(\Gamma-\frac{\dot{\tilde{Z}}}{\xi}\right)d\xi = \infty \tag{C- 6}$$

Therefore, the closed-loop system in (C- 4) converges to the small neighborhood of the sliding surface by selecting proper control parameters (K, Γ).

b) Solving the sliding surface dynamic equation:

The sliding surface dynamic equation presented in (C- 3) is recalled here as follows.

$$\dot{S} + KS + \int \Gamma S = \tilde{Z} \tag{C- 7}$$

The design parameters *K* and Γ are diagonal positive definite; therefore, the vector differential equations of this equation are decoupled and can be treated as a scalar ordinary differential equation by considering each row of vector $\tilde{Z}$. The solution of the jth row of (C- 7) is shown in the following [53]:

$$
\begin{aligned}
& S_j(t) \\
& = D_1\, e^{\left(\frac{-K_j+\sqrt{K_j^2-4\Gamma_j}}{2}\right)t} + D_2 e^{\left(\frac{-K_j-\sqrt{K_j^2-4\Gamma_j}}{2}\right)t} \\
& + \left(\left(\left(\int \frac{d}{dt}\tilde{Z}_j(t) \right) e^{\left(\frac{K_j-\sqrt{K_j^2-4\Gamma_j}}{2}\right)t} dt \right) e^{\left(\frac{K_j+\sqrt{K_j^2-4\Gamma_j}}{2}\right)t} \right. \\
& \left. - \left(\left(\int \frac{d}{dt}\tilde{Z}_j(t) \right) e^{\left(\frac{K_j+\sqrt{K_j^2-4\Gamma_j}}{2}\right)t} dt \right) e^{\left(\frac{K_j-\sqrt{K_j^2-4\Gamma_j}}{2}\right)t} \right) \frac{e_j^{-tK}}{\sqrt{K_j^2-4\Gamma_j}}
\end{aligned}
\qquad \text{(C- 8)}
$$

where D_1 and D_2 are the integration constants calculated by considering the initial conditions, e denotes the exponential function, and j is the row number of the sliding surface.

Equation (C- 8) shows that by selecting proper values for K and Γ, the sliding surface will converge to the neighborhood of the sliding surface, $S(t)=0$.

Appendix D

Simulation Models

In this appendix, the simulation models designed and used in this current thesis are shown.

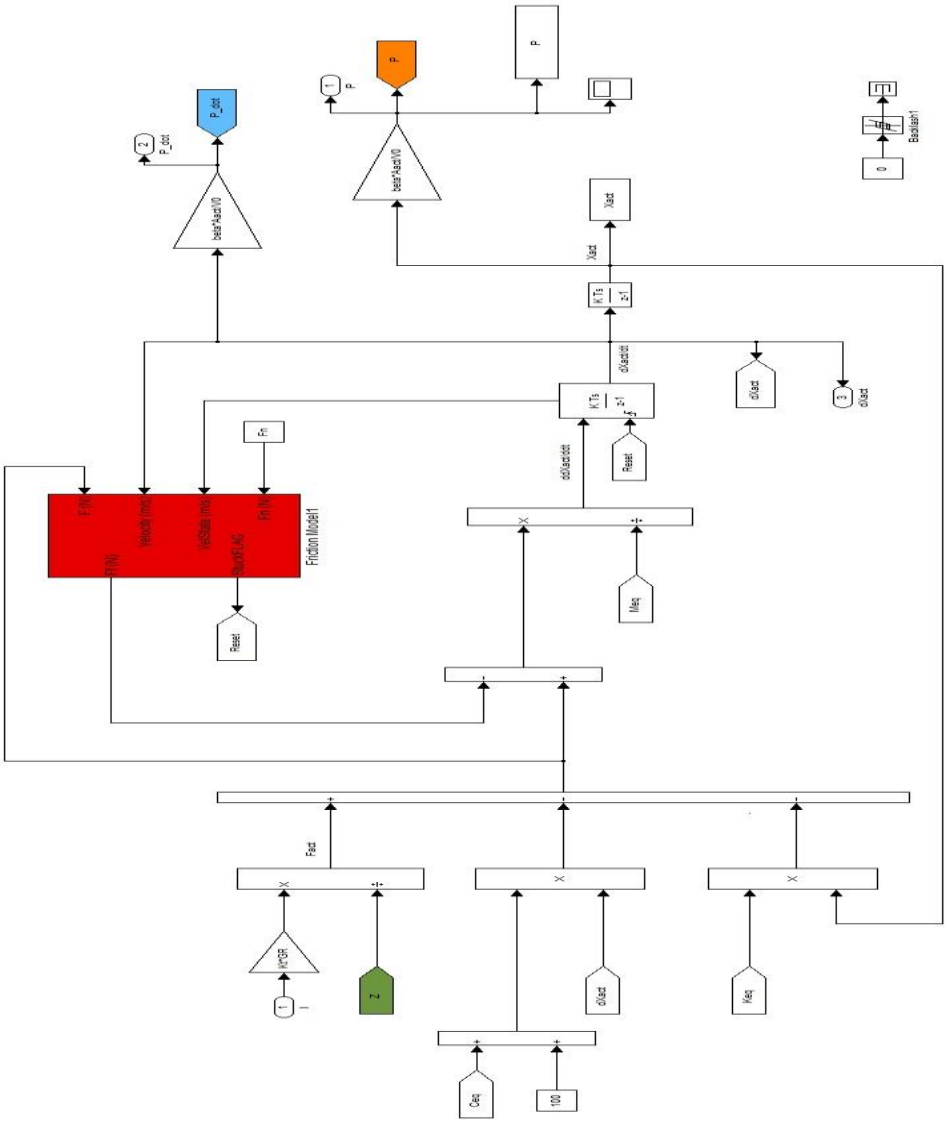

Figure D- 1 Plant simulation model

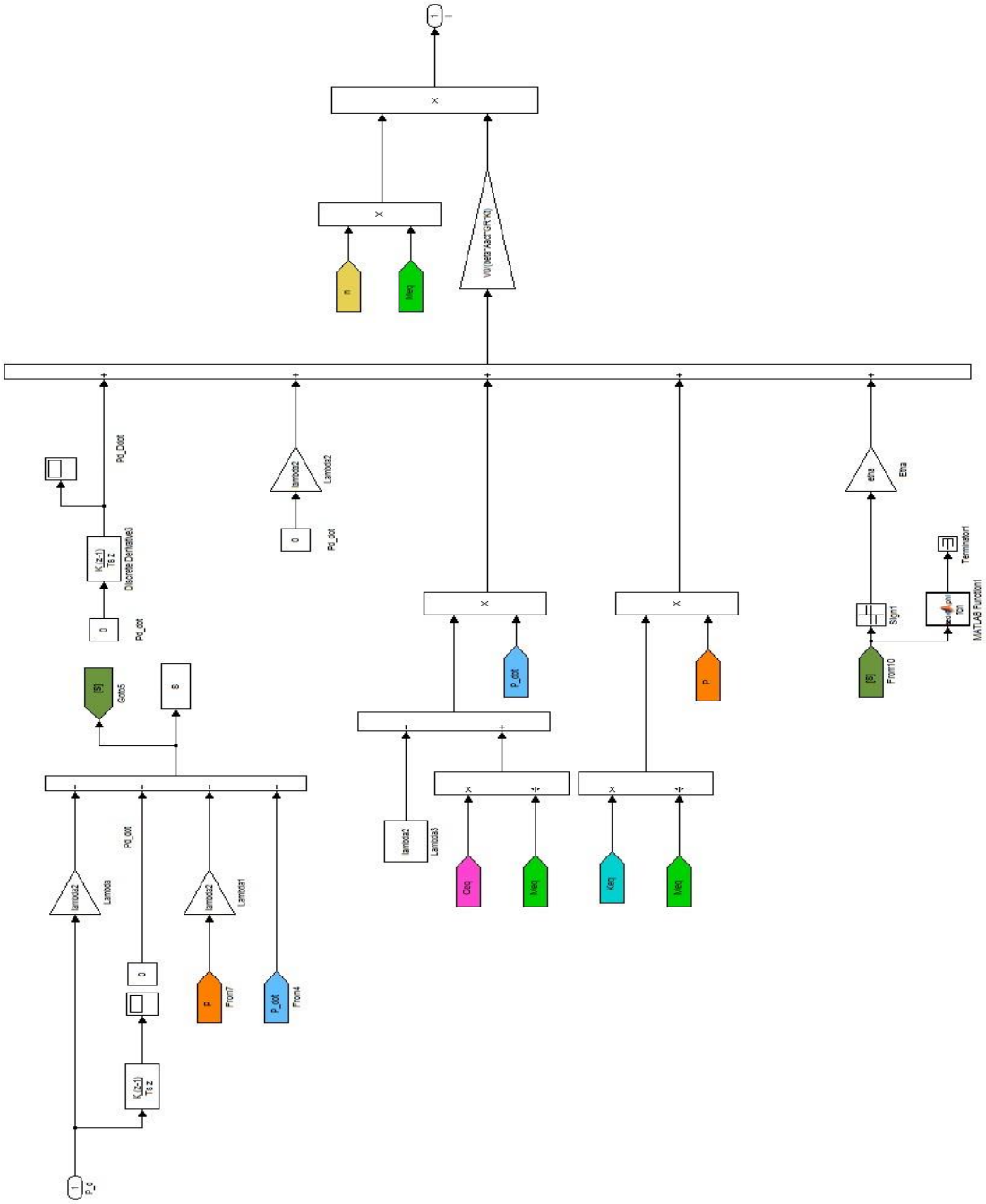

Figure D- 2 Sliding Mode Control simulation moel

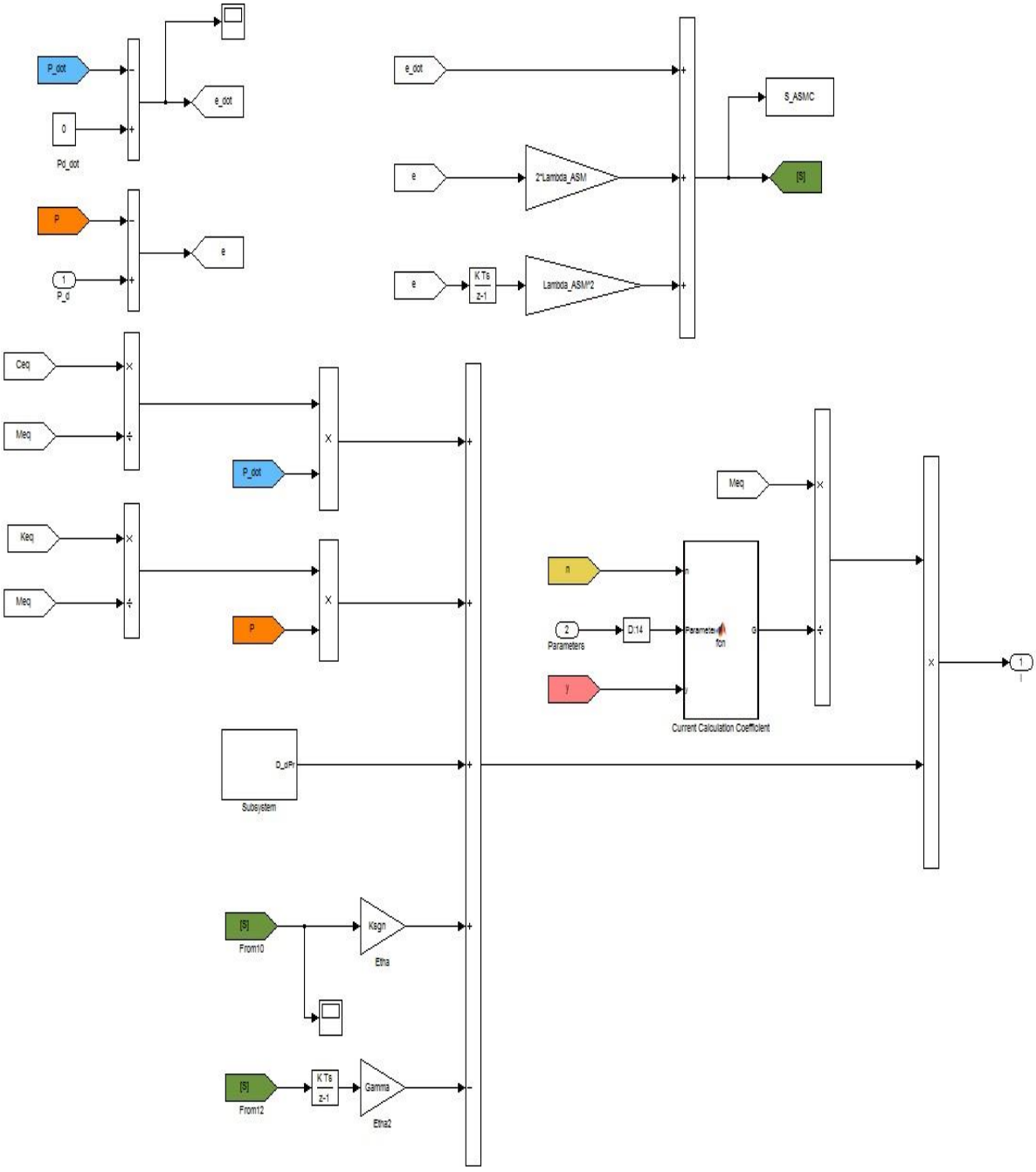

Figure D- 3 Adaptive Sliding Mode Control simulation model

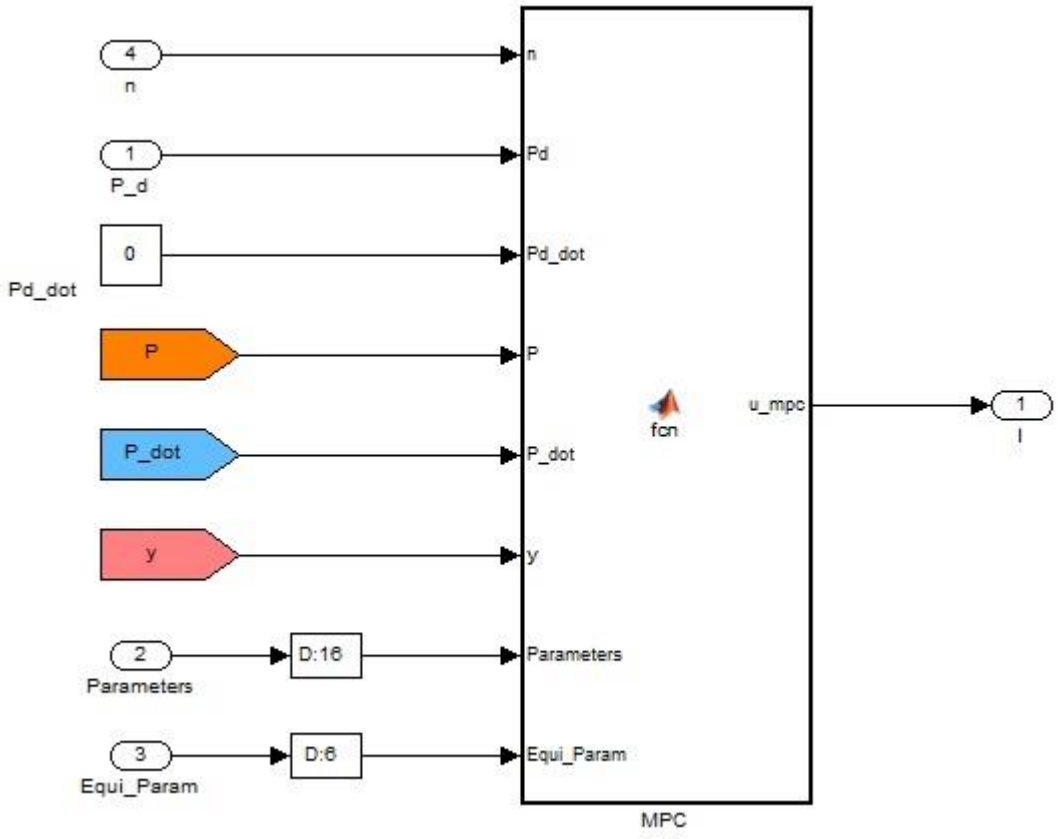

Figure D- 4 MPC simulation model

MPC Design Code

```
function u_mpc = fcn(n,Pd,Pd_dot,P,P_dot,y,Parameters,Equi_Param)
%#codegen

Meq_C=Equi_Param(4);
Keq_C=Equi_Param(5);
Ceq_C=Equi_Param(6);
beta_C=Parameters(16);
Aact=Parameters(2);
GR=Parameters(3);
Kt=Parameters(4);
V0=Parameters(5);
Rb=Parameters(10);
Rr=Parameters(11);
e=Parameters(12);

Z=((sqrt((Rb+Rr)^2-e^2)+y)/((e*(sqrt((Rb+Rr)^2-e^2)+y))+((Rb+Rr+y)*(n-
e))))*(GR*Kt);
```

```
u_mpc=0;
%==========================================================================
=
%%
Xd=[Pd;Pd_dot]; X0=[P;P_dot];

DeltaT=0.001;
n_s=2;

Ks0=0;%100;
C0=100;

Keq2=Keq_C+Ks0;                 % Oil stiffness
Beq2=Ceq_C+C0;                  % Equivalent damping in actuator side

Ac=[0 1;-Keq2/Meq_C -Beq2/Meq_C];
Bc=[0;GR*beta_C*Aact*Kt*Z/(Meq_C*V0)];

A = expm(Ac*DeltaT);
Bd_p = Ac\(A - eye(2,2));
B = Bd_p *Bc;

N=5;
Sx=zeros(n_s*(N+1),n_s);    X_desire=zeros(n_s*(N+1),1);
for r=1:N+1
    Sx(n_s*(r-1)+1:n_s*r,:)=A^(r-1);
    X_desire(n_s*(r-1)+1:n_s*r,:)=Xd;
end

Su=zeros(n_s*(N+1),N);
lb=zeros(N,1);
ub=zeros(N,1);

lb2=-30;
ub2=30;


for r=1:N
    for c=1:r
        Su(2*r+1:2*(r+1),c)=(A^(r-c))*B;
    end
    lb(r,:)=lb2;
    ub(r,:)=ub2;
end

Q=[1 0;0 0];
q=9.5229e-10;     % weigth of each state, eleman of matrix

Q_bar=zeros(n_s*(N+1),n_s*(N+1));

for r=1:N+1
```

```
    Q_bar(n_s*(r-1)+1:n_s*r,n_s*(r-1)+1:n_s*r)=q*Q;
end

r=9.8708e-2;%weight of inputs, inputs are n(amplification ratio) for this
problem
R_bar=r*eye(N);

H2=((Su')*Q_bar*Su)+R_bar;
F=(2*X0'*Sx'*Q_bar*Su)-(2*X_desire'*Q_bar*Su);
Hqp=2*(H2+H2')/2;
Fqp=1*F;

coder.extrinsic('optimset','quadprog')
%options = optimset( 'Algorithm' , 'interior-point-convex');
I2=quadprog(Hqp,Fqp,[],[],[],[],lb,ub,[]);

output=zeros(1,N);
output(1,1)=1;
current=output*I2;
u_mpc=current;
```

Bibliography

[1] R. Bosch, *Bosch automotive handbook*. Vol 74. Bentley, Cambridge, 2004.

[2] C. Line, C. Manzie, and M. C. Good, "Electromechanical brake modeling and control: from PI to MPC," *Control Syst. Technol. IEEE Trans.*, vol. 16, no. 3, pp. 446–457, 2008.

[3] J. Fox, R. Roberts, C. Baier-Welt, L. M. Ho, L. Lacraru, and B. Gombert, "Modeling and control of a single motor electronic wedge brake," No. 2007-01-0866. SAE Technical Paper, 2007.

[4] Z. Wang, L. Yu, Y. Wang, C. You, L. Ma, and J. Song, "Prototype of distributed electro-hydraulic braking system and its fail-safe control strategy," No. 2013-01-2066. SAE Technical Paper, 2013.

[5] B. Breuer and K. H. Bill, *Brake technology handbook*. 2008.

[6] N. Manring, *Hydraulic control systems*. Wiley, 2005.

[7] D. F. Reuter, E. W. Lloyd, J. W. Zehnder, and J. A. Elliott, "Hydraulic design considerations for EHB systems," No. 2003-01-0324. SAE Technical Paper, 2003.

[8] A. L. Harris, "Electro-hydraulic braking system." U.S. Patent No. 6,588,855, 08-Jul-2003.

[9] D. S. Crombez, "Electro-Hydraulic Brake Brake-By-Wire System and Method." U.S. Patent Application 12/702,378., 09-Feb-2010.

[10] Y. Hwang, "Electro-hydraulic brake system." U.S. Patent Application 11/524,760, 20-Sep-2006.

[11] A. Kusano and T. Kuno, "Hydraulic brake system for vehicles." U.S. Patent No.6,709,072., 23-Mar-2004.

[12] U. Gottwick and M. Kunz, "Electrohydraulic braking system." U.S. Patent No. 7,770,982., 10-Aug-2010.

[13] W.-R. Pasterkamp and W. Quirant, "Hydraulic vehicle braking system." U.S. Patent No. 6,733,090., 11-May-2004.

[14] E. Nakamura, M. Soga, A. Sakai, A. Otomo, and T. Kobayashi, "Development of electronically controlled brake system for hybrid vehicle," No. 2002-01-0300. SAE Technical Paper, 2002.

[15] M. Soga, M. Shimada, J.-I. Sakamoto, and A. Otomo, "Development of vehicle dynamics management system for hybrid vehicles: ECB system for improved environmental and vehicle dynamic performance," *JSAE Rev.*, vol. 23, no. 4, pp. 459–464, 2002.

[16] M. Park, S. Kim, L. Yang, and K. Kim, "Development of the control logic of electronically controlled hydraulic brake system for hybrid vehicle," No. 2009-01-1215. SAE Technical Paper, 2009.

[17] C. von Albrichsfeld and J. Karner, “Brake system for hybrid and electric vehicles,” No. 2009-01-1217. SAE Technical Paper, 2009.

[18] Z. L. Jin, Y. Q. Zhao, R. K. Shi, L. S. Guo, and Z. T. Shi, “Modeling and Analysis of Electro Hydraulic Brake System Based on AMESim/Matlab,” in *Advanced Materials Research*, 2012, vol. 383, pp. 1994–1999.

[19] V. Milanés, C. González, J. E. Naranjo, E. Onieva, and T. De Pedro, “Electro-hydraulic braking system for autonomous vehicles,” *Int. J. Automot. Technol.*, vol. 11, no. 1, pp. 89–95, 2010.

[20] D. H. Kim, J. M. Kim, S. H. Hwang, and H. S. Kim, “Optimal brake torque distribution for a four-wheeldrive hybrid electric vehicle stability enhancement,” *Proc. Inst. Mech. Eng. Part D J. Automob. Eng.*, vol. 221, no. 11, pp. 1357–1366, 2007.

[21] N. D’alfio, A. Morgando, and A. Sorniotti, “Electro-hydraulic brake systems: design and test through hardware-in-the-loop simulation,” *Veh. Syst. Dyn.*, vol. 44, no. sup1, pp. 378–392, 2006.

[22] S. Anwar, “An anti-lock braking control system for a hybrid electromagnetic/electrohydraulic brake-by-wire system,” in *American Control Conference, 2004. Proceedings of the 2004*, 2004, vol. 3, pp. 2699–2704.

[23] S. Semmler, R. Isermann, R. Schwarz, and P. Rieth, “Wheel slip control for antilock braking systems using brake-by-wire actuators,” No. 2003-01-0325. SAE Technical Paper, 2003.

[24] D. Kim and H. Kim, “Vehicle stability control with regenerative braking and electronic brake force distribution for a four-wheel drive hybrid electric vehicle,” *Proc. Inst. Mech. Eng. Part D J. Automob. Eng.*, vol. 220, no. 6, pp. 683–693, 2006.

[25] C. F. Lee, “Brake force control and judder compensation of an automotive electromechanical brake,” 2013.

[26] C. L. J. Line, “Modelling and control of an automotive electromechanical brake,” 2007.

[27] C. Jo, S. Hwang, and H. Kim, “Clamping-force control for electromechanical brake,” *Veh. Technol. IEEE Trans.*, vol. 59, no. 7, pp. 3205–3212, 2010.

[28] R. Hoseinnezhad, A. Bab-Hadiashar, and T. Rocco, “Real-time clamp force measurement in electromechanical brake calipers,” *Veh. Technol. IEEE Trans.*, vol. 57, no. 2, pp. 770–777, 2008.

[29] C. F. Lee and C. Manzie, “Adaptive Brake Torque Variation Compensation for an Electromechanical Brake,” No. 2012-01-1840. SAE Technical Paper, 2012.

[30] C. F. Lee, C. Manzie, and C. Line, “Explicit nonlinear MPC of an automotive electromechanical brake,” *IFAC Proc. Vol.*, vol. 17, no. 1 PART 1, pp. 10758–10763, 2008.

[31] H. Olsson, K. J. Åström, C. C. De Wit, M. Gäfvert, and P. Lischinsky, "Friction models and friction compensation," *Eur. J. Control*, vol. 4, no. 3, pp. 176–195, 1998.

[32] Y. Lee and W.-S. Lee, "Hardware-in-the-loop Simulation for Electro-mechanical Brake," in *SICE-ICASE, 2006. International Joint Conference*, pp. 1513–1516, 2006.

[33] J. K. Ahn, K. H. Jung, D. H. Kim, H. B. Jin, H. S. Kim, and S. H. Hwang, "Analysis of a regenerative braking system for hybrid electric vehicles using an electro-mechanical brake," *Int. J. Automot. Technol.*, vol. 10, no. 2, pp. 229–234, 2009.

[34] M. Kees, K. J. Burnham, F. P. Lockett, J. H. Tabor, and R. A. Williams, "Hydraulic actuated brake and electromechanically actuated brake systems," 2001.

[35] B. Hartmann, H., Schautt, M., Pascucci, A., and Gombert, "eBrake® - The Mechatronic Wedge Brake," in *No. 2002-01-2582. SAE Technical Paper*, 2002.

[36] C. H. Jo, S. M. Lee, H. L. Song, Y. S. Cho, I. Kim, D. Y. Hyun, and H. S. Kim, "Design and control of an upper-wedge-type electronic brake," *Proc. Inst. Mech. Eng. Part D J. Automob. Eng.*, vol. 224, no. 11, pp. 1393–1405, 2010.

[37] R. Roberts, M. Schautt, H. Hartmann, and B. Gombert, "Modelling and validation of the mechatronic wedge brake," No. 2003-01-3331. SAE Technical Paper, 2003.

[38] R. Roberts, B. Gombert, H. Hartmann, D. Lange, and M. Schautt, "Testing the mechatronic wedge brake," No. 2004-01-2766. SAE Technical Paper, 2004.

[39] L. Balogh, T. Streli, H. Nemeth, and L. Palkovics, "Modelling and simulating of self-energizing brake system," *Veh. Syst. Dyn.*, vol. 44, no. sup1, pp. 368–377, 2006.

[40] L. M. Ho, R. Roberts, H. Hartmann, and B. Gombert, "The electronic wedge brake-EWB," No. 2006-01-3196. SAE Technical Paper, 2006.

[41] Á. Semsey and R. Roberts, "Simulation in the development of the electronic wedge brake," No. 2006-01-0298. SAE Technical Paper, 2006.

[42] J. G. Kim, M. J. Kim, J. K. Kim, and K.-H. Noh, "Developing of electronic wedge brake with cross wedge," No. 2009-01-0856. SAE Technical Paper, 2009.

[43] K. Han, K. Huh, W. Hwang, M. Kim, and D. Kim, "EWB Control Based on the Estimated Clamping Force," No. 2012-01-1797. SAE Technical Paper, 2012.

[44] D. E. Schenk, R. L. Wells, and J. E. Miller, "Intelligent braking for current and future vehicles," No. 950762. SAE Technical Paper, 1995.

[45] Y. Wang, Z. Wang, L. Yu, and J. Song, "DEHB (Distributed Electro-hydraulic Braking System) Having a Holding Function," No. 2015-01-0017. SAE Technical Paper, 2015.

[46] S. J. Chapman, *Electric machinery fundamentals*. Tata McGraw-Hill Education, 1985.

[47] R. L. Norton, *Cam design and manufacturing handbook*. Industrial Press Inc., 2009.

[48] P. Flores, "A Computational Approach for Cam Size Optimization of Disc Cam-Follower Mechanisms With Translating Roller Followers," *J. Mech. Robot.*, vol. 5, no. 4, p. 041010, 2013.

[49] A. Akers, M. Gassman, and R. Smith, *Hydraulic power system analysis*. CRC press, 2010.

[50] F. M. M. Tarawneh and S. Muafag, "Friction forces in o-ring sealing," *Am. J. Appl. Sci.*, vol. 2, no. 3, pp. 626–632, 2005.

[51] The MathWorks, "Genetic Algorithm Options: User's Guide (r2015a)." The MathWorks, Inc., p. http://www.mathworks.com/help/gads/gaoptimset.html, 2015.

[52] J.-J. E. Slotine and W. Li, *Applied nonlinear control*, vol. 60. Prentice-Hall Englewood Cliffs, NJ, 1991.

[53] M. Zeinali and L. Notash, "Adaptive sliding mode control with uncertainty estimator for robot manipulators," *Mech. Mach. Theory*, vol. 45, no. 1, pp. 80–90, 2010.

[54] M. Zeinali and A. Khajepour, "Height control in laser cladding using adaptive sliding mode technique: theory and experiment," *J. Manuf. Sci. Eng.*, vol. 132, no. 4, p. 41016, 2010.

[55] Y. Shtessel, C. Edwards, L. Fridman, and A. Levant, *Sliding mode control and observation*. Springer, 2014.

[56] D. Seborg, T. F. Edgar, and D. Mellichamp, *Process dynamics & control*. John Wiley & Sons, 2006.

[57] M. Morari, J. H. Lee, C. Garcia, and D. M. Prett, "Model predictive control," *Preprint*, 2002.

[58] F. Borrelli, A. Bemporad, and M. Morari, "Predictive Control for linear and hybrid systems," *In Preperation*, 2014.

[59] "Maple." [Online]. Available: http://www.maplesoft.com/products/maple/.

[60] "The Computational Geometry Algorithms Library." [Online]. Available: http://www.cgal.org/.

[61] J. C. Gerdes and J. K. Hedrick, "Brake system modeling for simulation and control," *J. Dyn. Syst. Meas. Control*, vol. 121, no. 3, pp. 496–503, 1999.

[62] A. Fazeli, M. Zeinali, and A. Khajepour, "Application of adaptive sliding mode control for regenerative braking torque control," *Mechatronics, IEEE/ASME Trans.*, vol. 17, no. 4, pp. 745–755, 2012.

[63] J. Sugie, D.-L. Chen, and H. Matsunaga, “On global asymptotic stability of systems of Liénard type,” *J. Math. Anal. Appl.*, vol. 219, no. 1, pp. 140–164, 1998.